

國立交通大學

多媒體工程研究所

碩士論文

以物理為基礎的彩妝顯像方法

A Physically-Based Cosmetic Rendering

研究生：黃程國

指導教授：莊榮宏 教授

林文杰 教授

中華民國一百年十月

以物理為基礎的彩妝顯像方法  
A Physically-Based Cosmetic Rendering

研究生：黃程國

Student : Cheng-Guo Huang

指導教授：莊榮宏

Advisor : Jung-Hong Chuang

林文杰

Wen-Chieh Lin



Submitted to Institute of Multimedia Engineering

College of Computer Science

National Chiao Tung University

in partial Fulfillment of the Requirements

for the Degree of

Master

in

Computer Science

October 2011

Hsinchu, Taiwan, Republic of China

中華民國一百年十月

# 以物理為基礎的彩妝顯像方法

研究生：黃程國

指導教授：莊榮宏 博士

林文杰 博士



## 摘要

在3D人臉動畫領域中，如何模擬逼真的彩妝效果是一項重要的議題。在傳統的化妝顯像方法中，通常是使用影像處理的方式，將彩妝效果轉換至目標圖片上，但是這種方法具有天生的缺陷，即彩妝形狀的變形和需要相似的觀察角度拍攝模型。此外，影像處理的方法需要在相似的打光效果拍攝影像，例如：如果拍攝的打光條件不同，通常在結果上會造成不自然的效果。因此，我們提出一個整合型的方法，結合螢幕空間的顯像方式和庫貝卡-蒙克理論顯像彩妝效果。在實驗過程中，我們量測眾多的化妝品，像液態粉底液、腮紅和唇膏，然後再經由庫貝卡-蒙克模型計算出相關的參數資料。顯像步驟分為兩個階段，皮膚顯像和彩妝顯像。在皮膚顯像的過程中，考慮光通過彩妝品後的能量，並將其能量套入直接光照的結果，然後再進行原始的螢幕空間的顯像方法計算皮膚表層能量。最後，藉由多層次理論，將皮膚和彩妝效果合併，以獲得最後的顯像結果。

# A Physically-Based Cosmetic Rendering

Student: Cheng-Guo Huang

Advisor: Dr. Jung-Hong Chuang

Dr. Wen-Chieh Lin

Institute of Multimedia Engineering

College of Computer Science

National Chiao Tung University



Simulating realistic makeup effect is one of important research issues in the 3D facial animation and cosmetic industry. In tradition, people usually use image processing such as warping to transfer one's makeup to another subject. But there are many disadvantages that consist of shape distortion and restriction on the similar viewing position. Besides, these methods disregard the lighting condition. Hence, we propose an integrated approach, which combines the screen-space rendering technique with the Kubelka-Munk theory, to render the 3D makeup effect. We measure many cosmetics, such as foundations, blushes and lipsticks, and we compute the parameters of Kubelka-Munk model from these data. In the rendering stage, we consider that light penetrates through the cosmetic. Therefore, we use Kubelka-Munk model to compute the total transmittance, and then we apply this value to render the appearance of human skin. Finally, we use the multi-layer theory to combine each layer together.

## Acknowledgments

I would like to thank my advisors, Professor Jung-Hong Chuang, and Wen-Chieh Lin for their guidance, inspirations, and encouragement. I also want to thank my senior colleague Tsung-Shian Huang, for supporting me to measure data and help me to solve some rendering problems. Thanks to my colleagues during these two years: Jen-Chieh Liao, Jen-Hao Liao, Yi-Shan Li, Bo-Yin Yao, Mu-Shiue Li and Shao-Ti Lee for their assistances and discussions. Especially thanks to Chuan-Chang Wang (NEXT MEDIA®) which gives us many scanning data of human head (digital Coco and Orange), and thanks to Huey-Min Lai and Kuo-Jui Ho (Industrial Technology Research Institute®) which support us to measuring data. I am very thanks for my colleague Fu-His Huang who helps me to design cosmetic maps. Lastly I would like to thank my family for their love and support.

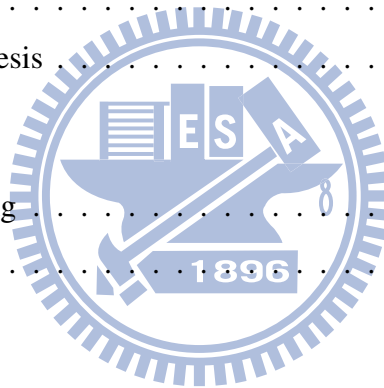


---

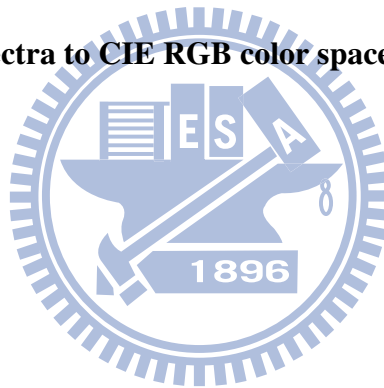
# Contents

---

<b>1</b>	<b>Introduction</b>	<b>1</b>
1.1	Contribution . . . . .	2
1.2	Organization of the thesis . . . . .	2
<b>2</b>	<b>Related Work</b>	<b>3</b>
2.1	The cosmetic rendering . . . . .	3
2.2	Translucent rendering . . . . .	8
<b>3</b>	<b>Approach</b>	<b>13</b>
3.1	Framework . . . . .	13
3.2	The method of human skin rendering . . . . .	15
3.2.1	Human skin rendering . . . . .	16
3.3	The makeup effect of each layer and layered composition . . . . .	22
3.3.1	Kubelka-Munk theory . . . . .	22
3.4	The integration of two techniques . . . . .	27
3.4.1	The skin pass . . . . .	27
3.4.2	The cosmetic pass . . . . .	32
3.4.3	The computation of specular term . . . . .	34
3.5	Implementation . . . . .	37



<b>4</b>	<b>Measurement</b>	<b>39</b>
4.1	Measuring data by spectroradiometer . . . . .	39
4.2	Approximation way to obtain Kubelka-Munk coefficients . . . . .	47
<b>5</b>	<b>Result</b>	<b>50</b>
5.1	The measuring data of cosmetic . . . . .	51
5.2	The makeup rendering . . . . .	88
<b>6</b>	<b>Conclusions</b>	<b>94</b>
6.1	Summary . . . . .	94
6.2	Limitation and Future work . . . . .	95
<b>A</b>	<b>Converting reflectance spectra to CIE RGB color space</b>	<b>96</b>
	<b>Bibliography</b>	<b>100</b>



---

# List of Figures

---

2.1	divide two example images to obtain cosmetic map[1] . . . . .	4
2.2	the workflow of digital face makeup by example [2] . . . . .	5
2.3	the synthesis cosmetic map[3] . . . . .	6
2.4	the results of computer-suggested makeup[3] . . . . .	7
2.5	the fitting result of the foundation [4] . . . . .	7
2.6	the rendering result of [4] . . . . .	8
2.7	the schema of the two dipole source [5] . . . . .	9
2.8	the render result of Donner and Jensen [6] . . . . .	10
2.9	the approximating Dipole profiles with sum-of-Gaussian [7] . . . . .	11
2.10	the simple diagram of [8] . . . . .	11
3.1	Framework of our simulation system . . . . .	14
3.2	The screen-space human skin rendering pipeline . . . . .	16
3.3	The workflow of texture-space and screen-space . . . . .	17
3.4	the result of softness shadow boundary . . . . .	18
3.5	The influence of different global subsurface scattering value . . . . .	19
3.6	blurred operation . . . . .	20
3.7	Fitting result by six Gaussian weights and four Gaussian weights . . . . .	21
3.8	the simple view of Schuster's assumption . . . . .	23
3.9	The chromaticity coordinate of liquid-foundation from four different observation. . . . .	24



3.10	The reflectance of liquid-foundation from four different observation. . . . .	24
3.11	Reflectance and transmittance of two non-homogeneous layers . . . . .	26
3.12	the pass of light between foundation and skin . . . . .	28
3.13	the flow chart about the skin pass . . . . .	29
3.14	the cosmetic map . . . . .	30
3.15	the total transmittance after the light goes through the foundation . . . . .	31
3.16	the irradiance map and applying the transmittance (w/o SSSS) . . . . .	31
3.17	the irradiance map and applying the transmittance (with SSSS) . . . . .	32
3.18	the work flow about the cosmetic pass . . . . .	33
3.19	rendering result . . . . .	34
3.20	enlarging of skin surface . . . . .	35
3.21	the rendering result of specular effect . . . . .	36
3.22	the architecture of simulation system . . . . .	38
4.1	Our capture device and environment . . . . .	40
4.2	Radiant energy of liquid foundation . . . . .	41
4.3	Radiant energy of CIE standard illuminant D55 . . . . .	41
4.4	Radiant energy of CIE standard illuminant E . . . . .	42
4.5	the reflectance of barium sulfate and barium sulfate sample . . . . .	43
4.6	Reflectance of liquid foundation . . . . .	44
4.7	Liquid foundation sample. Left: background. Mid: thickness layer. Right: thin layer . . . . .	44
4.8	The sample of our simple container . . . . .	45
4.9	The reflectance of $R_i$ , $R$ and $R_g$ . . . . .	45
4.10	The coefficient S and K for each wavelength . . . . .	46
4.11	The original reflectance and the fitting result . . . . .	46

4.12	CIERGB color of fitting curve and measured curve. Left: Original data (R0) and the color is (0.62, 0.58, 0.51). Right: Fitting result and the color is (0.60, 0.57, 0.5) . . . . .	47
4.13	CIERGB color of fitting curve and measured curve. Left: Original data (R0), color (0.62, 0.48, 0.38). Right: Fitting result, color (0.60, 0.47, 0.38) . . . . .	47
4.14	Selecting two colors and obtaining S and K . . . . .	48
4.15	capture coefficient S and K by camera . . . . .	48
4.16	liquid foundation sample . . . . .	49
4.17	diffuse color captured by our simple device . . . . .	49
5.1	original appearance of skin rendering . . . . .	51
5.2	the measuring data of sample F1 . . . . .	53
5.3	the fitting data of sample F1 . . . . .	53
5.4	the comparison between R and R0 of sample F1 . . . . .	54
5.5	the rendering result of sample F1 . . . . .	55
5.6	the measuring data of sample F2 . . . . .	56
5.7	the fitting data of sample F2 . . . . .	56
5.8	the comparison between R and R0 of sample F2 . . . . .	57
5.9	the rendering result of sample F2 . . . . .	58
5.10	the measuring data of sample F3 . . . . .	59
5.11	the fitting data of sample F3 . . . . .	59
5.12	the comparison between R and R0 of sample F3 . . . . .	60
5.13	the rendering result of sample F3 . . . . .	61
5.14	the measuring data of sample F4 . . . . .	62
5.15	the fitting data of sample F4 . . . . .	62
5.16	the comparison between R and R0 of sample F4 . . . . .	63
5.17	the rendering result of sample F4 . . . . .	64
5.18	the measuring data of sample F5 . . . . .	65

5.19	the fitting data of sample F5 . . . . .	65
5.20	the comparison between R and R0 of sample F5 . . . . .	66
5.21	the rendering result of sample F5 . . . . .	67
5.22	the measuring data of sample B1 . . . . .	68
5.23	the fitting data of sample B1 . . . . .	69
5.24	the comparison between R and R0 of sample B1 . . . . .	69
5.25	the rendering result of sample B1 . . . . .	70
5.26	the measuring data of sample B2 . . . . .	71
5.27	the fitting data of sample B2 . . . . .	71
5.28	the comparison between R and R0 of sample B2 . . . . .	72
5.29	the rendering result of sample B2 . . . . .	73
5.30	the measuring data of sample L1 . . . . .	74
5.31	the fitting data of sample L1 . . . . .	75
5.32	the comparison between R and R0 of sample L1 . . . . .	75
5.33	the rendering result of sample L1 . . . . .	76
5.34	the measuring data of sample L2 . . . . .	76
5.35	the fitting data of sample L2 . . . . .	77
5.36	the comparison between R and R0 of sample L2 . . . . .	77
5.37	the rendering result of sample L2 . . . . .	78
5.38	the measuring data of sample L3 . . . . .	78
5.39	the fitting data of sample L3 . . . . .	79
5.40	the comparison between R and R0 of sample L3 . . . . .	79
5.41	the rendering result of sample L3 . . . . .	80
5.42	the measuring data of sample L4 . . . . .	80
5.43	the fitting data of sample L4 . . . . .	81
5.44	the comparison between R and R0 of sample L4 . . . . .	81
5.45	the rendering result of sample L4 . . . . .	82
5.46	the measuring data of sample L5 . . . . .	82

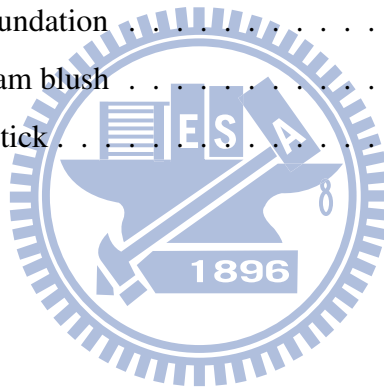
5.47	the fitting data of sample L5 . . . . .	83
5.48	the comparison between R and R0 of sample L5 . . . . .	83
5.49	the rendering result of sample L5 . . . . .	84
5.50	the measuring data of sample L6 . . . . .	84
5.51	the fitting data of sample L6 . . . . .	85
5.52	the comparison between R and R0 of sample L6 . . . . .	85
5.53	the rendering result of sample L6 . . . . .	86
5.54	the measuring data of sample L7 . . . . .	86
5.55	the fitting data of sample L7 . . . . .	87
5.56	the comparison between R and R0 of sample L7 . . . . .	87
5.57	the rendering result of sample L7 . . . . .	88
5.58	the comparing result of with SSS and without SSS . . . . .	89
5.59	combination with different cosmetics and apply on Digital Coco . . . . .	90
5.60	combination with different cosmetics and apply on a man head . . . . .	91
5.61	combination with different cosmetics and apply on Digital Orange . . . . .	92
5.62	comparison rendering result with reference image . . . . .	93
5.63	comparison rendering result with reference image. (do not contain eyelashes and eyebrows) . . . . .	93
A.1	Obtaining reflectance by remove light effect . . . . .	97
A.2	CIE 2-degree color matching functions . . . . .	98
A.3	converting diagram . . . . .	99

---

# List of Tables

---

3.1	blend weight . . . . .	20
5.1	The brand of liquid foundation . . . . .	52
5.2	The brand of each cream blush . . . . .	68
5.3	The brand of each lipstick . . . . .	74

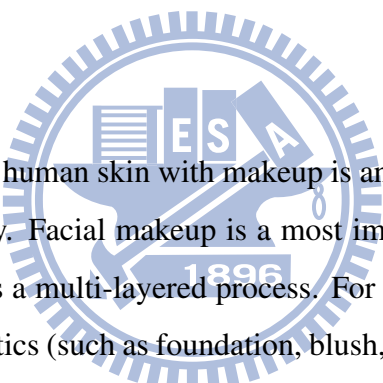


# CHAPTER 1

---

## Introduction

---



Rendering the realistic image of human skin with makeup is an important issue in the 3D facial animation and cosmetic industry. Facial makeup is a most important routine for some female or some men, and the makeup is a multi-layered process. For example, we usually do the skin care first and smear some cosmetics (such as foundation, blush, lipstick and eye-shadow) on our face. By smearing the cosmetics on our face, we can change our facial appearance in different style.

There are many researches to render the makeup effect and can be divide into two main categories cosmetic transfer and makeup simulation. Cosmetic transfer uses the example image to transfer the makeup effect, and makeup simulation uses some properties to simulate the makeup effect. Both of them have some individual advantages. By using the transfer technique, we can directly change the makeup effect and this technique can obtain additional business value by employing to salon. Makeup simulation can be used in cosmetic industry or be used to simulate different makeup style. We can even render the makeup effect under different situation. For example, in nightclub, in the party or under the sunlight.

In our work, we expect to simulate the realistic image of human skin with the makeup effect.

We use the technique of screen-space to render the human skin and combine it with the Kubelka-Munk theory to simulate the makeup effect. The cosmetics include many special effects, such as pearl effect and glitter effect. However, these effects are difficult to simulate, because these effects are view-dependent. Therefore, our simulation does not process these complex effects. We concentrate on the cosmetics without the pearl effect and glitter effect, and we support the color changing with the assumption that the cosmetics are homogenous material.

## 1.1 Contribution

- We propose a complete algorithm to combines the screen-space skin rendering method and the Kubelka-Munk theory to obtain the makeup result.
- The makeup simulation system performs in real-time, and user can modify the style of cosmetic in interactive frame rate.

## 1.2 Organization of the thesis

The thesis is organized as follows: Chapter 2 gives some related work about the cosmetic rendering and the diffuse approximation of translucent rendering. Chapter 4 explains how to obtain the parameters from the measuring data, and shows other approximate method to get parameters. Chapter 3 illustrates the framework and explains our approach in detail. Chapter 5 shows the results of our simulation system. Finally, we summarize our approach and discuss the future work in Chapter 6.

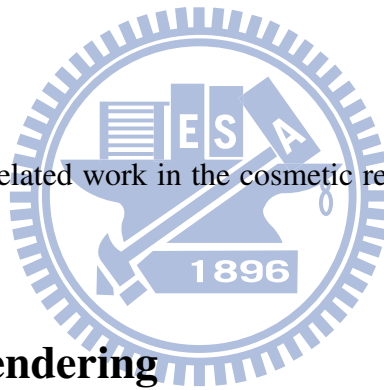
## CHAPTER 2

---

# Related Work

---

In this chapter, we review the related work in the cosmetic rendering and the diffuse approximation.



### 2.1 The cosmetic rendering

Cosmetic rendering can be divided into two main categories: cosmetic transfer and cosmetic simulation.

#### Cosmetic transfer

Cosmetic transfer means to transfer one's makeup information to another subject. Such methods usually require one or more examples to obtain cosmetic information (or the cosmetic map). The cosmetic map represents the change caused by the makeup effect. There are some researches in this field, such as Tong et al. [1], Dong Guo and Terence Sim [2] and Scherbaum et al. [3].

Tong et al. [1] use a pair of 2D example images of the same face "before" and "after" makeup to find the cosmetic map, and apply the cosmetic map to the subject. In their work, their first



step is to remove the non-skin feature. For example: eyebrows, eyelashes and some inherent skin features (such as freckles, moles and blemishes), and then warp two example images to the subject image. After the warping, they divide the "after" image by the "before" image to obtain the cosmetic map. In this map, each value of this map is the Bidirectional reflectance distribution function (BRDF) value in this view (Figure 2.1). Then the subject is multiplied by the cosmetic map to obtain the makeup result.

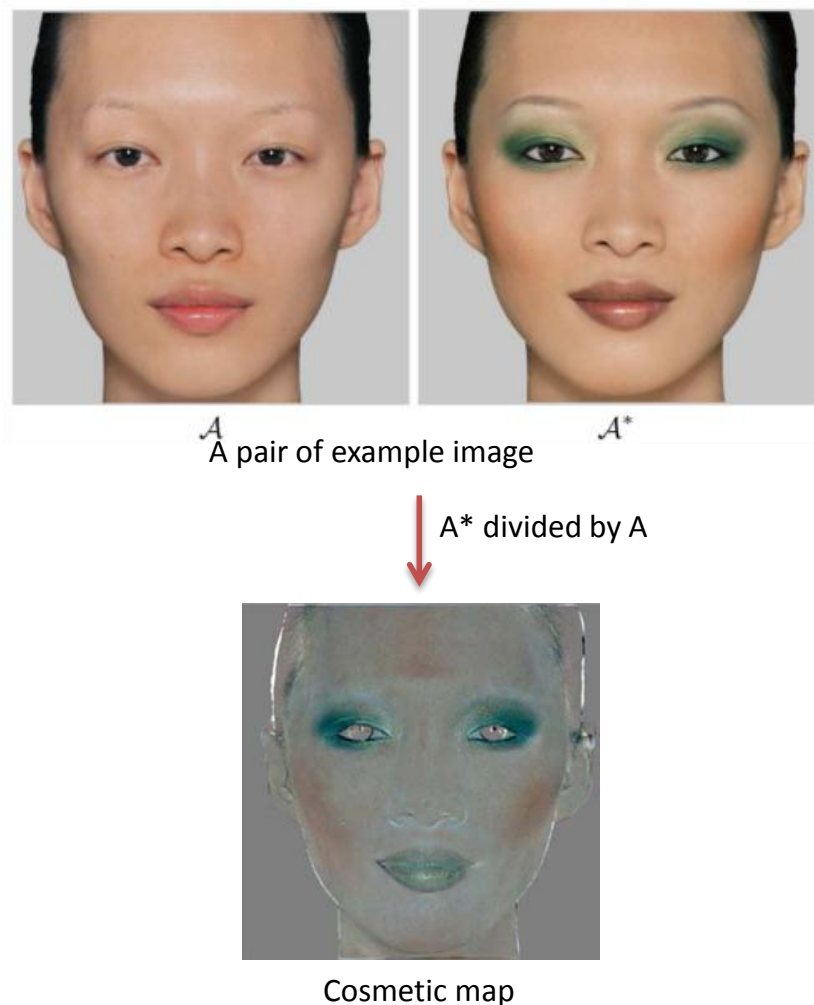


Figure 2.1: divide two example images to obtain cosmetic map.[1]

Dong Guo and Terence Sim [2] propose another convenient approach to transfer cosmetic effect. In their work, they use one example image and one subject image as input. There are four main steps in this approach: face alignment and warping, layer decomposition, synthesis and combination. This method use the image warping to transfer the makeup effect, so it needs a fully alignment before transferring. First, they warp the example image to the subject. Second, they analyze the example image and the subject image to extract the face structure, the skin detail and the color. After decomposition is finished, the information from each layer of example is transferred to corresponding layer of the subject in different way: skin detail is transferred by additive way; color is transferred by alpha blending; shading effect and highlight in the face structure will be transferred by gradient editing. Finally, each layer are composed together and the final result is obtained. The workflow of their approach is illustrated in the figure 2.2.

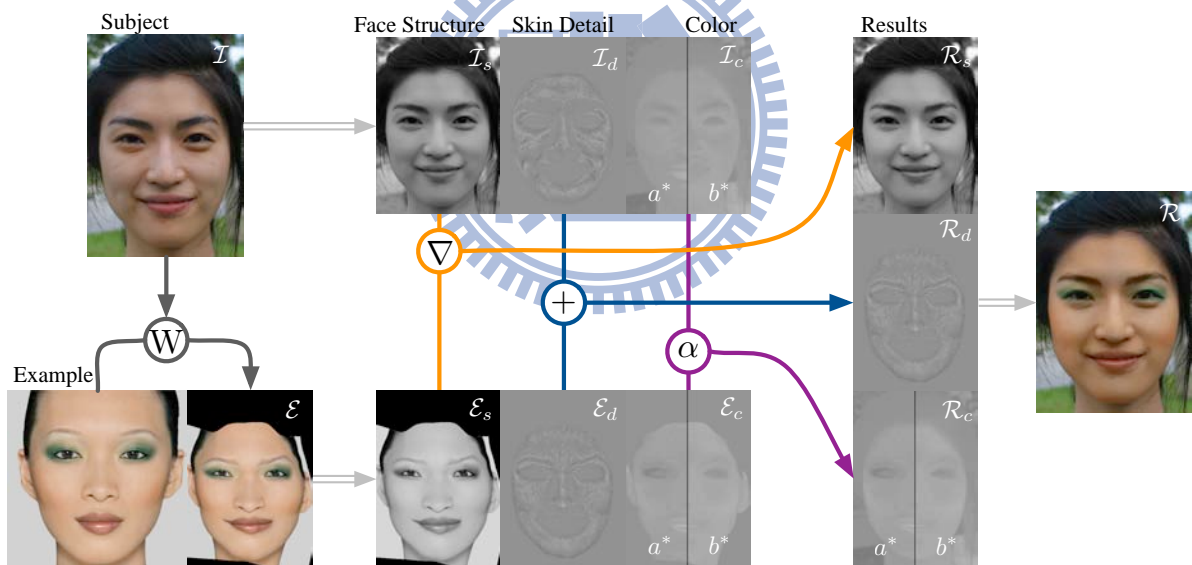


Figure 2.2: the workflow of digital face makeup by example. [2]

Both two methods have a fatal problem by 2D image warping which causes the shape of makeup to be deformed, and they need to capture the image at the same or similar viewing position. Dong Guo and Terence Sim [2] use one example image to transfer the cosmetic effect, but it loses much information. For example, they transfer the color by blending operation, and

the color of makeup effect cannot be transferred correctly. (Because each appearance of human skin has different properties, such as skin color.)

Scherbaum et al. [3] build a database by the device of structure light and use the database to re-synthesize the makeup effect. They capture human faces that include makeup effect and without makeup effect, and then extract the information from the pair of images, such as position, normal, diffuse map, scattering profile, specular and the cosmetic map, etc. In the run-time, user inputs a 2D image to query the appropriate 3D face and the 3D face is morphed to fit the 2D image. After fetch the suitable face, they query the database to find to best-match facial appearance and cosmetic map by PCA. Then, the system re-synthesizes the cosmetic and applies it to diffuse map. They provide a better way to transfer the makeup effect, but there are many problems about it. First, the style of makeup is fixed. Second, the system needs give more constrains to re-synthesizes the credible cosmetic map. Final, the system needs many examples to give the appearance correctly. Figure 2.3 shows the synthesis cosmetic map and figure 2.4 gives some results.

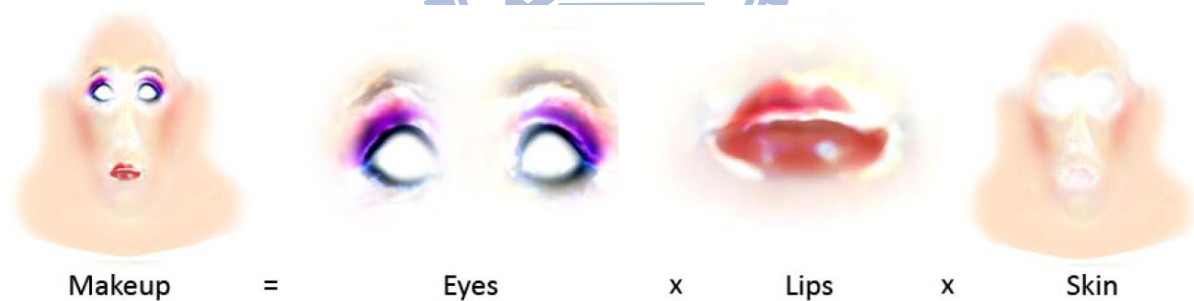


Figure 2.3: the synthesis cosmetic map. [3]



Figure 2.4: the results of computer-suggested makeup. [3]

### Cosmetic simulation

Moriuchi et al. [4] use a physical model and a statistical approach to simulate the foundation. They measure the foundation from different view angle and capture its reflectance between 400 nm and 700 nm. Then, they use the Cook-Torrance model to find appropriate parameters. Using Cook-Torrance model to describe the translucent material is not enough, because this model is used to describe the Lambert material. Therefore, they employ the statistical approach to analyze the reflectance data by PCA. Figure 2.5 shows the fitting result and Figure 2.6 shows the rendering result.

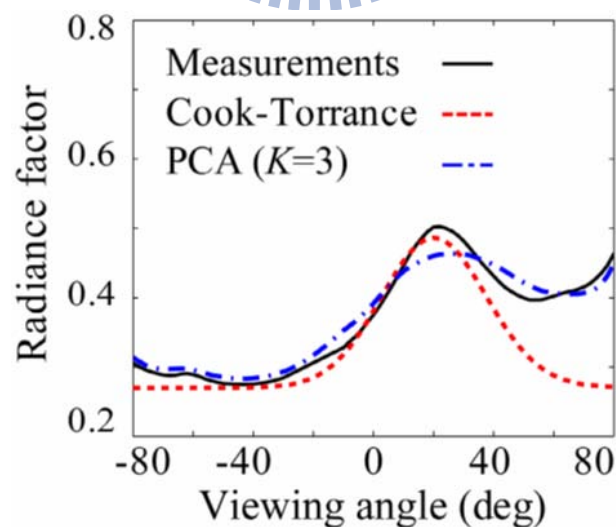


Figure 2.5: the fitting result of the foundation. [4]

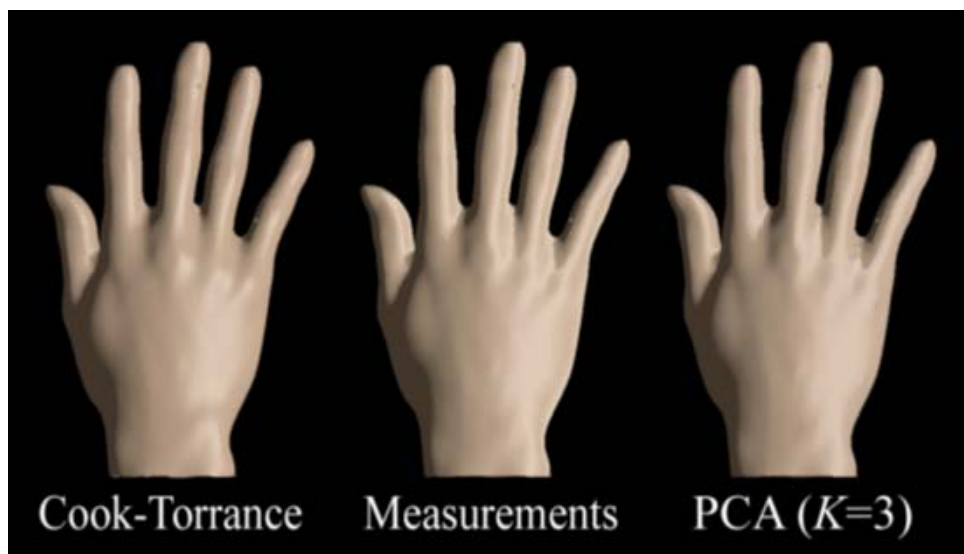


Figure 2.6: the rendering result of [4]

Doi et al. [9] use the Kubelka-Munk theory to render the foundation on the skin. They measure the reflectance of many skins and liquid foundations, and then use the Kubelka-Munk theory to render result. Even they use a good way to simulate the makeup effect, they do not consider an important issue that measuring the reflectance of skin cannot obtain the translucent appearance. We extend this approach to 3D space, and provide a complete algorithm to render it.

## 2.2 Translucent rendering

Human skin is a kind of translucent materials. There some rendering technique to render translucent material, but the diffuse approximation is a better way to render translucent materials.

Jensen et al. [5] introduce to use diffuse approximation to solve the radiant transfer equation. By using the diffuse approximation, they translate the computation of complex interior-behavior to the function of distance-related. By this way, they use dipole to compute the diffuse reflectance. Figure 2.7 shows a pair of dipole source. They assume the thickness of material

is infinity and the scattering coefficient  $\sigma_s$  is much larger than the absorption coefficient  $\sigma_a$ . Hence, the render result is more translucent.

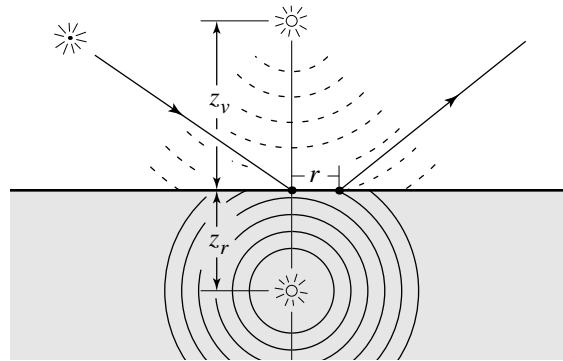


Figure 2.7: the schema of the two dipole source. [5]

Donner and Jensen [6] extend the dipole approximation. They use the multi-pole to approximate the thin layer's material, such as skin and leaves. After computing the reflectance of each layer, they use multi-layered model to combine each layer. Figure 2.8 shows the render result of Donner and Jensen [6].



Figure 2.8: the render result of Donner and Jensen [6].

Both of the above methods take long time to render an image. For example, Donner and Jensen [6] use one to five minutes to render an image. Jensen and Buhler [10] provide a hierarchical structure to reduce the computation time. They apply hierarchical structure to dipole method [5], and the rendering time takes 7-8 second per image. Therefore, using the hierarchical structure still cannot reach real-time performance.

d'Eon et al. [8] provide a texture-space algorithm to render the translucent materials in real-time frame rate. The multi-pole method [6] provide a good way to simulate translucent materials, but this process is double-integration for gathering energy. Hence, it needs much time to compute. d'Eon et al. [8] use sum-of-Gaussian to approximate the diffuse profile. After the diffusion profile is represented by sum-of-Gaussian, the complex integration of original equation can be approximated by multiple Gaussian-filters. In the run time, they render the irradiance map in texture-space, and then they use Gaussian-filter to blur this map many times. Finally, they combine each blurred result by the weights of sum-of-Gaussian. Figure 2.9 shows the approximating Dipole profiles with sum-of-Gaussian and Figure 2.10 shows a diagram of

this technique.

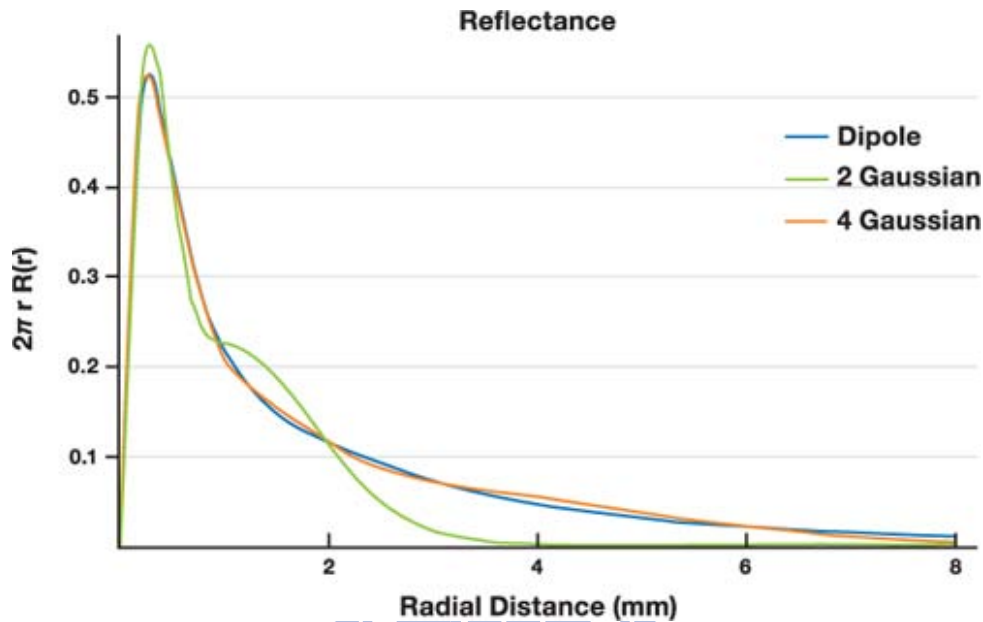


Figure 2.9: the approximating Dipole profiles with sum-of-Gaussian.[7].

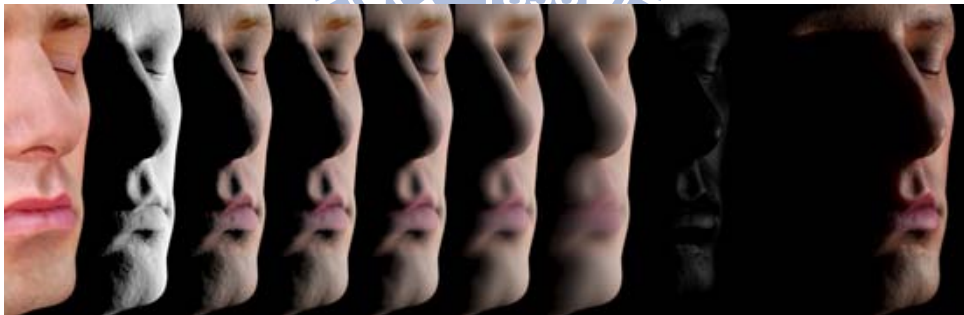
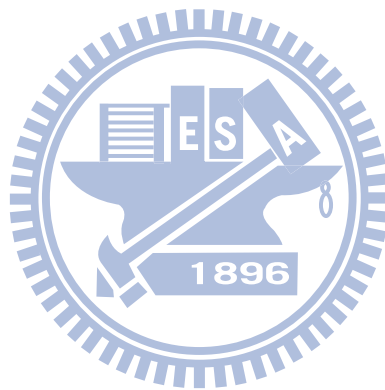


Figure 2.10: the simple diagram of [8].

Jimenez et al. [11] extend the texture-space technique to the screen-space. They render the shading result in screen-space and store it in render target. Then, they considered screen-space information to blur the result many times. In each blurring pass, they use the alpha blending to accumulate the blurring result and the blending weights are according to the sum-of-Gaussian. We apply this technique to our simulation system.



d'Eon and Irving [12] propose a quantized-diffusion model for rendering translucent material. In their work, they decompose the dipole function to sum-of-Gaussian, and extend the multi-layered structure [6] to support the decomposed sum-of-Gaussian. The model of d'Eon and Irving [12] can support many materials, such as low absorption materials and high absorption materials. They give an impressive result, but the rendering time of a frame need 20-30 minutes to render a frame.

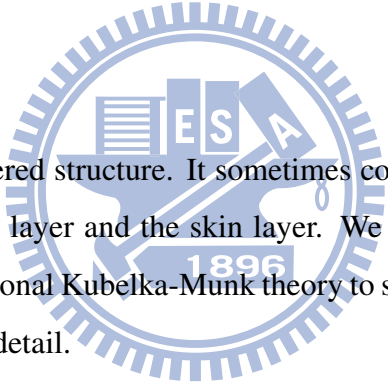


## CHAPTER 3

---

# Approach

---



The face make-up is a multilayered structure. It sometimes consisting of the foundation layer, the blush layer, the eye shadow layer and the skin layer. We combine a rendering method to translucent materials with traditional Kubelka-Munk theory to simulate the makeup appearance. In this chapter, we explain it in detail.

### 3.1 Framework

Our makeup simulation system can be divided into two main passes - skin rendering pass and makeup pass. In our simulation, we assume the cosmetics do not have the pearl effect and the sparkle effect. Figure 3.1 shows an overview of our simulation method.

In the skin pass, we use screen-space human skin rendering technique which is introduced by Jimenez et al [11] to simulate the appearance of human skin. In their work, they generate irradiance map in screen-space. Then, they blur the irradiance map many times and use alpha blending to acculturate each blurring result. Finally, they add specular part to the blurring result and obtains the final result. In order to use this technique to our makeup simulation, we

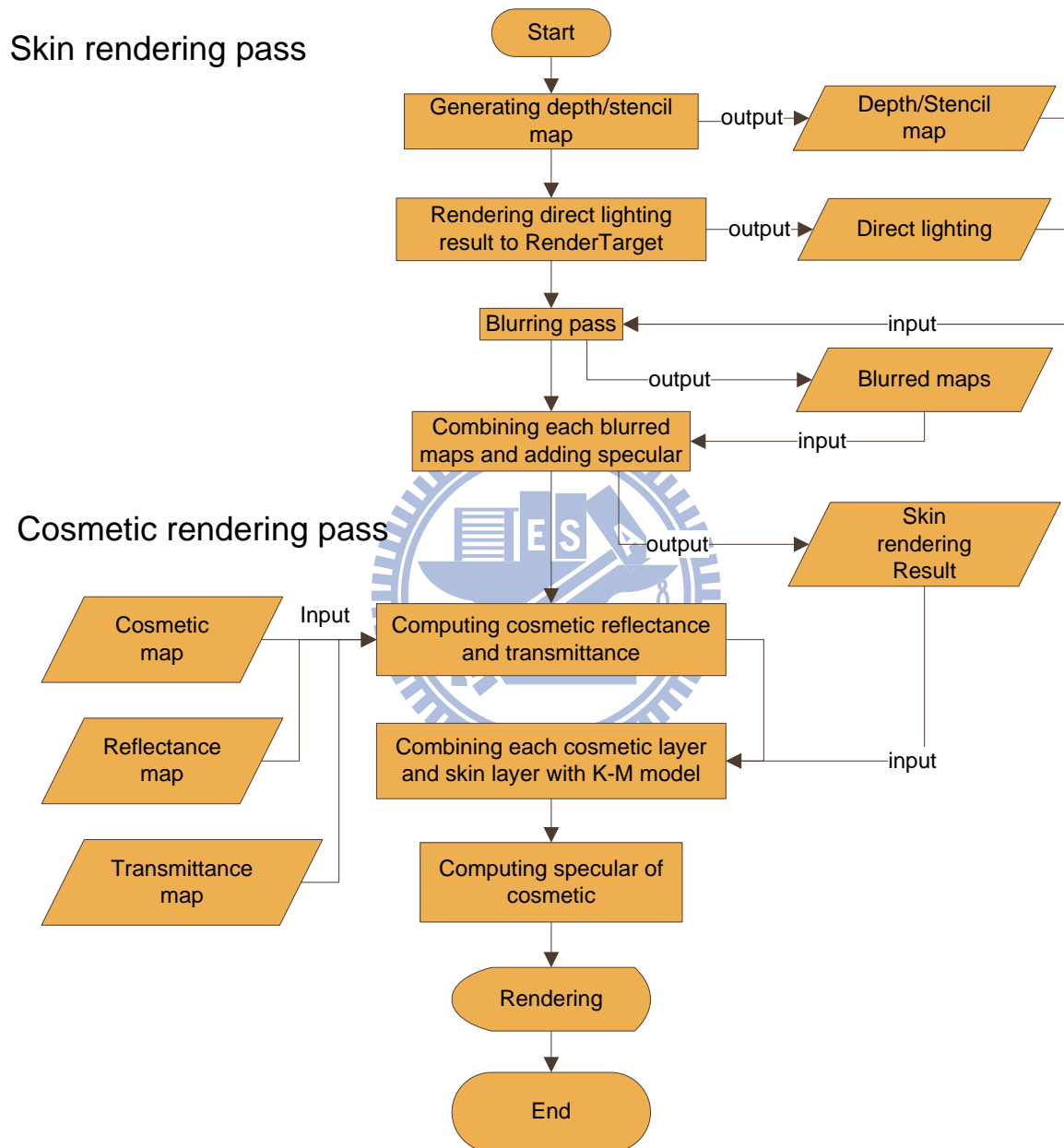


Figure 3.1: Framework of our simulation system.

considered whether the surface is covered by the cosmetics. If the skin surface is covered by the cosmetics, we compute the total energy of light penetration through the cosmetics and apply this energy to generate the irradiance map in screen-space. In subsection 3.4, we explain this part in detail.

In the cosmetic pass, we use Kubelka-Munk theory to compute the reflectance and the transmittance of each cosmetic layer, and then we use the multi-layered theory to compute final reflectance.

There are some advantages by using our approach to simulate the makeup appearance:

1. The makeup simulation system performs in real-time, and the thickness of cosmetics can be changed in interactive frame rate.
2. User can modify cosmetic map and render different makeup appearance immediately.
3. Unlike the traditional image warping method, our approach can render in different views and can be used in different environment.

In the following subsections: First, we introduce how to render the appearance of skin by a screen-space technique. Next, we introduce the Kubelka-Munk theory that is used to compute layered reflectance and transmittance. Our system combines each layer by its multi-layered model in our simulation. Finally, we describe how to merge these two techniques to render our result.

## 3.2 The method of human skin rendering

Human skin is a kind of translucent material. It contains many biological layers, such as epidermis, dermis and vein, etc. There are many methods to simulate human skin. The suitable way to render it is the diffusion approximate method (Jensen et al. [5], Donner and Jensen [6], d'Eon et al. [8], Jimenez et al. [11] and d'Eon and Irving [12]) and we follow the method proposed by Jimenez et al. [11] to simulate the appearance of human skin.

### 3.2.1 Human skin rendering

The screen-space approach translates the texture-space diffusion approximation to screen-space. Jimenez applies the convolution directly to final rendering rather than renders an irradiance map and convolves it many times with the diffusion profile. Figure 3.2 shows the original screen-space human skin rendering pipeline, and figure 3.3 gives a overview of the texture-space diffusion and the screen-space rendering pipeline. The texture-space diffusion has main cost in the blurring pass, because the texture-space diffusion blurs the irradiance map with full quad and it needs much memory to store the blurring result. Hence, the frame rate of texture-space diffusion is slower than the technique of screen-space. For this reason, we choose the screen-space method to render the appearance of human skin.

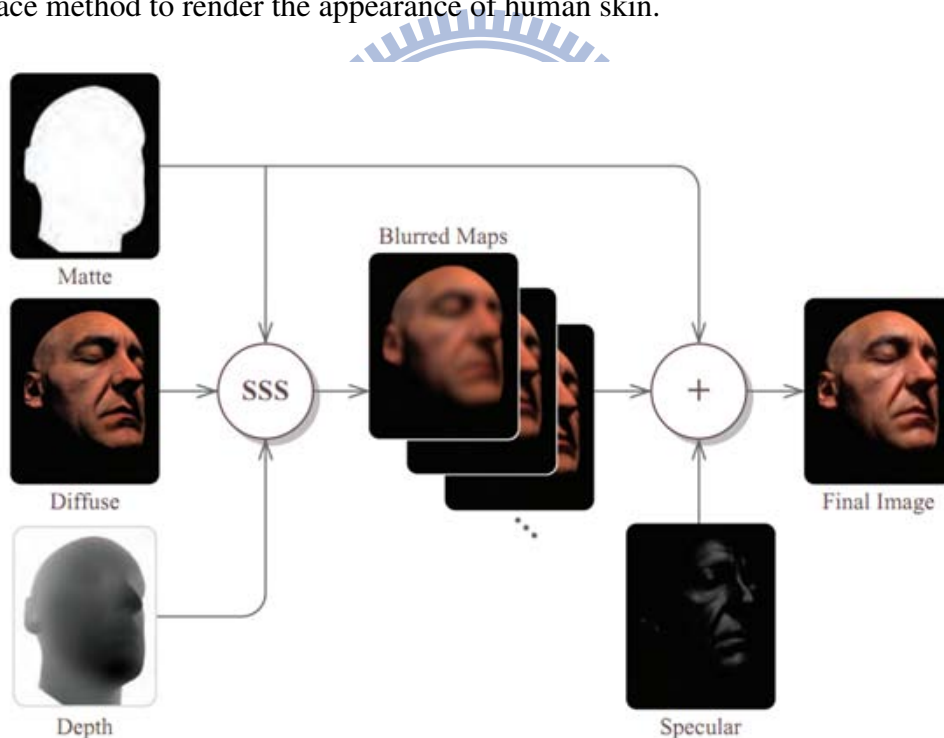


Figure 3.2: The screen-space human skin rendering pipeline [11].

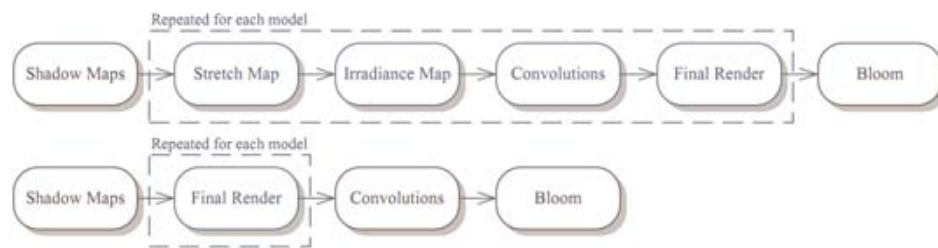


Figure 3.3: The workflow of texture-space and screen-space. Top: workflow about the texture-space diffusion. Bottom: screen-space diffusion.[11]

The screen-space human skin rendering is three main passes. In the first pass, it generates shadow map from light source and generates the depth map and the stencil (matte) map from viewing position. (The depth map is used to decide the stretch factor for blurred pass and the stencil map is used to restrict the blurred area.) Second, it uses shadow map and color map to generate the irradiance map, which takes shadow and lambert term into account, in screen-space. Finally, it uses depth map and stencil map to blur the irradiance map many times, and uses alpha blending to accumulate each blurring results. In general, it also puts specular term to the irradiance map, then the softness and smoothness highlight can be obtained after the blurring pass is finished. By adding shadow to the irradiance map, we can achieve softness shadow boundary and make rendering result more reliable. Figure 3.4 shows softness shadow boundary and original shadow boundary. In this case, we use PCF to compute shadow which is introduced by Reeves et al. [13].

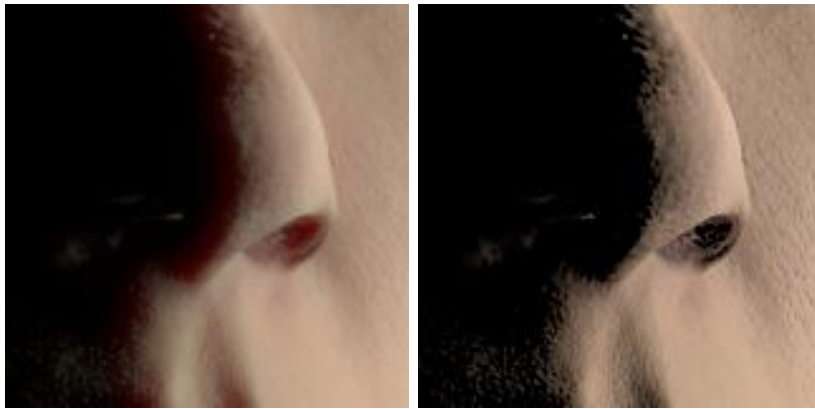


Figure 3.4: the result of softness shadow boundary.

In the traditional texture-space diffusion method, blurring pass needs a stretch map to obtain the stretch factor and uses it to decide the kernel width:

$$\text{Kernel width} = \text{stretch factor} * \text{Gaussian width}$$

In order to find a correct method to compute the stretch factors for screen-space approach, Jimenez observed several phenomena:

- The blurry kernels' widths are related to the distance between camera and object. For example, if the camera is far from the object, it needs narrower kernel widths than close one.
- If the pixel of object surface is at steep angles from the view of camera, it needs narrower kernels than flatten one.

According to the above considerations, Jimenez derives two equations to obtain approximate stretch factors:

$$S_x = \frac{\alpha}{d(x, y) + \beta * \text{abs}(\nabla_x * d(x, y))} \quad (3.1)$$

$$S_y = \frac{\alpha}{d(x, y) + \beta * \text{abs}(\nabla_y * d(x, y))} \quad (3.2)$$

where  $d(x, y)$  is the depth value captured from the viewing position which is stored in the depth map,  $\alpha$  indicates the global subsurface scattering level in the image,  $\beta$  controls the subsurface scattering which varies with the depth gradient, and  $\nabla$  means the object surface flatness. We can control  $\alpha$  value to change the appearance of subsurface scattering. Figure 3.5 demonstrates different global subsurface scattering values.



Figure 3.5: The influence of different global subsurface scattering value.  $\beta$  is fixed by 800 and varying global subsurface scattering values are 40, 28 and 12, respectively.

After determining the blurry kernels' widths, it blurs each pixel with 7-taps and multiplies each taps to specific weight. These weights are 0.006, 0.061, 0.242, 0.382, 0.242, 0.061, and



0.006 [7]. We fetch the texel and its 3 neighbors and multiplies these weight, respectively. Blurring operation can be separated to horizontal blurring and vertical blurring, and each blurred result can be directly accumulated by alpha blending. This process can be finished by multiple render targets (MRT). Figure 3.6 shows blurred operation.

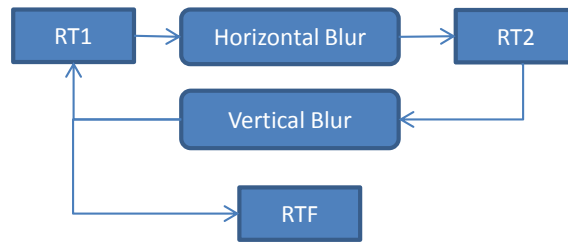


Figure 3.6: blurred operation.

In the above figure, RT1 means render target 1, RT2 means render target2 and RTF means final render target. RT1 is applied horizontal Gaussian blurring and store blurred result in RT2. Then, RT2 is applied vertical Gaussian blurring and outputs the result into both RT1 and RTF. For RTF, it uses alpha blending to accumulate each blurred values and the blend weights are listed in table 3.1.

Table 3.1: blend weight

Skin	$W_i$			$W'_i$		
	R	G	B	R	G	B
0.0064	0.2405	0.4474	0.6157	1.0	1.0	1.0
0.0516	0.1158	0.3661	0.3439	0.3251	0.45	0.3583
0.2719	0.1836	0.1864	0.0	0.34	0.1864	0.0
2.0062	0.46	0.0	0.0402	0.46	0.0	0.0402

Jimenez et al. use least square to fit original six Gaussian weights d'Eon et al. [7] into four Gaussian weights  $W_i$ . For producing normalized result, Jimenez et al. [14] normalizes these

value by equation 3.3, and these normalized weights are used in blending operation. Figure 3.7 plots six Gaussian weights and four Gaussian weights. Equation 3.3 generates a normalized weight at each step  $i$  of the previous sum, e.g. if we want to compute R channel's normalized weight in step 2, we use equation 3.3 and  $0.1158 / (0.2405 + 0.115) = 0.3251$ .  $W'_i$  is a blend weight and we can use equation 3.4 to compute the blend result. After blurred pass finishes, we can obtain the appearance of skin. In subsection 3.4, we describe how to use screen-space method to our simulation system.

$$W'_i = \frac{W_i}{\sum_{j=1}^i W_j} \quad (3.3)$$

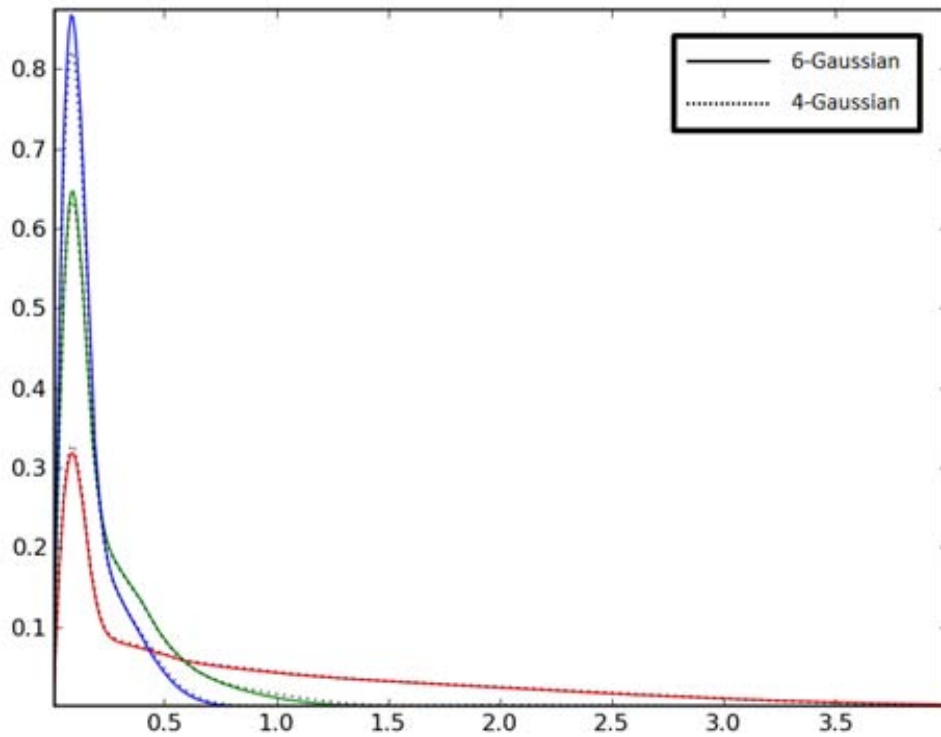


Figure 3.7: Fitting result by six Gaussian weights and four Gaussian weights.[14]

$$Color_{out} = Color_{src} * W'_i + Color_{dst} * (1 - W'_i) \quad (3.4)$$

### 3.3 The makeup effect of each layer and layered composition

Makeup is a multi-layered structure. It combines many color layers and colorless layers, e.g. Color layers include foundation, blush, eye-shadow and lipstick; colorless layers include toning water and Moisturizing gel. We focus on color layers and these color layers are simulated by the Kubelka-Munk theory which is famous for paints industry.

#### 3.3.1 Kubelka-Munk theory

The Kubelka-Munk model can be derived from radiation transfer equation. The Kubelka-Munk theory uses the scattering coefficient per unit length and the absorption coefficient per unit length to describe the properties of the whole medium; radiation transfer equation use some descriptive coefficients to represent the individual behavior of each particle, such as the absorption coefficient, the scattering coefficient and the scattering phase function. There are much research show the relationship between the coefficients of Kubelka-Munk and the coefficients of radiation transfer equation, such as Thennadil [15].

Schuster is the first attempt to use isotropic scattering to find the simplified equation of radiation transfer equation. In this process, Schuster assumes each layers are parallel and each scattering is isotropic, and simplifies radiation field into two opposite radiation fluxes I and J in the x and -x direction, respectively. In order to eliminate the boundary effect, Schuster assumes yz-plane is greater than thickness of layer. Figure 3.8 gives a simple view of these assumptions.

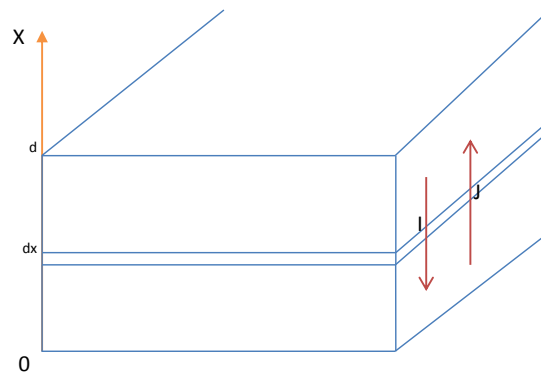


Figure 3.8: The simple view of Schuster's assumption

Kubelka-Munk extends the equation of Schuster and adds some assumptions to simplify complex in-scattering transmission and remission: each scattering is isotropic scattering; the particles are random distribution in the medium; the layer is subject only to diffuse irradiation. By the above conditions, Kubelka and Munk pointed out simplified the radiation transfer equation can be used to calculate the reflectance and transmittance of each layer. Gustav Kortum [16] gives more detail about the Kubelka-Munk theory in his book.

Because Kubelka-Munk assume each scattering is isotropic, we need to measure whether the reflectance of cosmetic from different observations are same or similar spectra. We select a liquid-foundation and measure same place from different observation (In this case, we rotate our sample around  $0, \pi/2, \pi$  and  $2\pi$ . Fig 3.9 gives the chromaticity coordinate and we can observe that the chromaticity from different observation places have similar coordinate and fig 3.10 shows measuring reflectance. Each reflectance has similar shape and the radiant energy are very closer. From the above observation, if the cosmetics do not have view-dependent effect, we almost can assume that the liquid-foundation, blush and lipstick are isotropic.

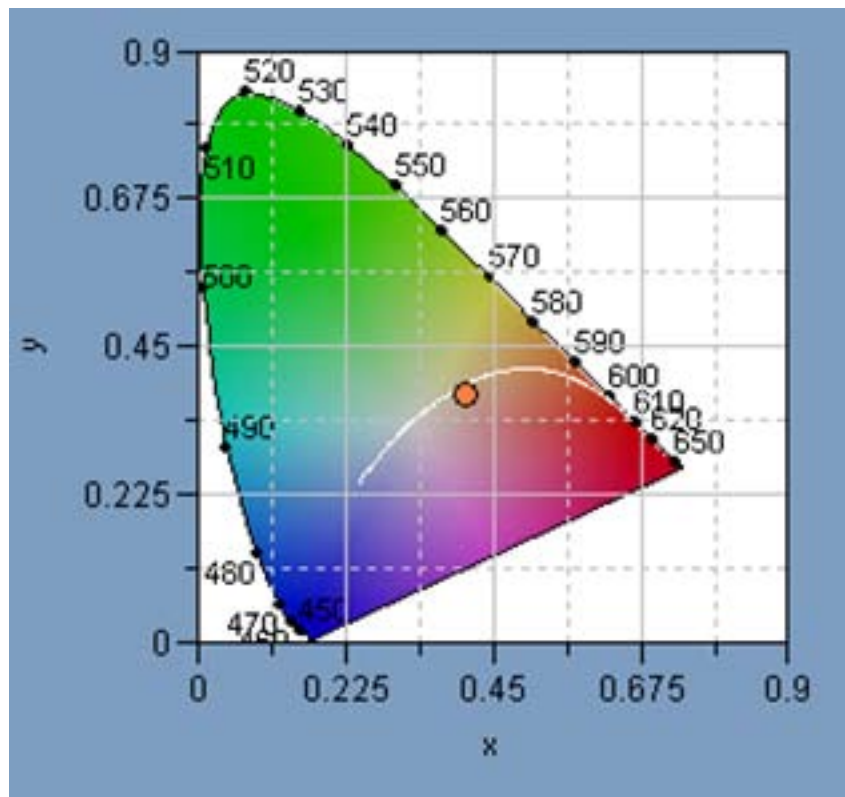


Figure 3.9: The chromaticity coordinate of liquid-foundation from four different observation

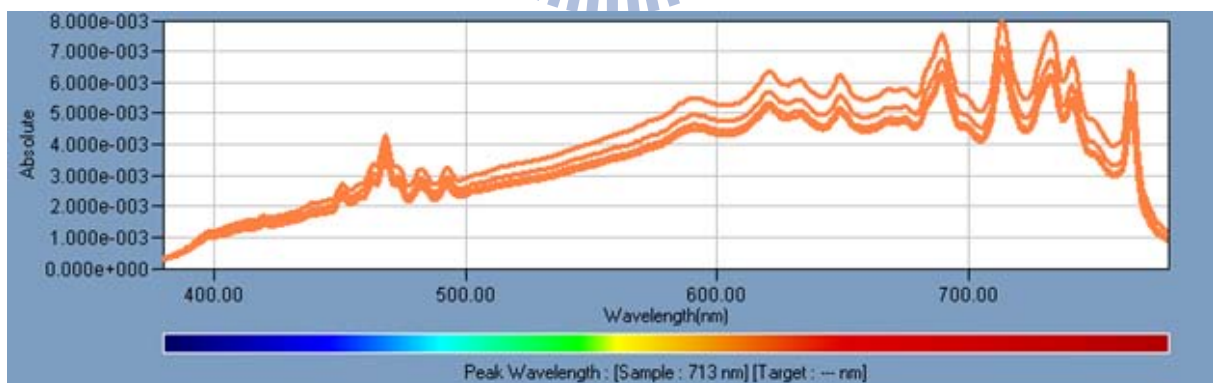


Figure 3.10: The reflectance of liquid-foundation from four different observation

## Reflectance and transmittance

The Kubelka-Munk model mainly uses the scattering coefficient  $S$ , the absorption coefficient  $K$  and the certain thickness to compute reflectance and transmittance. Equation 3.5 shows the reflectance equation.

$$R = \frac{1 - R_g (a - b \coth(bSX))}{a - R_g + b \coth(bSX)} \quad (3.5)$$

where

$$a = 1 + \left(\frac{K}{S}\right)$$

$$b = (a^2 - 1)^{\frac{1}{2}}$$

$X$  = thickness of layer

$R_g$  = reflectance of the background

$K$  = Absorption coefficient per unit length

$S$  = Scattering coefficient per unit length

The scattering coefficient  $S$  and the absorption coefficient  $K$  are wavelength-dependent and defined in per unit length rather than free mean path. When the material is sufficiently thick, we can ignore the reflectance of the background and equation 3.5 can be simplified as:

$$R_{\infty} = 1 + \left(\frac{K}{S}\right) - \left[ \left(\frac{K}{S}\right)^2 + 2 \left(\frac{K}{S}\right) \right]^{\frac{1}{2}} \quad (3.6)$$

where  $\frac{K}{S}$  is called constant ratio and defined in equation 3.7.

$$\left(\frac{K}{S}\right) = \frac{(1 - R_{\infty})^2}{2R_{\infty}} \quad (3.7)$$

Hence, we can measure the reflectance of thickness layer and use these spectrums to simulate the reflectance of thick layer directly.

In our simulation system, each cosmetic layer has a specified thickness value, and we can use equation 3.8 and 3.9 to compute its reflectance and transmittance, respectively.

$$R_0 = \frac{\sinh bSX}{a \sinh bSX + b \cosh bSX} \tag{3.8}$$

$$T = \frac{b}{a \sinh bSX + b \cosh bSX} \tag{3.9}$$

In the equation 3.8,  $R_0$  means the reflectance which is not affected by background. We usually use  $R_0$  and T to compute the reflectance and the transmittance of each layer rather than using R and T.

### Multilayered model

Another part of the Kubelka-Munk theory is multi-layered model. By using multi-layered model, we can combine each layer and obtain the final reflectance. Figure 3.11 gives the path of the diffusion radiation.

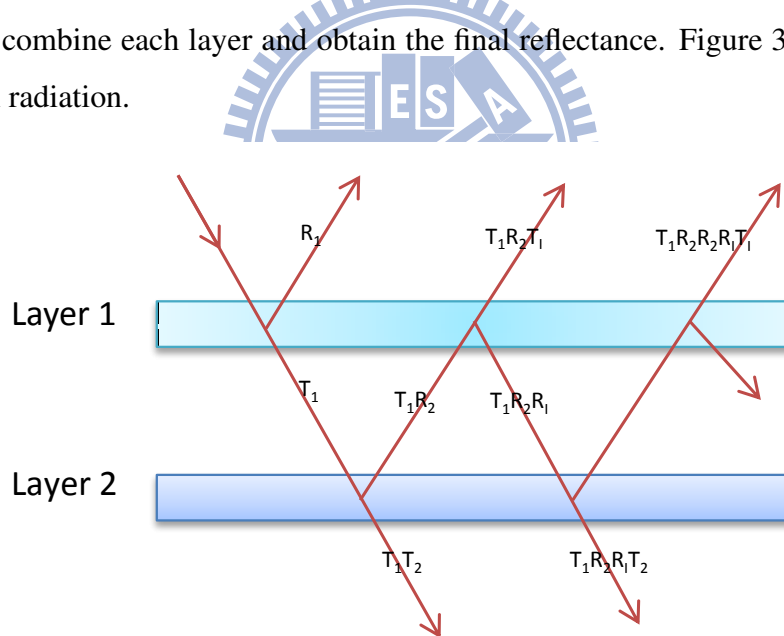


Figure 3.11: Reflectance and transmittance of two non-homogeneous layers.

The above figure can be translated to two geometrical series:

$$T_{1,2} = T_1T_2 (1 + R_1R_2 + R_1^2R_2^2 + \dots) = \frac{T_1T_2}{1 - R_1R_2} \tag{3.10}$$

$$R_{1,2} = R_1 + T_1 T_I T_2 (1 + R_I R_2 + R_I^2 R_2^2 + \dots) = R_1 + \frac{T_1 T_I T_2}{1 - R_I R_2} \quad (3.11)$$

and  $T_1 = T_I$ ,

$$R_{1,2} = R_1 + \frac{T_1 T_1 T_2}{1 - R_I R_2} \quad (3.12)$$

In many applications, we assume each layer is homogeneous material. Hence, we can focus on color change and the equation 3.10 and equation 3.11 can be rewritten as:

$$T_{1,2} = \frac{T_1 T_2}{1 - R_1 R_2} \quad (3.13)$$

$$R_{1,2} = R_1 + \frac{T_1 T_1 T_2}{1 - R_1 R_2} \quad (3.14)$$

In the multi-layered structure, we can use the above equation to solve more than two layered structure by recursive solving.

## 3.4 The integration of two techniques

In our system, we combine two different techniques to simulate the makeup effect on the human face. In this subsection, we describe rendering system in detail.

### 3.4.1 The skin pass

Before we explain what process in the skin pass, we need to figure out the interaction between human skin and makeup layers. Suppose we only apply the foundation to our face. In this situation, we have two layers structure, foundation and skin, and its schema is shown in Figure 3.12.



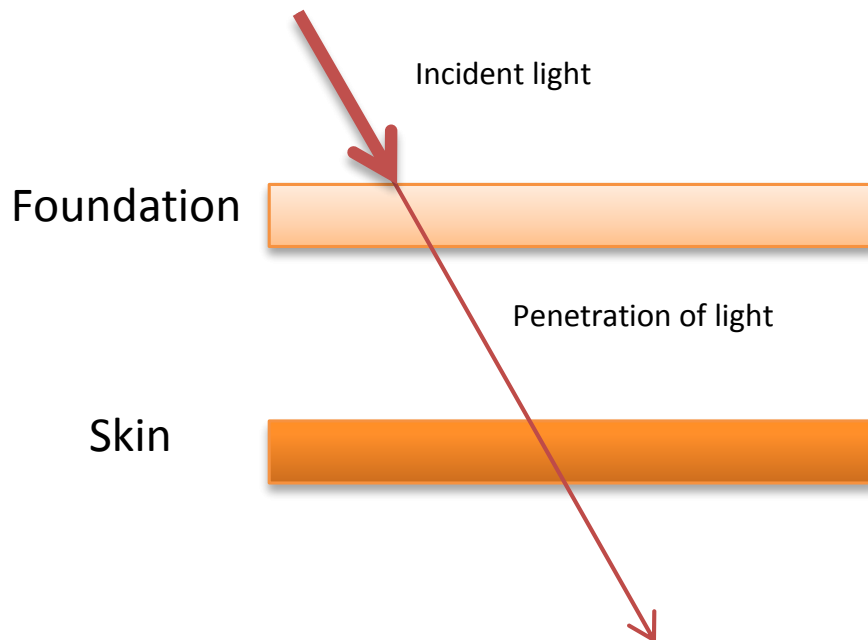


Figure 3.12: the pass of light between foundation and skin.

From the above figure, we can see the light through the foundation and reach the skin surface. Hence, we need to consider this situation rather than apply the intensity of light to skin directly. In our system, we compute the total transmittance before the light hits surface and apply this value to the color of skin. In order to facilitate the process, we use the cosmetic map to mark the area of each makeup layer. Therefore, we can fetch the corresponding texel to check whether this area is covered by cosmetic on surface. Figure 3.13 shows the flowchart about the skin pass and figure 3.14 shows the cosmetic map.

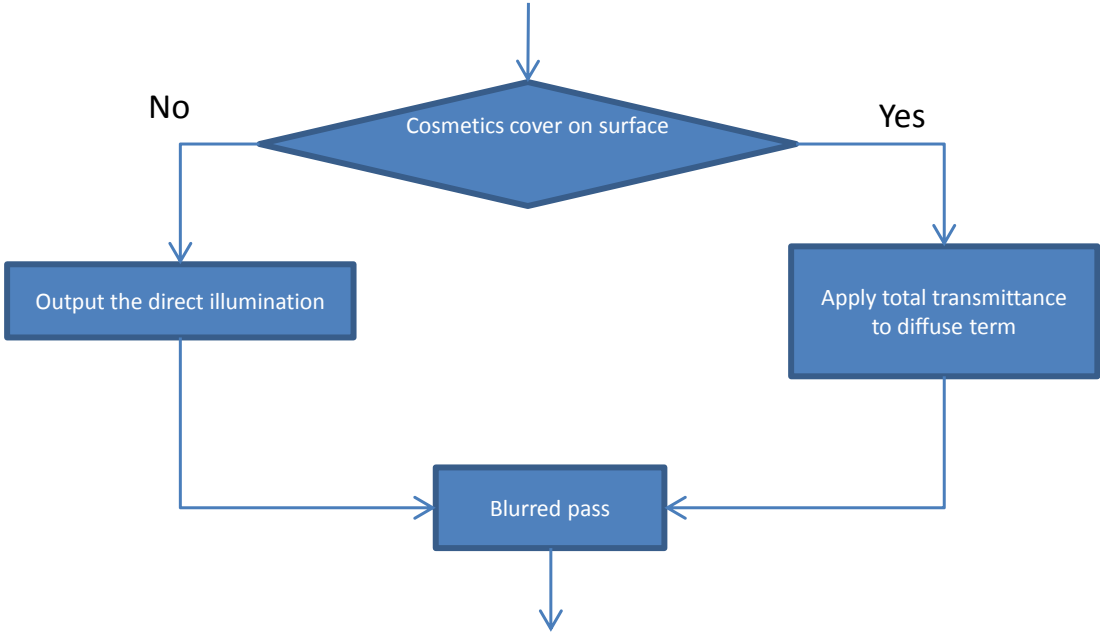


Figure 3.13: the flow chart about the skin pass.

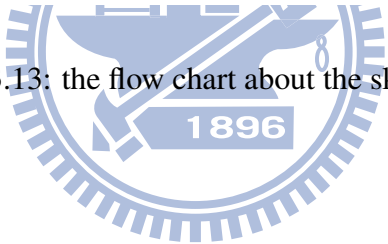




Figure 3.14: the cosmetic map. The red color is used to mark the foundation layer.

In the skin pass, we use two equations to compute the direct illumination map and list as follow:

if the skin covers with the cosmetic:

$$output_{color} = light_{color} * shadow * (diffuse + specular) * transmittance$$

else

$$output_{color} = light_{color} * shadow * (diffuse + specular)$$

The Kubelka-Munk theory compute the transmittance for each wavelength and we cannot use these value to compute the result. Hence, we first convert the spectra of the total transmittance to CIE RGB colors, and apply it to the diffuse color of human skin. Actually, we can use the approximate method to compute the transmittance which is introduced in chapter 4.2. Figure ?? shows the total transmittance after the light through the foundation and the value of total transmittance is converted from spectra. Figure 3.15 shows the irradiance map which does not apply screen-space technique and figure 3.17 shows the irradiance map of screen-space after

applies this transmittance.



Figure 3.15: the total transmittance after the light goes through the foundation.



Figure 3.16: the irradiance map and applying the transmittance. (without screen-space subsurface rendering)

After the skin pass, we can obtain the correct direct illumination map, and we blur this map many times to get the correct appearance of skin. Figure 3.17 shows the blurred result.



Figure 3.17: the irradiance map and applying the transmittance. (with SSSS)

### 3.4.2 The cosmetic pass

In the cosmetic pass, it computes the reflectance of each color and combines them to get the final diffuse result. Figure 3.18 shows the work flow about this pass.

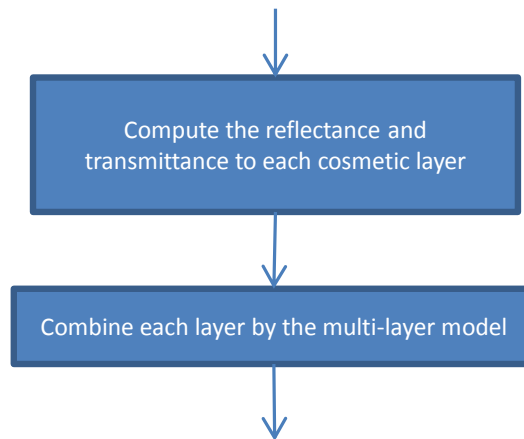
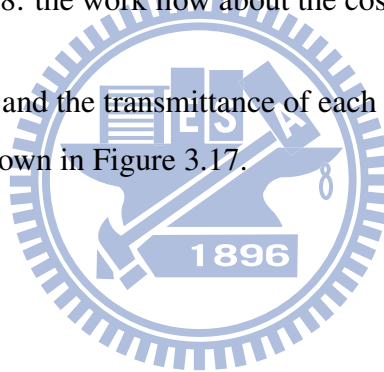


Figure 3.18: the work flow about the cosmetic pass.

We compute the reflectance and the transmittance of each layer by equation 3.13 and equation 3.14, and each result are shown in Figure 3.17.





(a) the rendering result

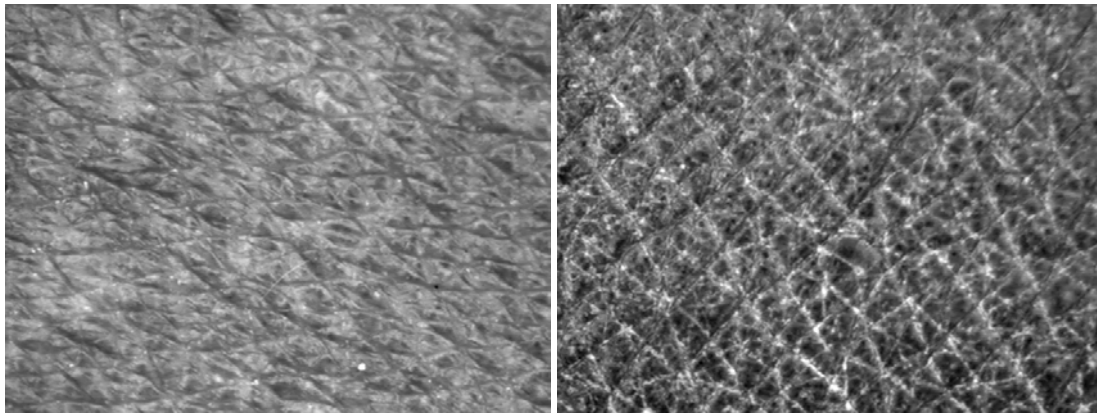
(b) the reflectance of foundation

Figure 3.19: rendering result.

### 3.4.3 The computation of specular term

#### Surface observation

Specular term is the most important term to describe the highlight effect. In our observations, if we apply the cosmetics to the skin, it gives the smooth appearance. Figure 3.20 shows the original skin surface and the surface which applied the foundation. We obtain this information by Skin Visiometer (SV 600).



(a) the original skin surface

(b) the skin surface with foundation

Figure 3.20: enlarging of skin surface.

We can observe that many cutin and fine line on the original surface. After we apply the foundation, the fine lines of the surface are filled with the foundation. Hence, we can obtain the smooth appearance. We can observe that the makeup changes the microeffect of skin and let surface more smoothness.

### Computing the specular term

In our system, we use the Kubelka-Munk theory to compute reflectance, transmittance and compose each layer together. But, the Kubelka-Munk theory does not consider specular term. Dorsey and Hanrahan [17] propose a simple way to solve this problem. For each layer, they use the Kubelka-Munk theory to compute the reflectance and transmittance and add specular effect by a simple model. Therefore, we use a similar way to simulate the specular of each layer. Figure 3.21 shows the result of specular effect and we render this result with foundation. The left result is only compute the specular term on skin; the medium result is compute the specular term on foundation; the right result compute the specular term for each layer.





Figure 3.21: the rendering result of specular effect. Left: only applying specular effect on skin surface. Medium: only applying specular effect on foundation. Right: computing specular on each layer.

For each layer, we use the BRDF specular model introduced by Kelemen et al. [18] to compute the specular term, and this model needs some parameters to compute the equation 3.15, such as the normalized of light direction, the normalized of view direction and surface roughness.

$$f_{r,spec}(\vec{L}, \vec{V}) = P_{\vec{H}}(\vec{H}) * \frac{F(\vec{H} \cdot \vec{L})}{2(1 + \vec{L} \cdot \vec{V})} \quad (3.15)$$

where  $F(\vec{H} \cdot \vec{L})$  is the Fresnel term and  $P_{\vec{H}}(\vec{H})$  is Beckmann distribution function. For the Fresnel term, we usually use Schlick's approximation to simulate the non-metal materials. The Beckmann distribution function is defined as:

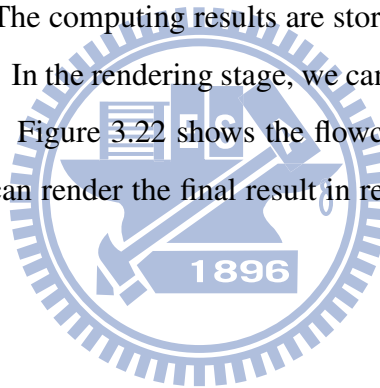
$$P_{\vec{H},Beckmann}(\vec{H}) = \frac{1}{m^2 \cos^4 \alpha} * e^{-\left(\frac{\tan^2 \alpha}{m^2}\right)}$$

where  $m$  is the roughness and this parameter affects the smoothness of microfacet, e.g. the bigger roughness gives broader specular area and smaller value of highlight; the smaller value gives small area and bigger value of highlight. In the specular computation, because we do not measure the roughness and index of refraction accurately, we simply adjust the roughness to

control the highlight and set a constant value as index of refraction. We believe that if we can obtain these parameters of each layer, it can render more realistic.

### 3.5 Implementation

In our simulation system, we do not need to compute the reflectance, the transmittance and the combination of each layer in every frames. In the simulation, both the scattering coefficient  $S$  and the absorption coefficient  $K$  are fixed. Hence, both the reflectance and the transmittance are changed when the thickness is modified. We add an extra pass to compute the reflectance and the transmittance. So, when the thickness is modified, we recomputed the reflectance and the transmittance by this pass. The computing results are stored in the reflectance map and the transmittance map, respectively. In the rendering stage, we can fetch the color from these maps, and apply to each pass directly. Figure 3.22 shows the flowchart with our simulation system. By using this architecture, we can render the final result in real time and change the thickness in interactive rate.



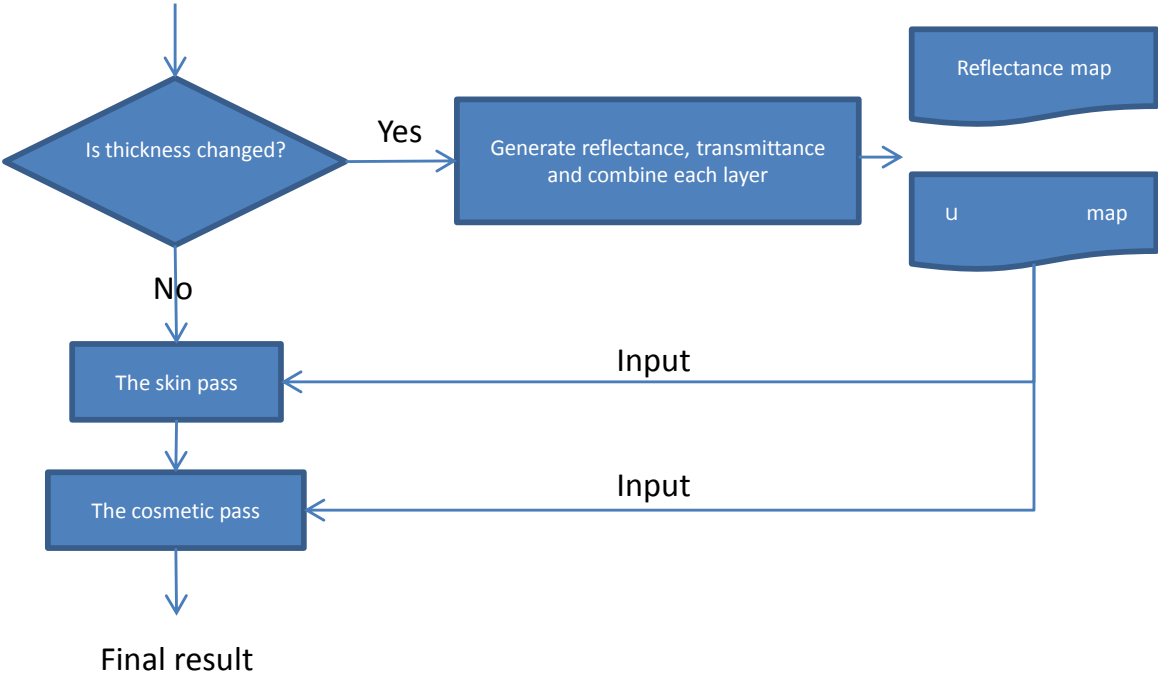
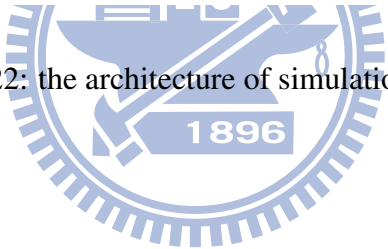


Figure 3.22: the architecture of simulation system.



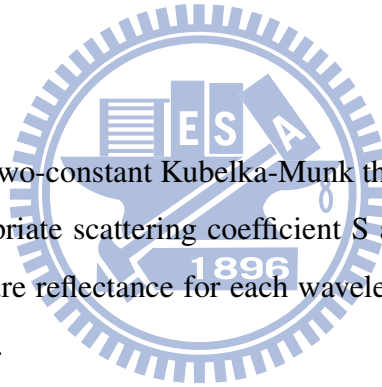
## CHAPTER 4

---

# Measurement

---

Our rendering system uses the two-constant Kubelka-Munk theory to simulate makeup appearance. In order to obtain appropriate scattering coefficient  $S$  and absorption coefficient  $K$ , we use spectroradiometer to measure reflectance for each wavelength and other approximation to obtain approximate coefficients.



### 4.1 Measuring data by spectroradiometer

The two-constant Kubelka-Munk theory gives Equation 4.1 and 4.2 that shows how to evaluate scattering coefficient  $S$  and absorption coefficient  $K$ , respectively. Both scattering coefficient  $S$  and absorption coefficient  $K$  are wavelength-dependent.

$$S = \frac{1}{bD} \left[ \coth^{-1} \frac{a - R}{b} - \coth^{-1} \frac{a - R_g}{b} \right] \quad (4.1)$$

$$K = S(a - 1) \quad (4.2)$$

where  $a = \frac{1}{2} \left[ \frac{1}{R_\infty} + R_\infty \right]$  and  $b = (a^2 - 1)^{\frac{1}{2}}$

In the above equation,  $R_i$  means the reflectance of the thick layer,  $R$  means the reflectance of two layers (the thin layer painted on background), and  $R_g$  means the reflectance of the background. Solving both scattering coefficient  $S$  and absorption coefficient  $K$  needs corresponding  $R_i$ ,  $R$  and  $R_g$  values to compute coefficient for each wavelength.

Our measurement uses spectroradiometer (MINOLTA CS-2000) to measure liquid foundations, cream blushes, cream eye-shadows and lipsticks. We use D55 light source and measure wavelength between 380 nm and 780 nm with the interval of 5nm. Figure 4.1 shows our device and environment.

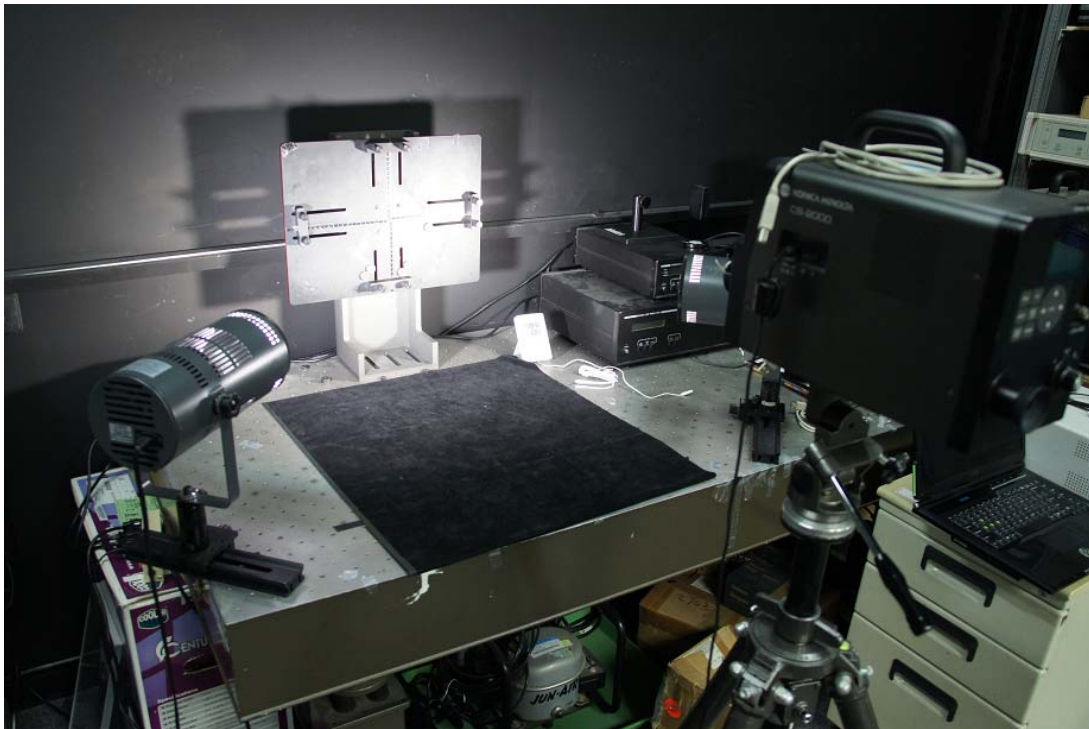


Figure 4.1: Our capture device and environment.

Our spectroradiometer device gives the radiant energy which is the convolution radiant energy of light with reflectance of material. Radiant energy is defined by equation 4.3.

$$E_m(\lambda) = E_L(\lambda) * R(\lambda) \quad (4.3)$$

$$R(\lambda) = \frac{E_m(\lambda)}{E_L(\lambda)}$$

$E_m(\lambda)$  is radiant energy which means the amount of the energy of light hit the surface and reflected to observer.  $R(\lambda)$  is the reflectance of material and  $E_L(\lambda)$  is radiant energy of light source. Figure 4.2 shows the radiant energy of liquid foundation. We graph two useful light source's radiant energy D55 and E in Figure 4.3 and Figure 4.4, respectively.

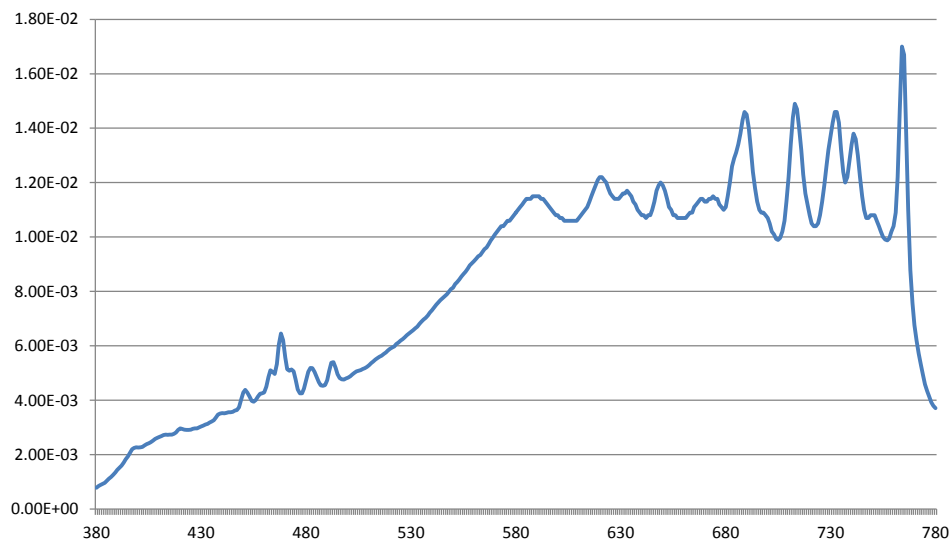


Figure 4.2: Radiant energy of liquid foundation.

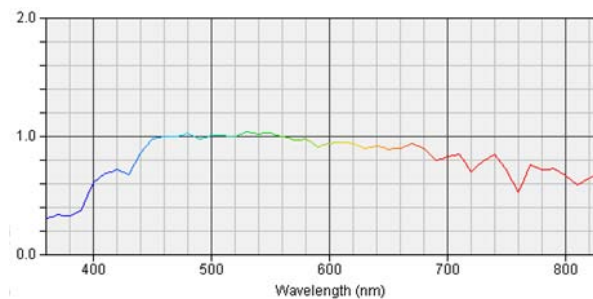


Figure 4.3: Radiant energy of CIE standard illuminant D55.

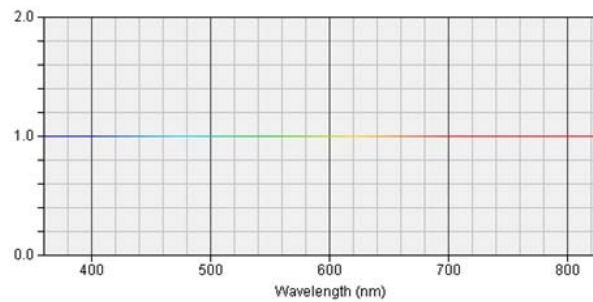
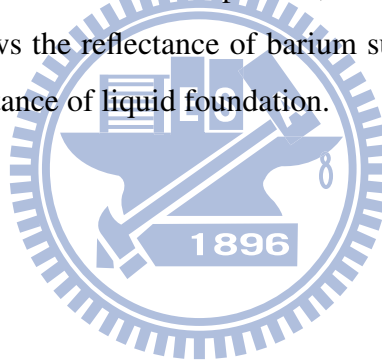
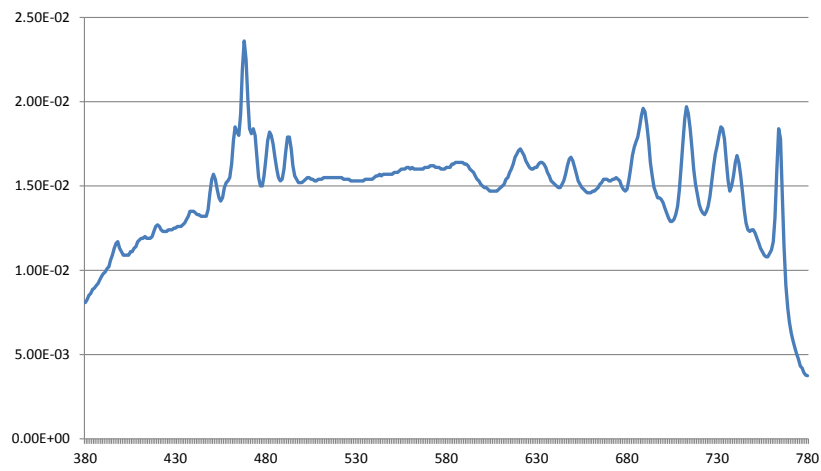


Figure 4.4: Radiant energy of CIE standard illuminant E.

We can use equation 4.3 to convert energy to reflectance. We use white material to measure radiant energy of light source  $E_L$  by using purity of 99% barium sulfate, and use equation 4.3 to compute the reflectance of material. After this process, we can obtain the reflectance of each material  $R(\lambda)$ . Figure 4.1 shows the reflectance of barium sulfate and barium sulfate sample and Figure 4.6 shows the reflectance of liquid foundation.





(a) Radiant energy of barium sulfate



(b) The sample of 99% barium sulfate

Figure 4.5: the reflectance of barium sulfate and barium sulfate sample



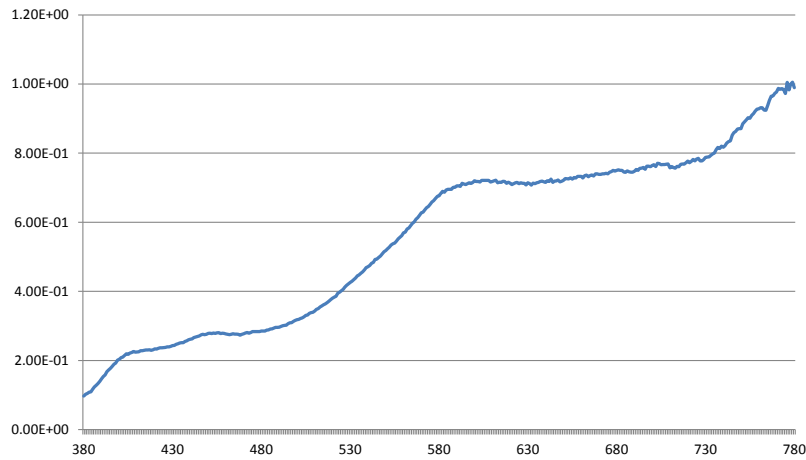


Figure 4.6: Reflectance of liquid foundation.

In our experiment, we paint sample with enough thickness to make it opaque, and we measure its reflectance to represent  $R_i$ . Then, we paint the sample to black background with certain thickness to measure  $R$ . Finally, we measure the reflectance of background to determine  $R_g$ . Figure 4.7 shows liquid foundation sample. We also make a simple container to load samples and figure 4.8 shows the container. By using this container, we can easily make the flat sample and easily measure the thickness of sample. Figure 4.9 shows the reflectance of  $R_i, R$  and  $R_g$ .



Figure 4.7: Liquid foundation sample. Left: background. Mid: thickness layer. Right: thin layer.

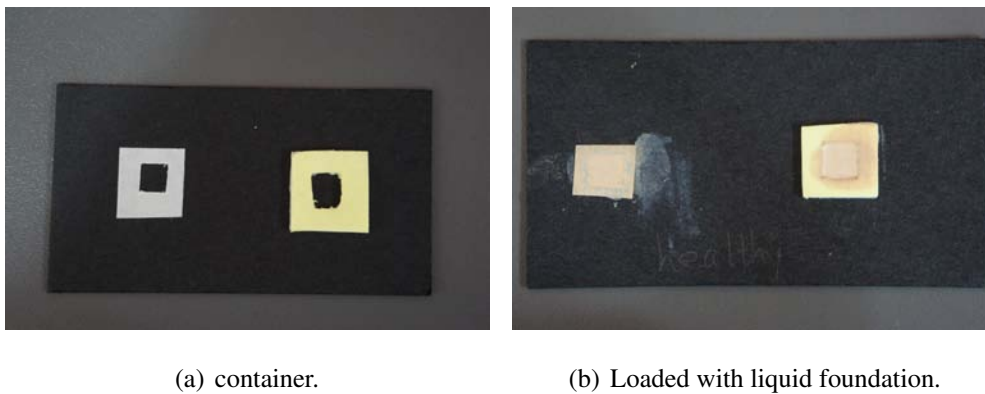
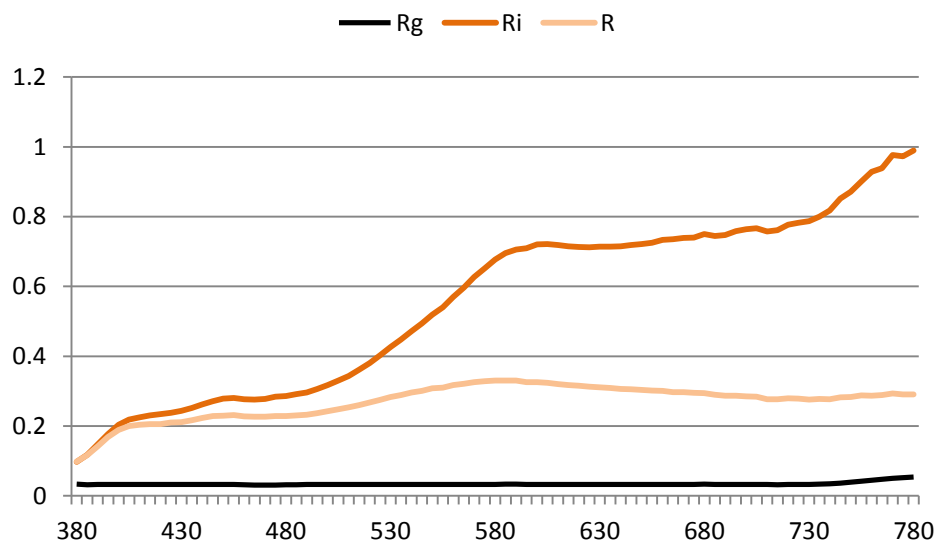


Figure 4.8: The sample of our simple container.

Figure 4.9: The reflectance of  $R_i$ ,  $R$  and  $R_g$ .

We apply  $R_i$ ,  $R$  and  $R_g$  to the equation 4.1 and equation 4.2 for obtaining the scattering coefficient  $S$  and the absorption coefficient  $K$ , respectively. Figure 4.10 shows  $S$  and  $K$  for each wavelength. Each wavelength of coefficient  $S$  and coefficient  $K$  can be used in equation 4.4 to simulate the original reflectance spectral of thin layer  $R_0$ . Furthermore, we can use different thickness to describe the reflectance of material. Figure 4.11 shows the original reflectance and

the fitting result.

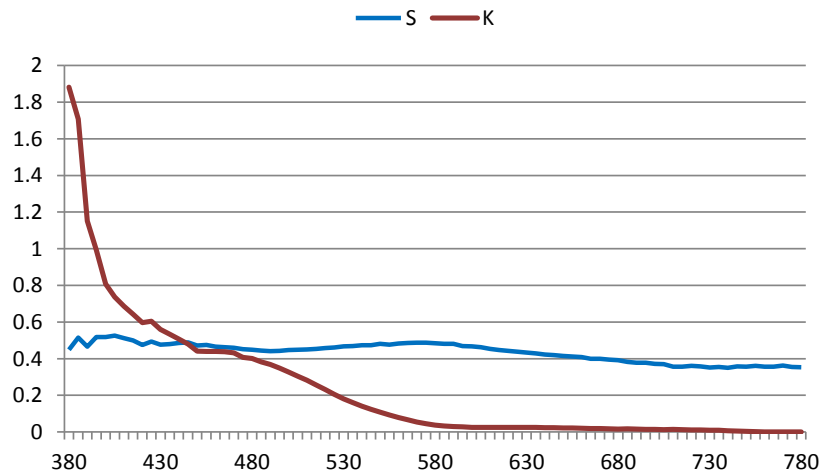


Figure 4.10: The coefficient S and K for each wavelength.

$$R_0 = \frac{\sinh bSX}{a \sinh bSX + b \cosh bSX} \tag{4.4}$$

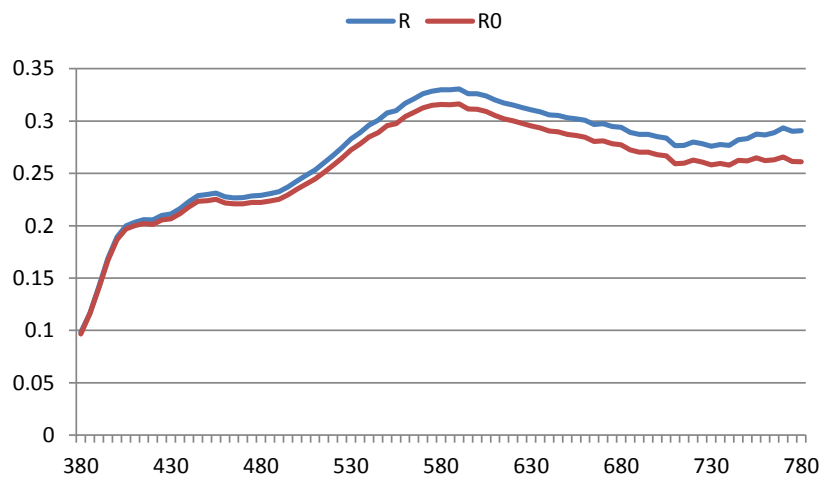


Figure 4.11: The original reflectance and the fitting result.

The fitting curve and measured curve have difference between 560 nm and 780 nm. The

fitting curve represents the reflectance of thin layer, and the measuring curve represents the reflectance of two layer, thin layer and background. These differences are not noticeable, if we convert these curve to RGB color space. Figure 4.12 shows the RGB color result of fitting curve and measurement curve. In figure 4.13, we apply D55 to RGB. (Appendix A provides the method for converting spectrum to CIE RGB color space.)



Figure 4.12: CIERGB color of fitting curve and measured curve. Left: Original data (R0) and the color is (0.62, 0.58, 0.51). Right: Fitting result and the color is (0.60, 0.57, 0.5).

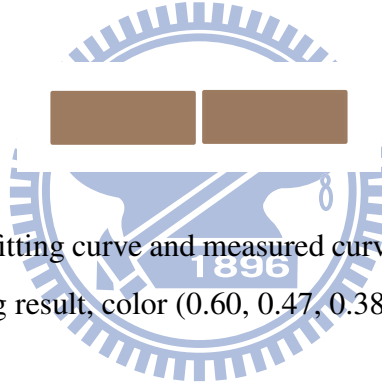


Figure 4.13: CIERGB color of fitting curve and measured curve. Left: Original data (R0), color (0.62, 0.48, 0.38). Right: Fitting result, color (0.60, 0.47, 0.38).

## 4.2 Approximation way to obtain Kubelka-Munk coefficients

Cassidy et al. [19] provide a simple inversion of the KM equation shown in equation 4.5 and equation 4.6.

$$S = \frac{1}{bX} \cosh^{-1} \left( \frac{b^2 - (a - R_W)(a - 1)}{b(1 - R_W)} \right) \quad (4.5)$$

$$K = S(a - 1) \quad (4.6)$$

where  $a = \frac{1}{2} \left( R_W + \frac{R_B - R_W + 1}{R_b} \right)$ ,  $b = (a^2 - 1)^{\frac{1}{2}}$ , and  $0 < R_B < R_W < 1$  for all channel. In above equation,  $R_B$  means the color of thin layer painted on black background and  $R_W$  means

the color of thin layer painted on white background. By using equation 4.5 and 4.6, we can select two colors  $R_B$  and  $R_W$  and then we can obtain scattering coefficient  $S$  and absorption coefficient  $K$ , respectively. Figure 4.14 shows a diagram about this process.

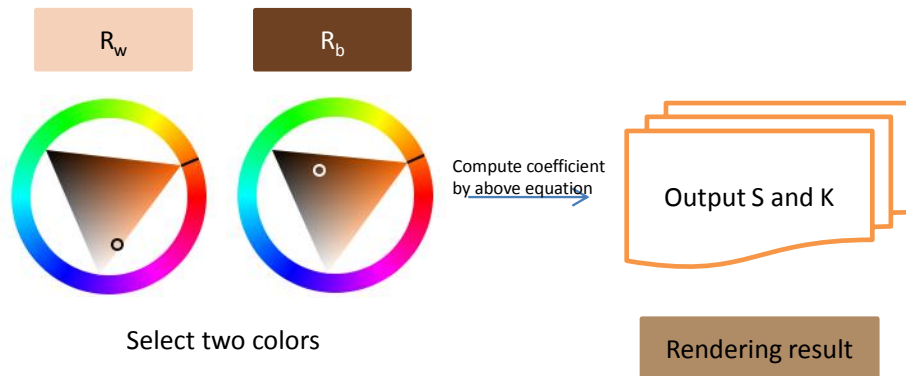


Figure 4.14: Selecting two colors and obtaining  $S$  and  $K$ .

In above case,  $S$  is (0.78, 0.39, 0.18) and  $K$  is (0.02, 0.10, 0.16).

In order to pick  $R_B$  and  $R_W$  from real material, we build a simple environment to obtain these colors. We use polarized light source and polarized lens to obtain diffuse color. Figure 12 shows our device and figure 13 shows a liquid foundation sample.

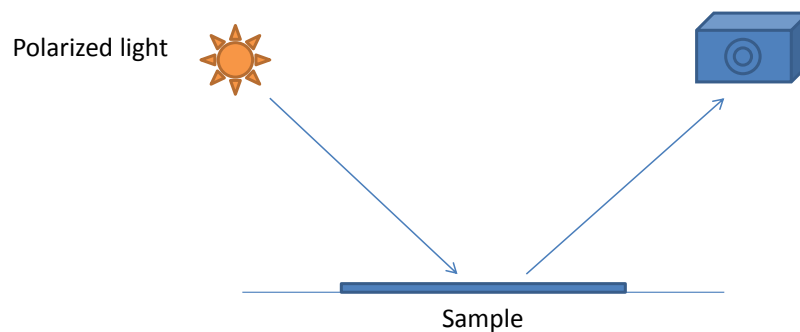


Figure 4.15: capture coefficient  $S$  and  $K$  by camera.



Figure 4.16: liquid foundation sample.

After capturing, we can pick color directly and use equation 4.5 and equation 4.6 to compute coefficient  $S$  and coefficient  $K$ . Because the light is polarized, we need multiply color by 2 to obtain approximate diffuse color. Figure 4.17 shows the diffuse color captured by this simple method. After estimating coefficient  $S$  and coefficient  $K$ , we can use these values to describe reflectance and transmittance in our simulation system.

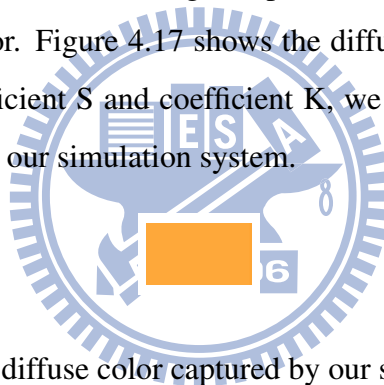


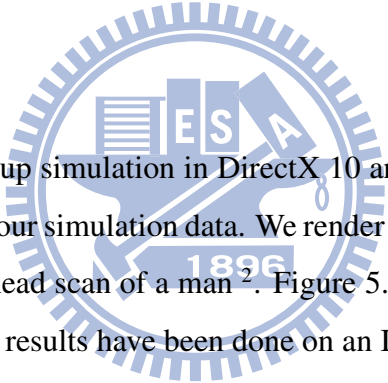
Figure 4.17: diffuse color captured by our simple device.

## CHAPTER 5

---

# Result

---



We have implemented the makeup simulation in DirectX 10 and HLSL, and in this section we present our rendering result and our simulation data. We render the makeup effect on two human head, Digital Coco <sup>1</sup> and a 3D head scan of a man <sup>2</sup>. Figure 5.1 shows the original appearance of skin rendering. All rendering results have been done on an Intel Core i5 750 2.67GHz CPU, 4GB RAM, and an NVIDIA GTX 260 graphics card. The resolution of each image is 1280 x 720. The frame rate of rendering is 170-175fps with makeup effect.

---

<sup>1</sup>©Next Media CO., LTD.

<sup>2</sup>INFINITE-REALITIES ®- <http://www.ir-ltd.net/infinite-3d-head-scan-released>



Figure 5.1: original appearance of skin rendering. (Left: Digital Coco. Right: Digital Orange.)

We divide this chapter into two parts - the measuring data of cosmetic and the makeup rendering. First, we show our measuring data and fitting data of each cosmetic, and then we show each rendering result individually. Then, we choose some cosmetics to compose different makeup result. We also provide some cosmetic map to show different makeup Patten.

## 5.1 The measuring data of cosmetic

We collect several cosmetics and measured their parameters. Our subjects include liquid foundations, cream blushes and lipsticks.



## Liquid foundation

We first show the liquid foundation. We measure five subjects. Table 5.1 shows the brand of each liquid foundation.

Table 5.1: The brand of liquid foundation.

	Sample F1	Sample F2	Sample F3	Sample F4	Sample F5
Brand	Maybelline (No 22. Natural Beige)	Orbis (N03)	Integrate (00)	BOURJOIS Healthy (#51)	BOURJOIS Healthy (#52)

The following figures show the measuring data of each sample, the fitting data of each sample, the comparing of  $R$  and  $R_0$  of each sample and the rendering result with different thicknesses as 0.1, 0.5 and 1.0. We can observe the detail of skin if the thickness is smaller.

There are some measuring mistakes which causes the fitting data error, such as Sample F2. In general, the reflectance spectrum increases when the layer becomes thicker, however the reflectance between 380-500 nm does not follow this rule. There are some reasons causes this effect. For example, the sample is not flat or the thickness is not thin enough. In our experience, the problem is usually caused by the first reason.

In our analysis, we found a phenomenon. If the subject is more opaque, the reflectance of  $R$  and  $R_0$  are similar. Hence, the reflectance of  $R$  and  $R_0$  of each lipstick are similar.

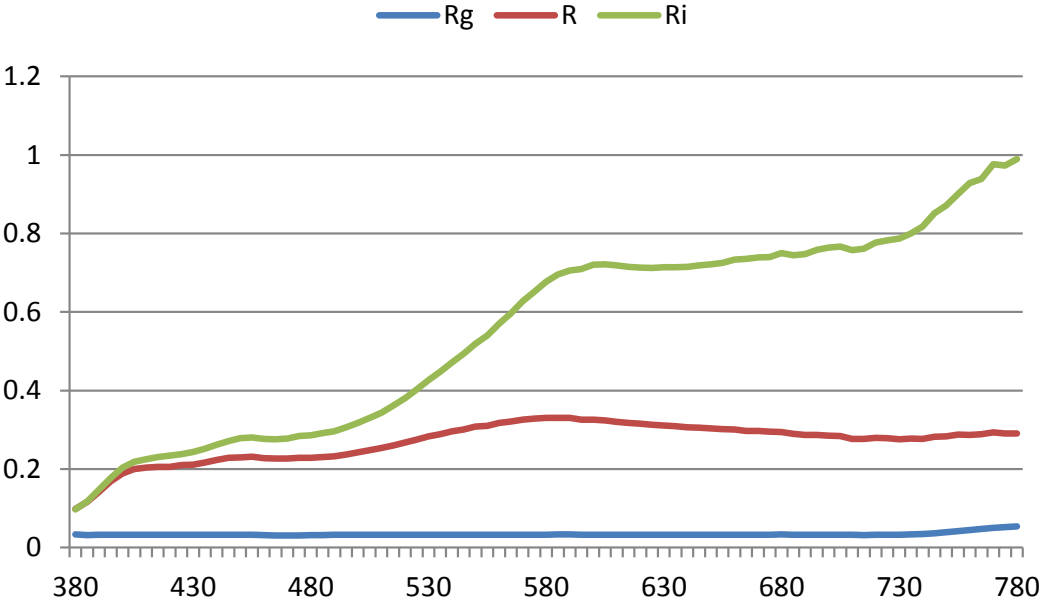


Figure 5.2: the measuring data of sample F1.

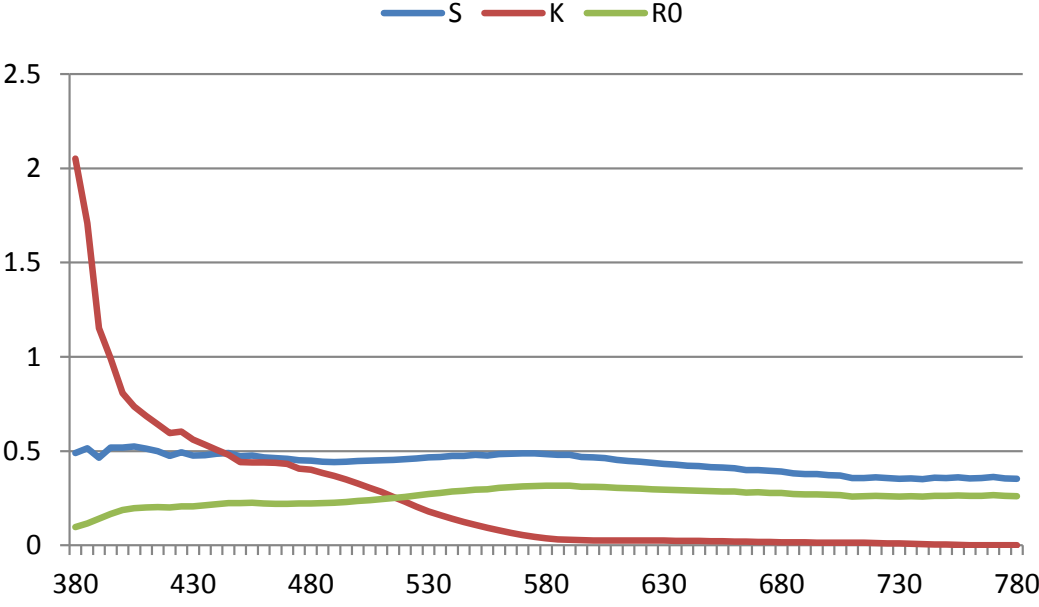


Figure 5.3: the fitting data of sample F1.

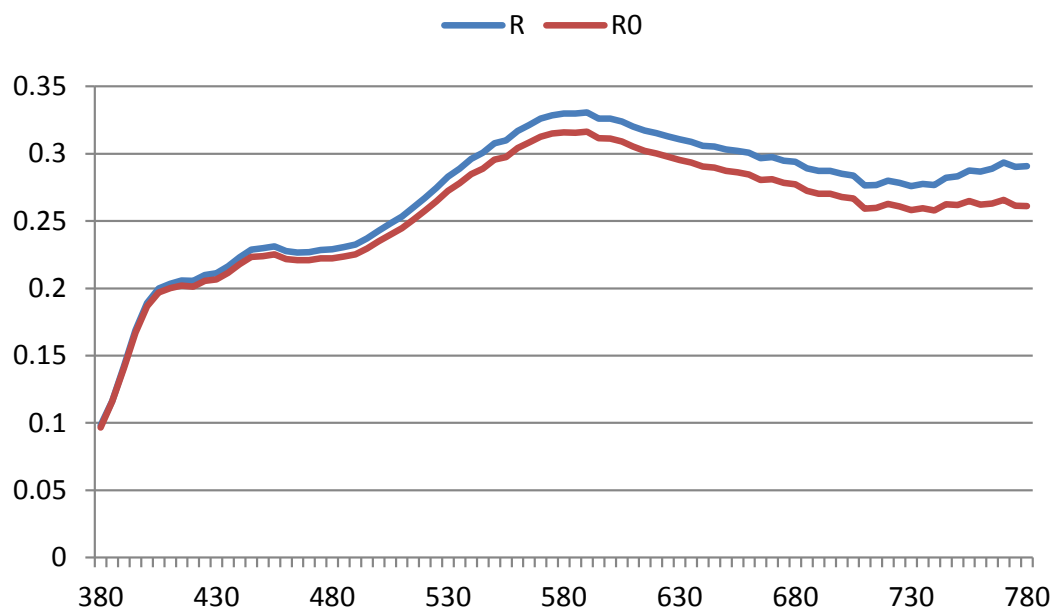


Figure 5.4: the comparison between R and R0 of sample F1.

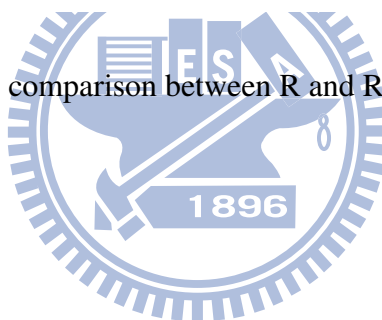




Figure 5.5: the rendering result of sample F1. Left: the thickness is 0.1. Mid: the thickness is 0.5. Right: the thickness is 1.0.(Each model uses different cosmetic map.)

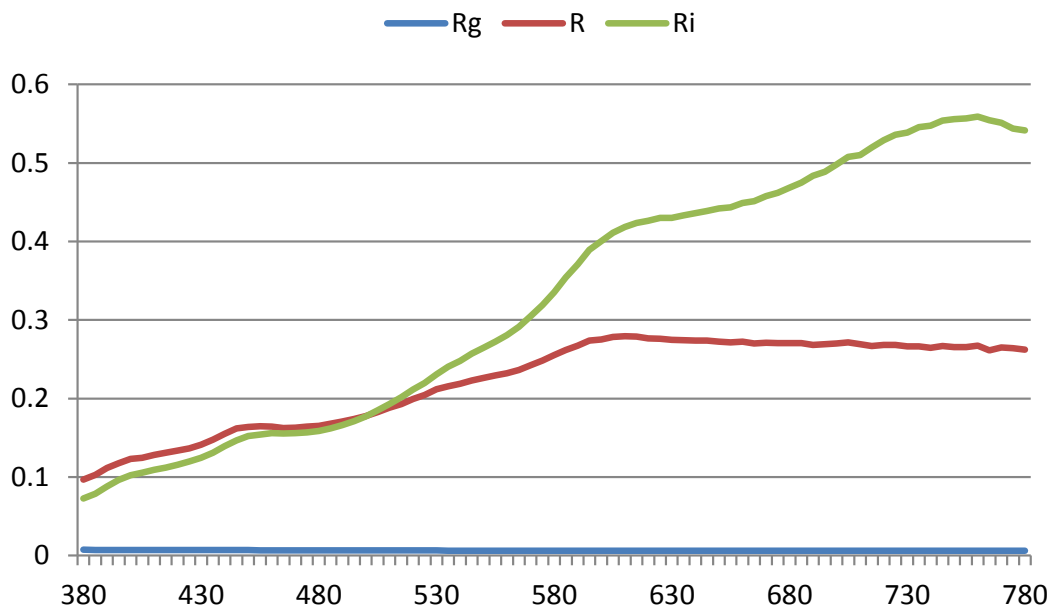


Figure 5.6: the measuring data of sample F2.

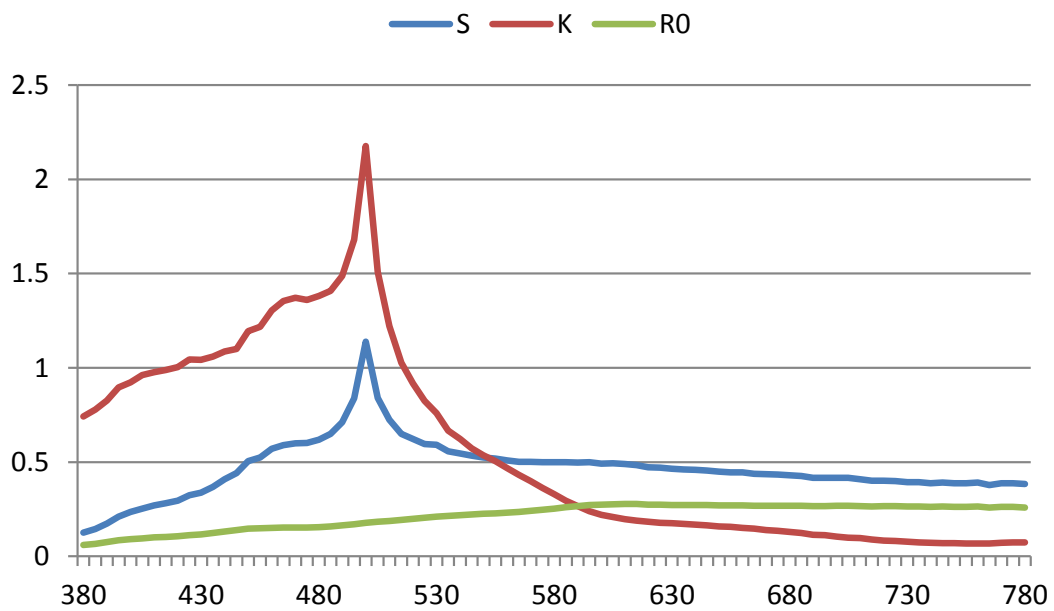


Figure 5.7: the fitting data of sample F2.

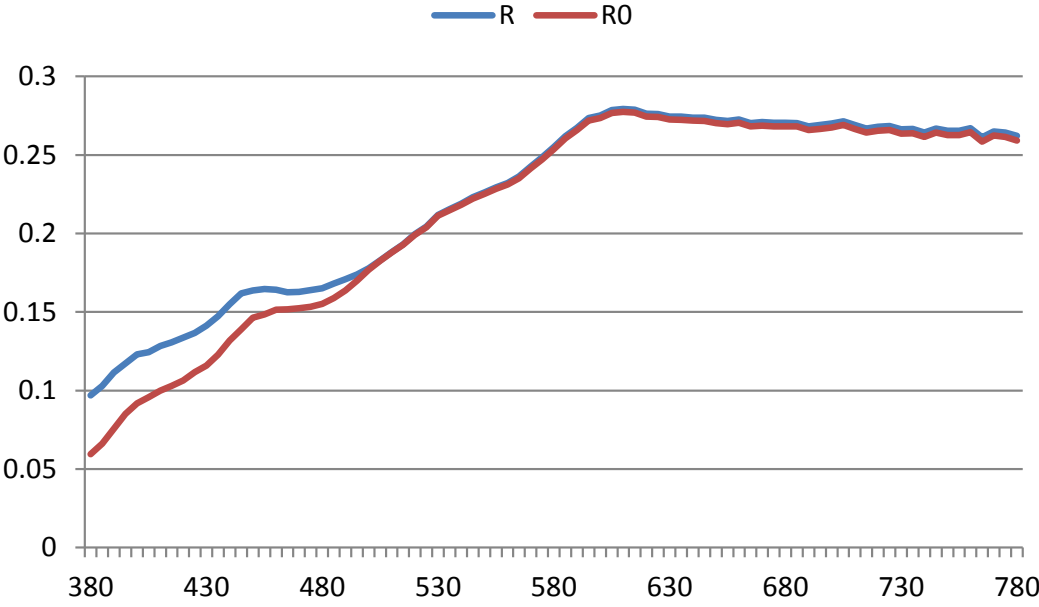


Figure 5.8: the comparison between R and R0 of sample F2.

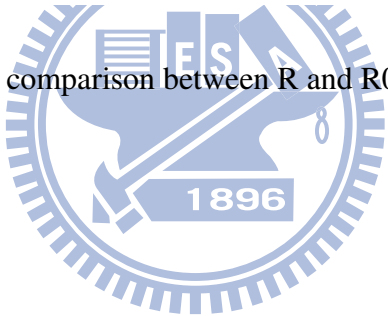




Figure 5.9: the rendering result of sample F2. Left: the thickness is 0.1. Mid: the thickness is 0.5. Right: the thickness is 1.0.(Each model uses different cosmetic map.)

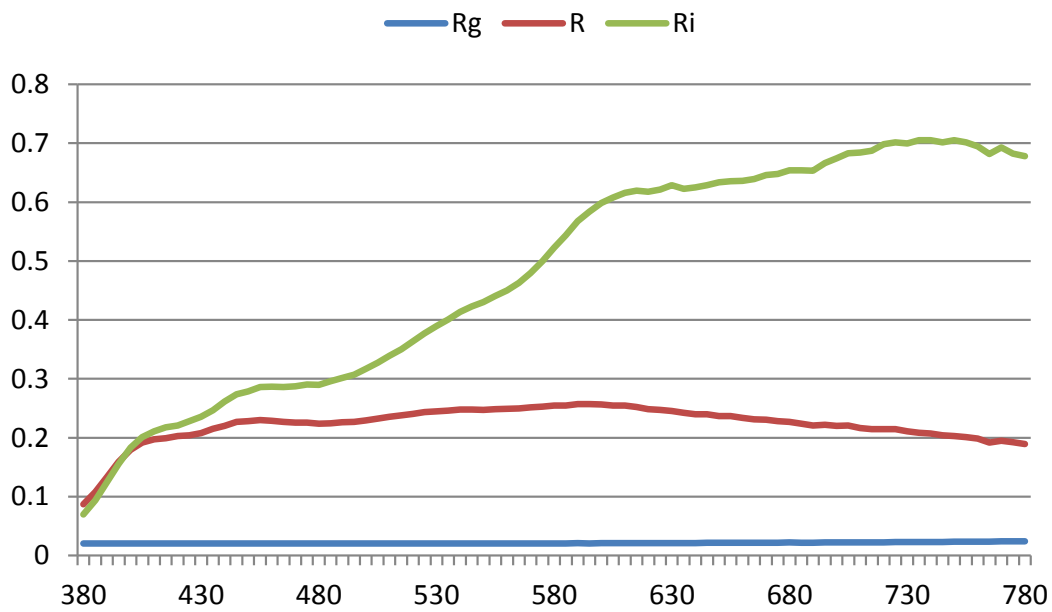


Figure 5.10: the measuring data of sample F3.

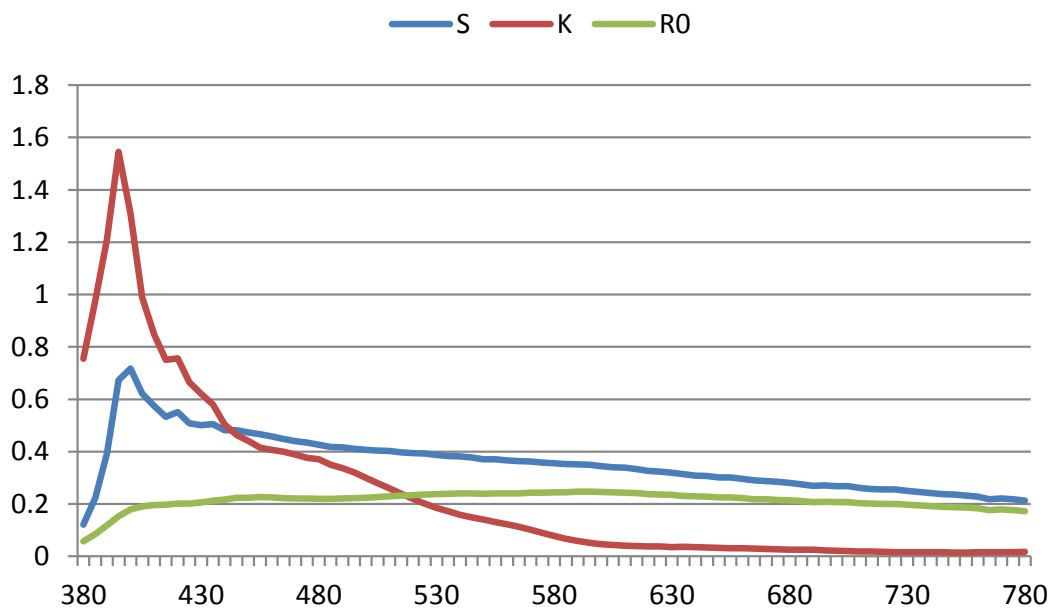


Figure 5.11: the fitting data of sample F3.



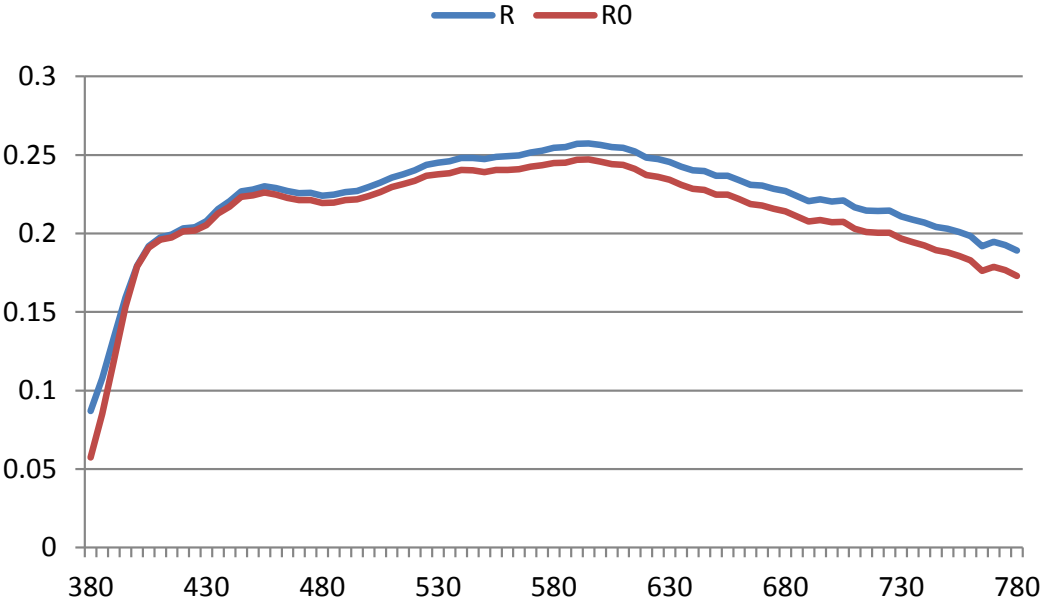


Figure 5.12: the comparison between R and R0 of sample F3.

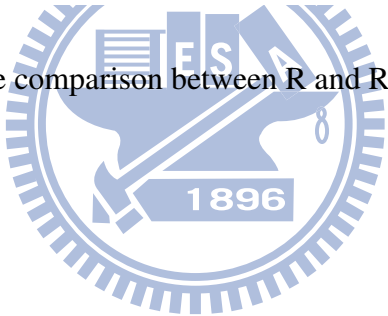




Figure 5.13: the rendering result of sample F3. Left: the thickness is 0.1. Mid: the thickness is 0.5. Right: the thickness is 1.0.(Each model uses different cosmetic map.)

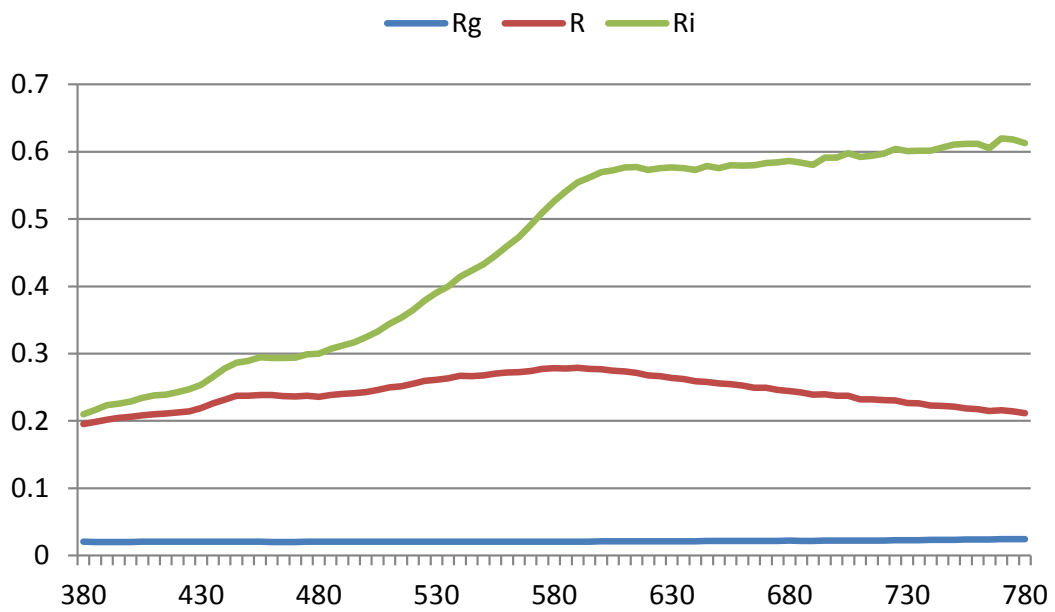


Figure 5.14: the measuring data of sample F4.

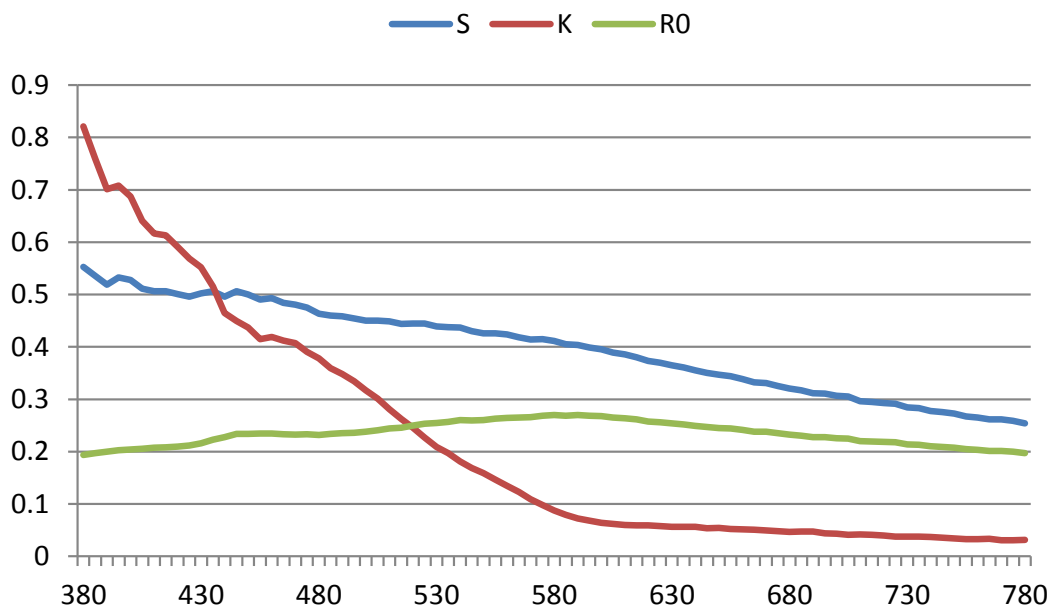


Figure 5.15: the fitting data of sample F4.

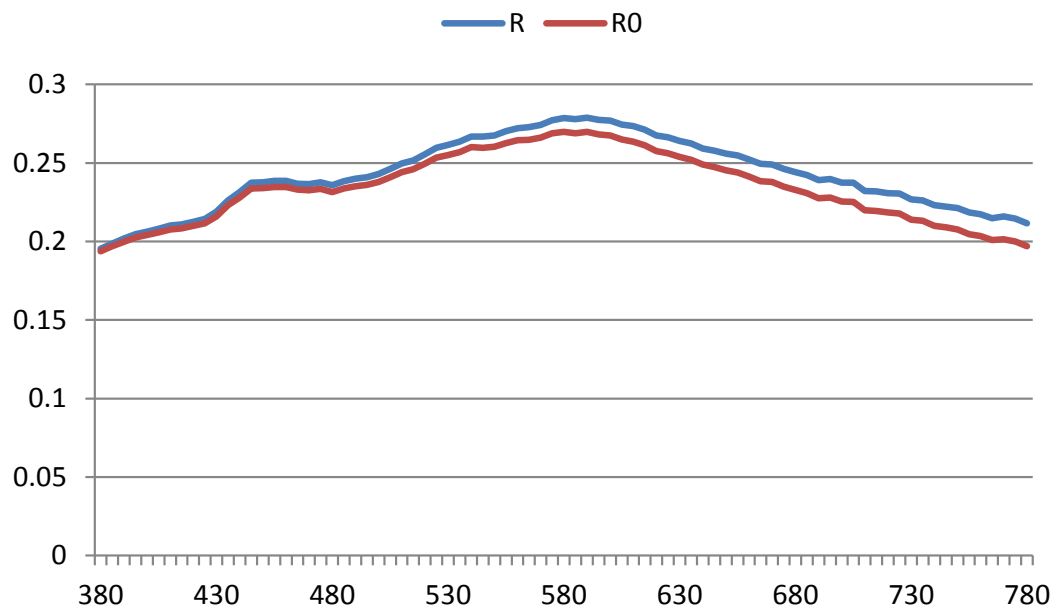


Figure 5.16: the comparison between R and R0 of sample F4.

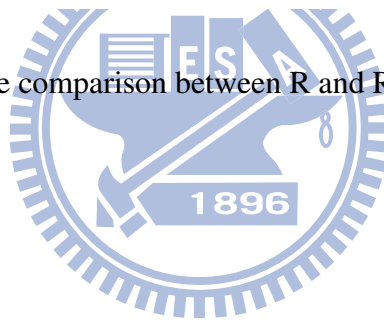




Figure 5.17: the rendering result of sample F4. Left: the thickness is 0.1. Mid: the thickness is 0.5. Right: the thickness is 1.0.(Each model uses different cosmetic map.)

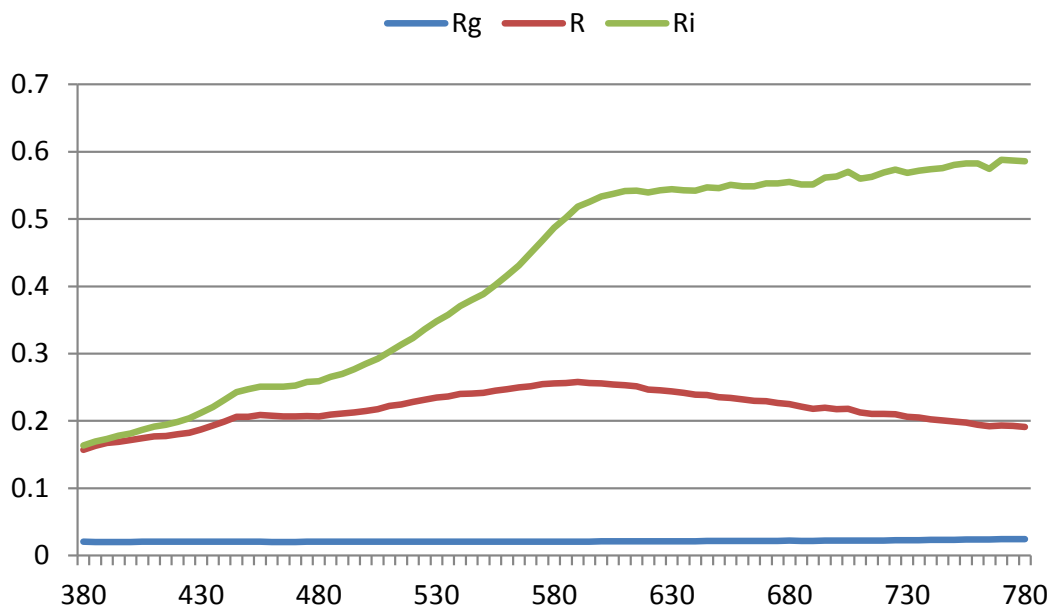


Figure 5.18: the measuring data of sample F5.

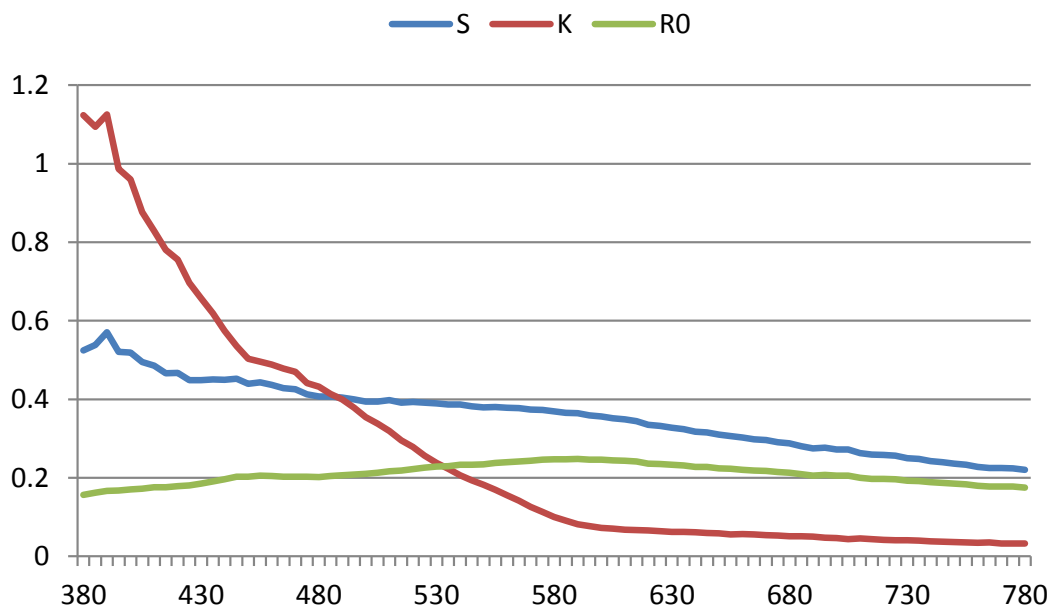


Figure 5.19: the fitting data of sample F5.

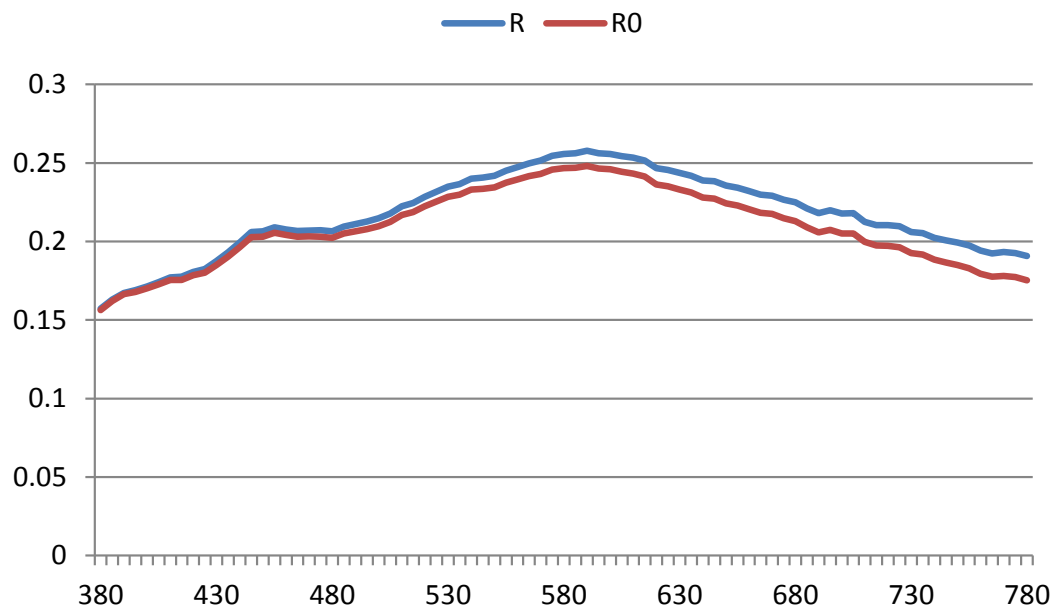


Figure 5.20: the comparison between R and R0 of sample F5.

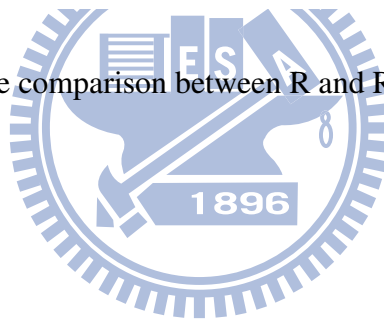




Figure 5.21: the rendering result of sample F5. Left: the thickness is 0.1. Mid: the thickness is 0.5. Right: the thickness is 1.0.(Each model uses different cosmetic map.)

### **Cream blush**

We measured two cream blushes and table 5.2 shows the brand of each cream blush. Because two blushes are too similar in the same thickness 1.0, we demonstrate two thicknesses of each blush, 1.0 and 2.0.



Table 5.2: The brand of each cream blush.

	Sample B1	Sample B2
Brand	MISSHA (No. 1 – Left)	MISSHA (No. 2 – Right)

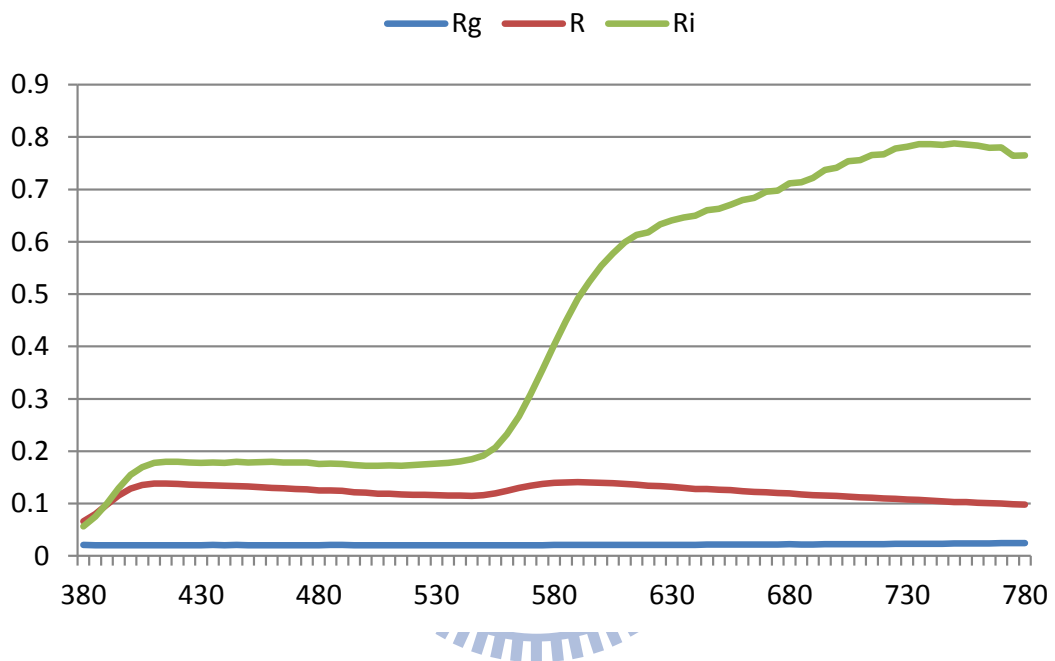


Figure 5.22: the measuring data of sample B1.

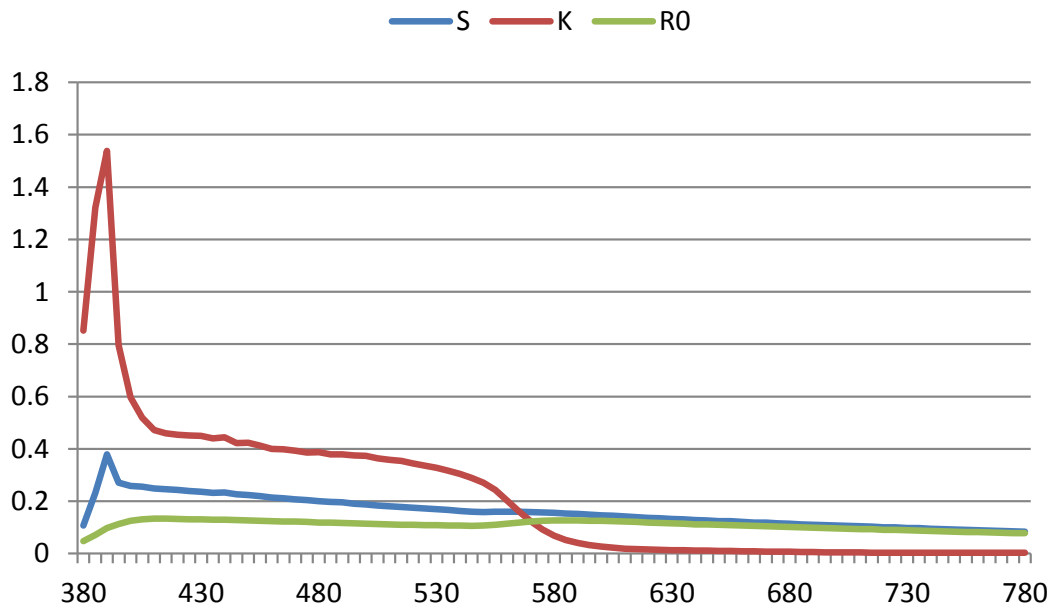


Figure 5.23: the fitting data of sample B1.

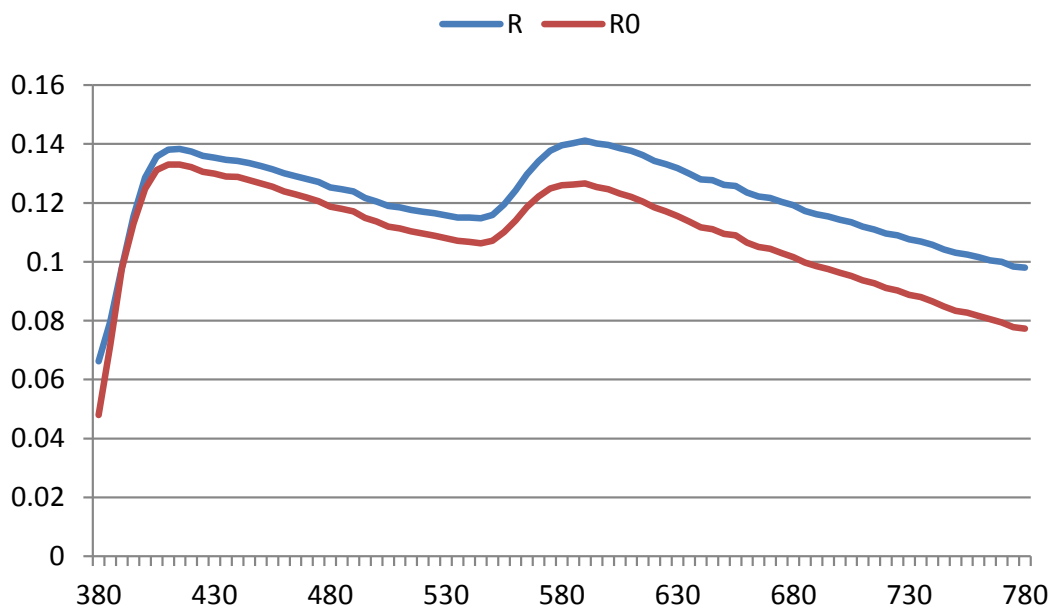


Figure 5.24: the comparison between R and R0 of sample B1.



Figure 5.25: the rendering result of sample B1. Left: the thickness is 1.0. Right: the thickness is 2.0. (Each model uses different cosmetic map.)

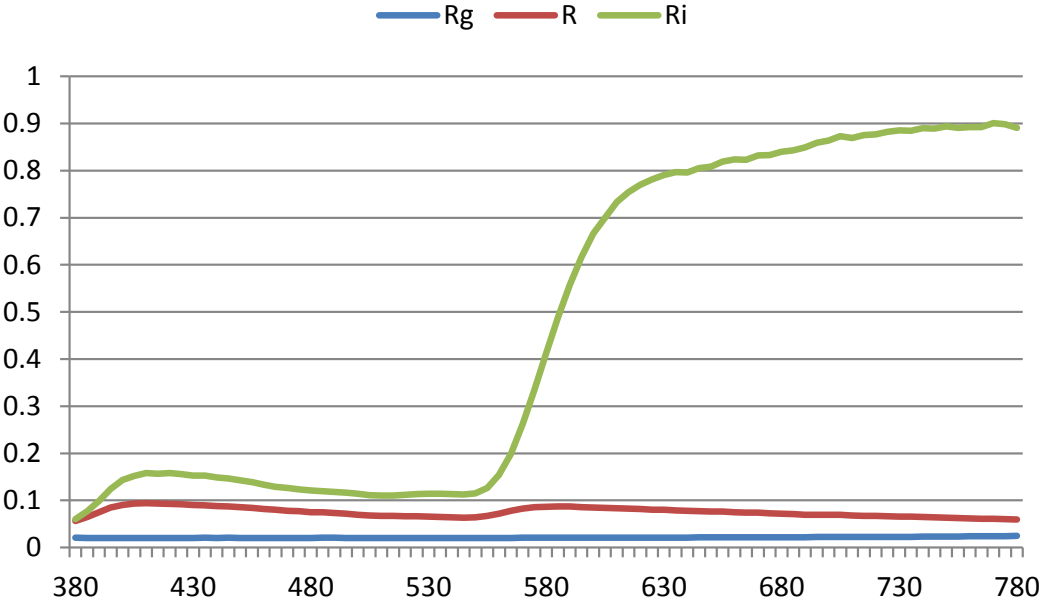


Figure 5.26: the measuring data of sample B2.

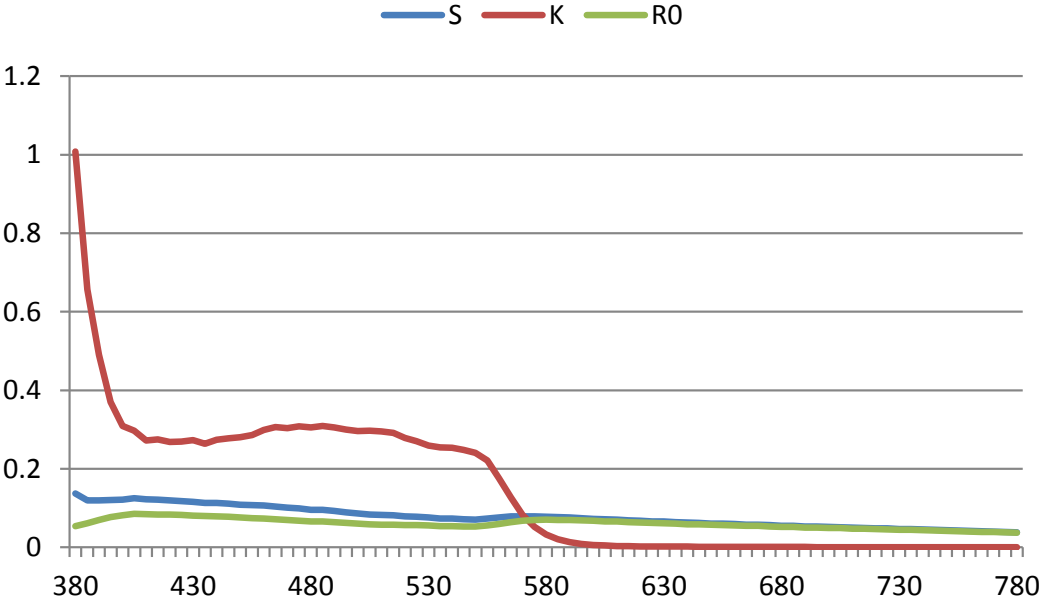


Figure 5.27: the fitting data of sample B2.

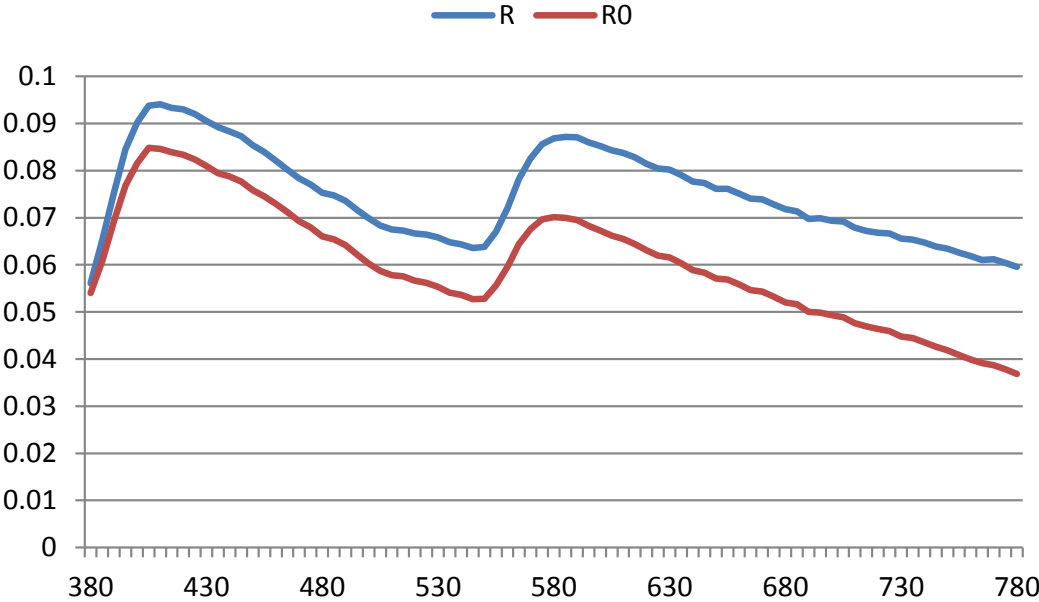


Figure 5.28: the comparison between R and R0 of sample B2.

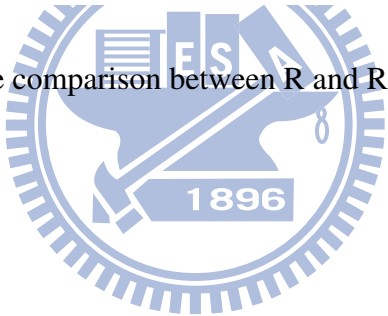




Figure 5.29: the rendering result of sample B2. Left: the thickness is 1.0. Right: the thickness is 2.0.(Each model uses different cosmetic map.)

### Lipstick

We measured five lipsticks and table 5.3 shows the brand of each lipstick.

Table 5.3: The brand of each lipstick.

	Sample L1	Sample L2	Sample L3	Sample L4	Sample L5
Brand	Orbis Rose Liqueur	Orbis Marshmallo w Pink	Orbis Pink Beige	Orbis Almond Beige	Orbis Beige Latte
	Sample L6	Sample L7			
Brand	Orbis Pink Margret	Orbis Apricot Chiffon			

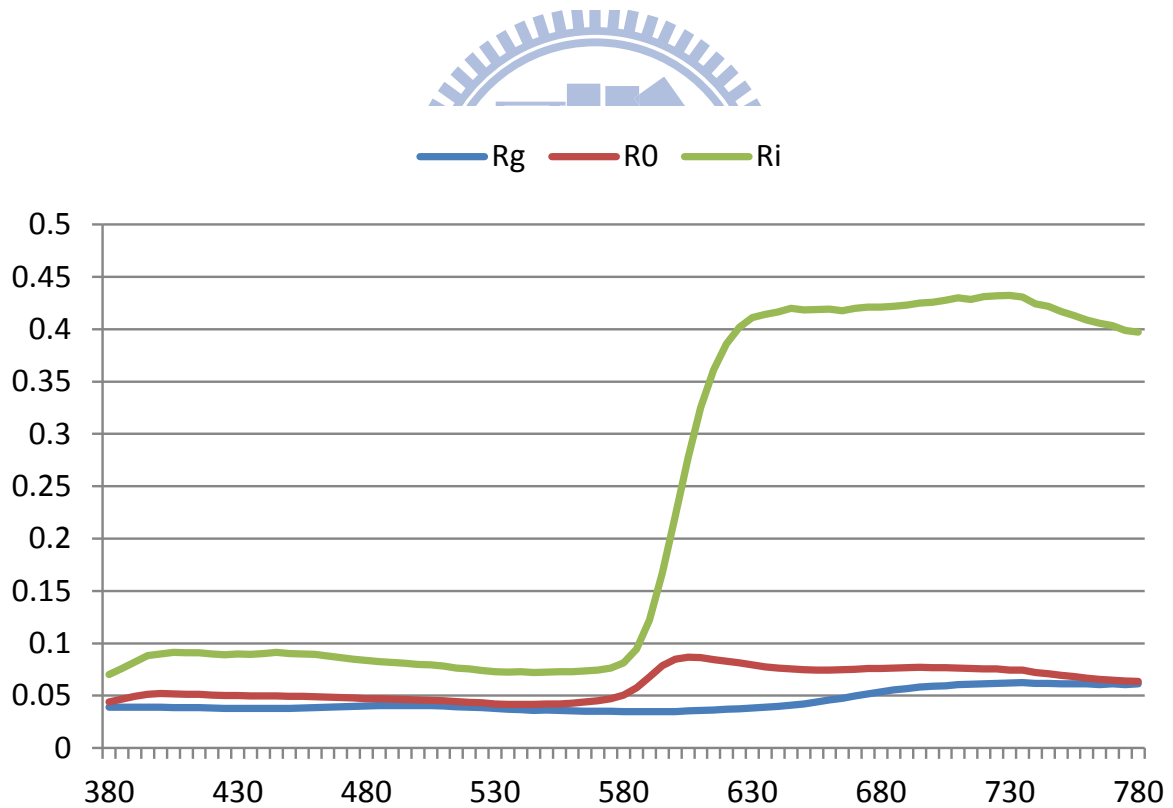


Figure 5.30: the measuring data of sample L1.

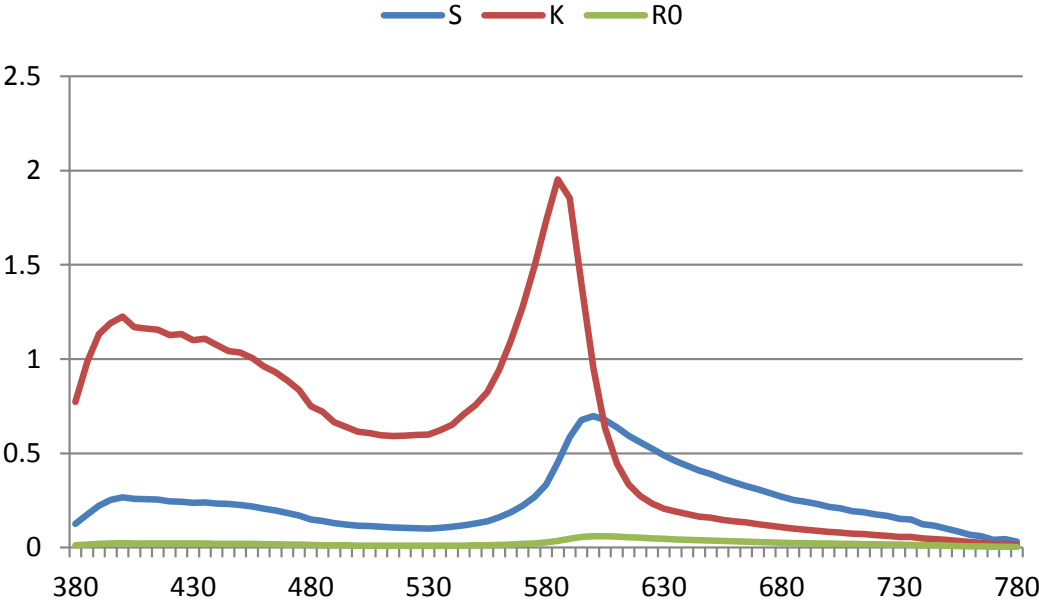


Figure 5.31: the fitting data of sample L1.

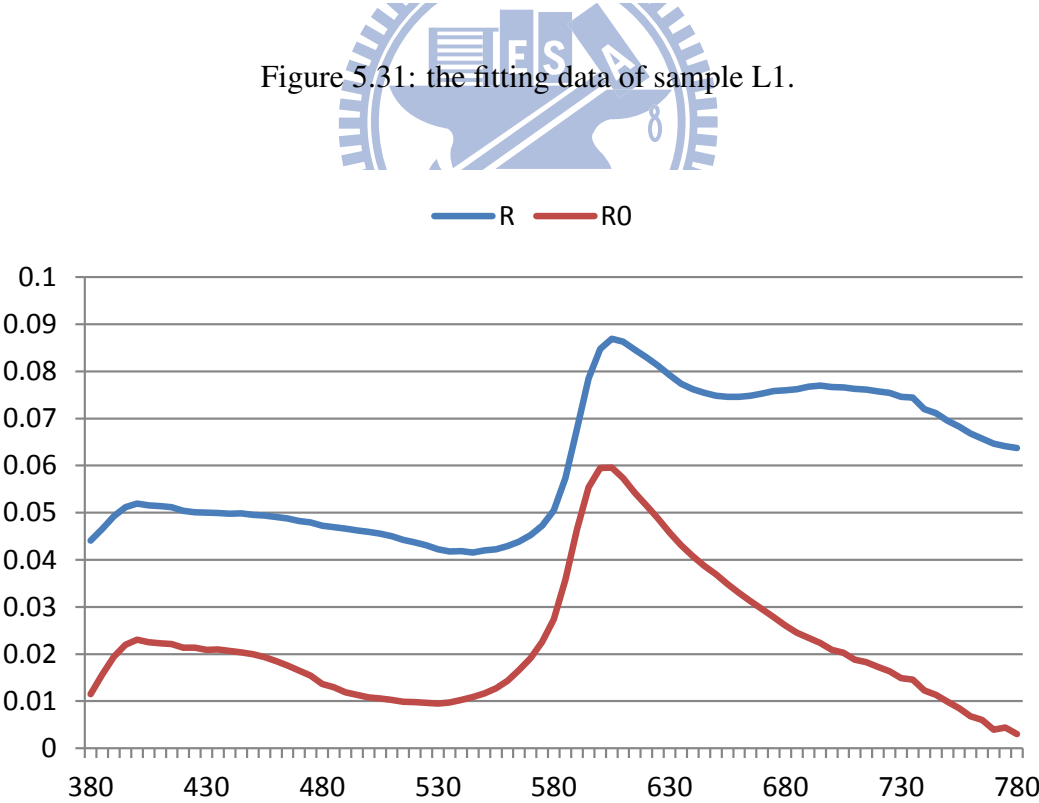


Figure 5.32: the comparison between and R0 of sample L1.





Figure 5.33: the rendering result of sample L1. Left: the thickness is 0.2. Medium: the thickness is 1.0. Right: the thickness is 2.0.

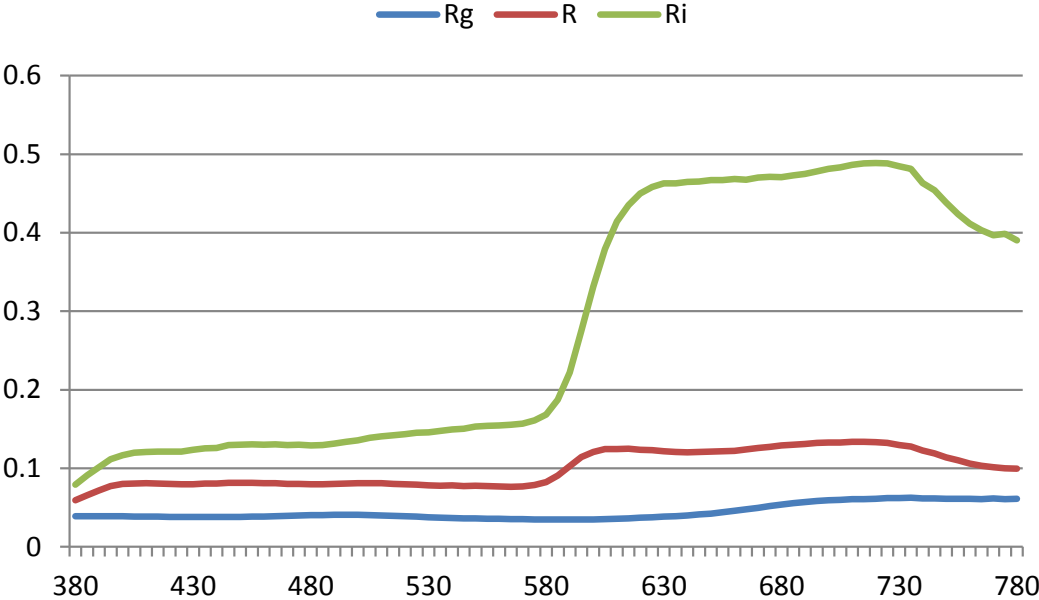


Figure 5.34: the measuring data of sample L2.

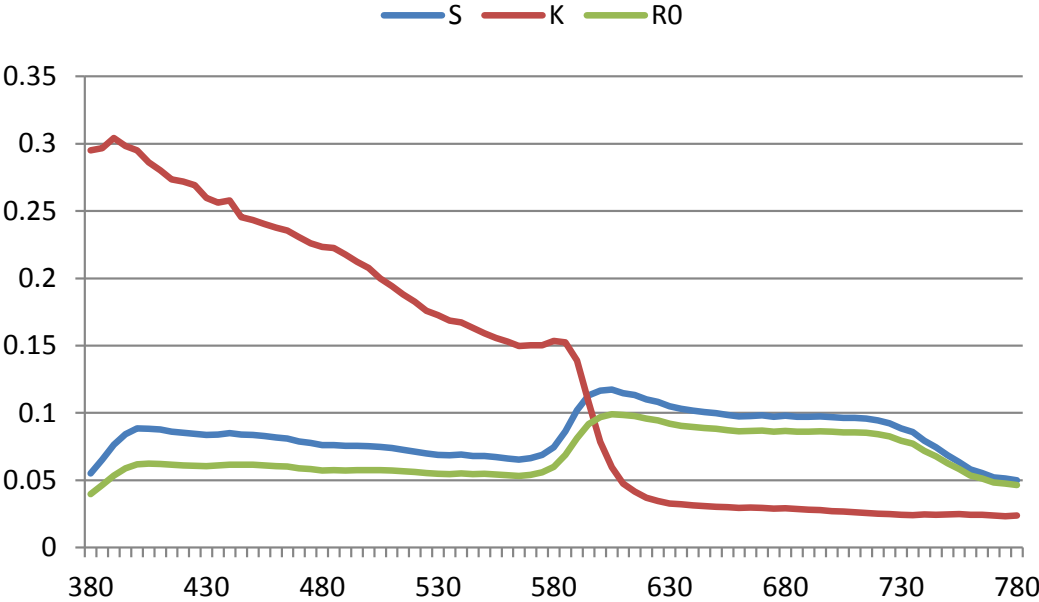


Figure 5.35: the fitting data of sample L2.

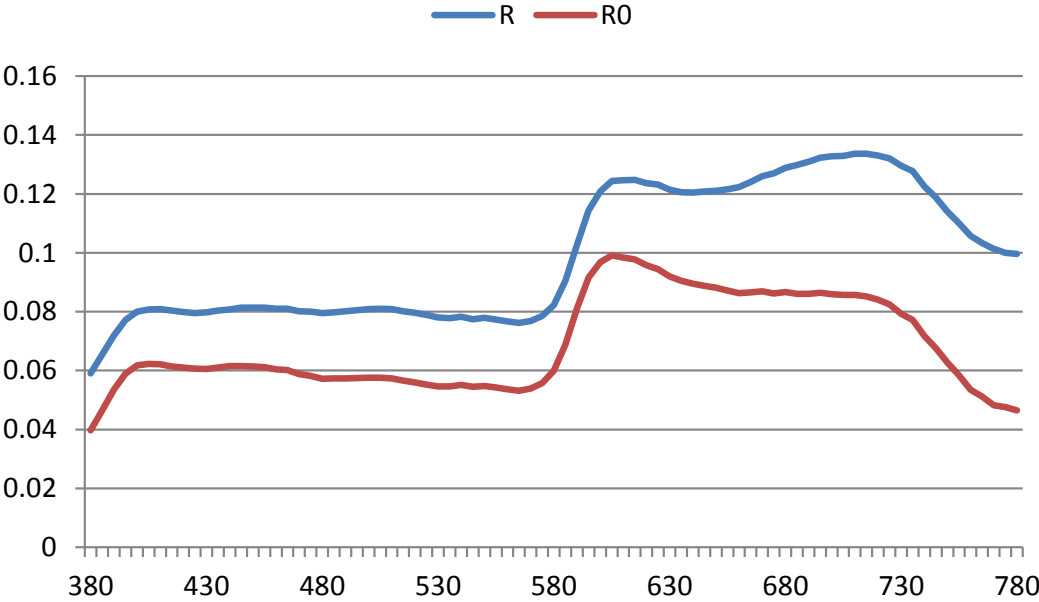


Figure 5.36: the comparison between R and R0 of sample L2.



Figure 5.37: the rendering result of sample L2. Left: the thickness is 0.2. Medium: the thickness is 1.0. Right: the thickness is 2.0.

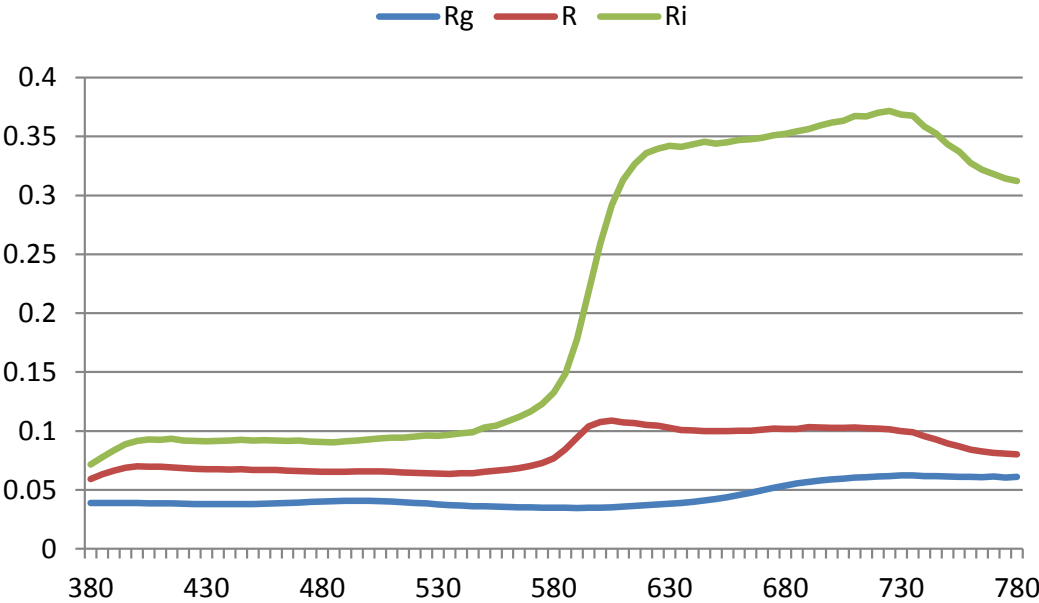


Figure 5.38: the measuring data of sample L3.

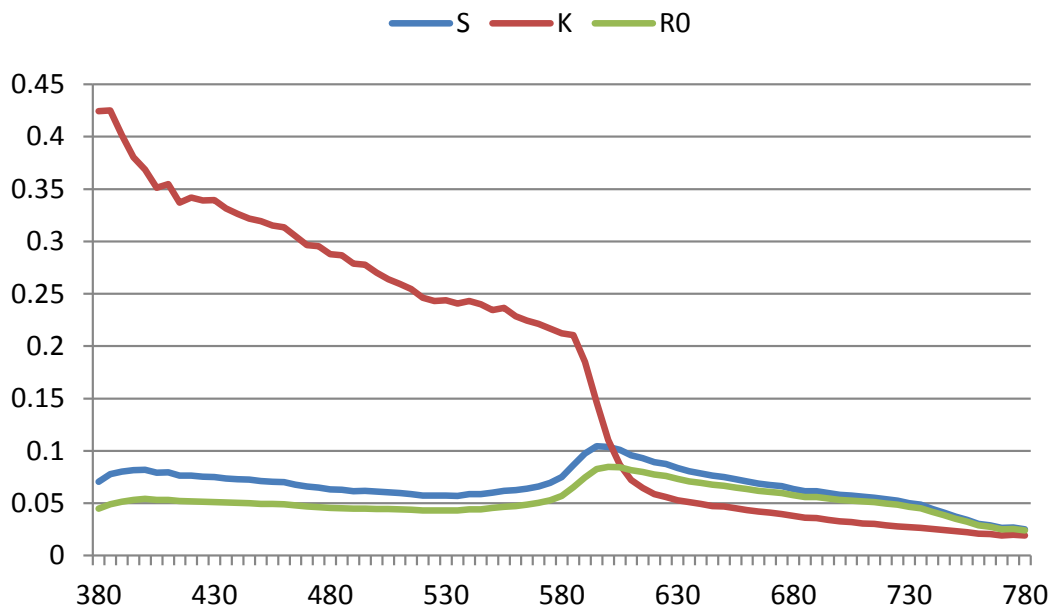


Figure 5.39: the fitting data of sample L3.

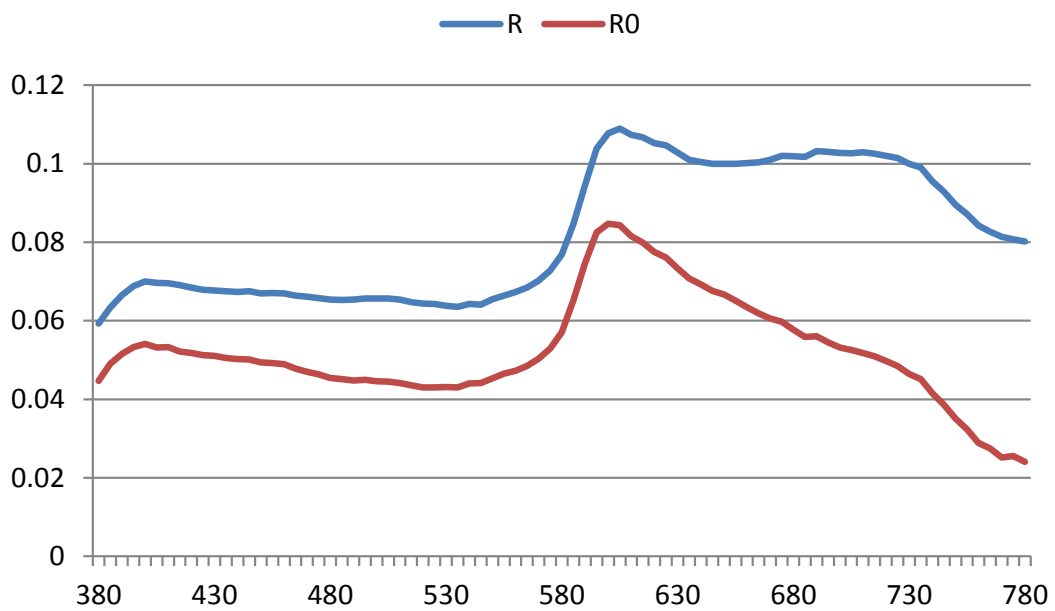


Figure 5.40: the comparison between R and R0 of sample L3.



Figure 5.41: the rendering result of sample L3. Left: the thickness is 0.2. Medium: the thickness is 1.0. Right: the thickness is 2.0.

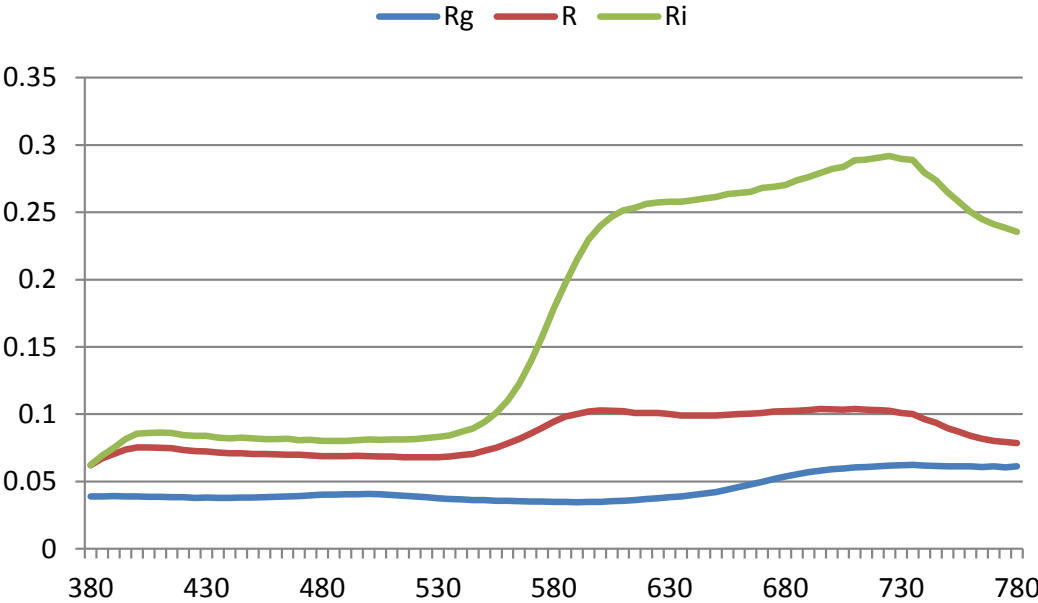


Figure 5.42: the measuring data of sample L4.

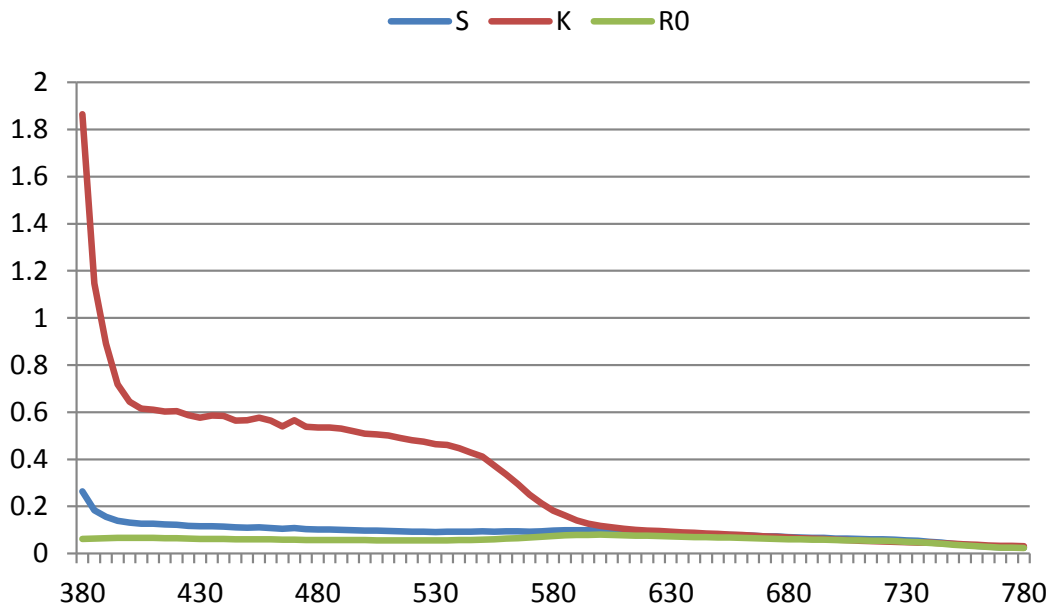


Figure 5.43: the fitting data of sample L4.

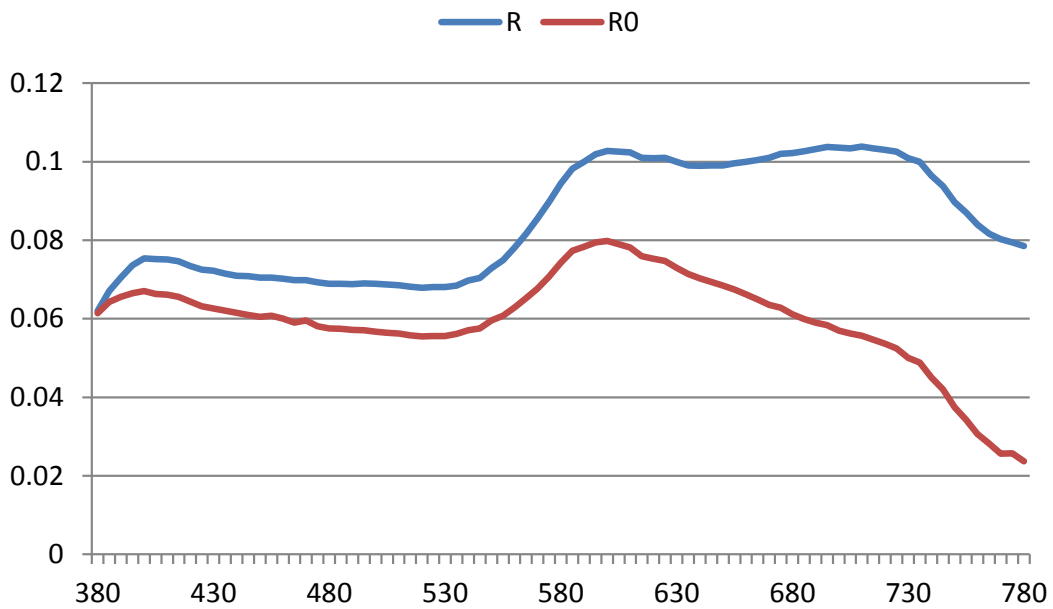


Figure 5.44: the comparison between R and R0 of sample L4.



Figure 5.45: the rendering result of sample L4. Left: the thickness is 0.2. Medium: the thickness is 1.0. Right: the thickness is 2.0.

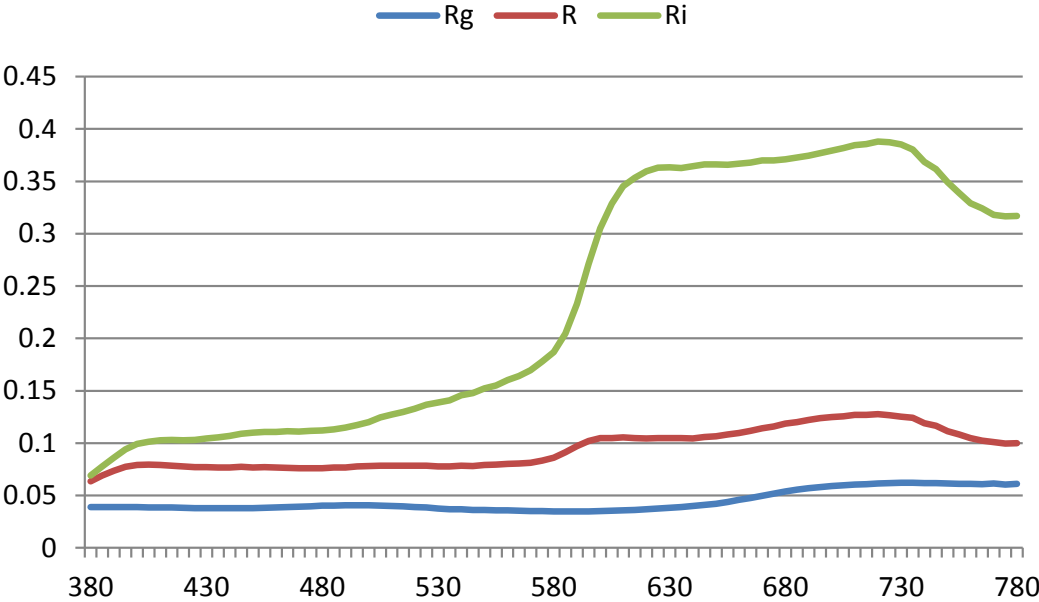


Figure 5.46: the measuring data of sample L5.

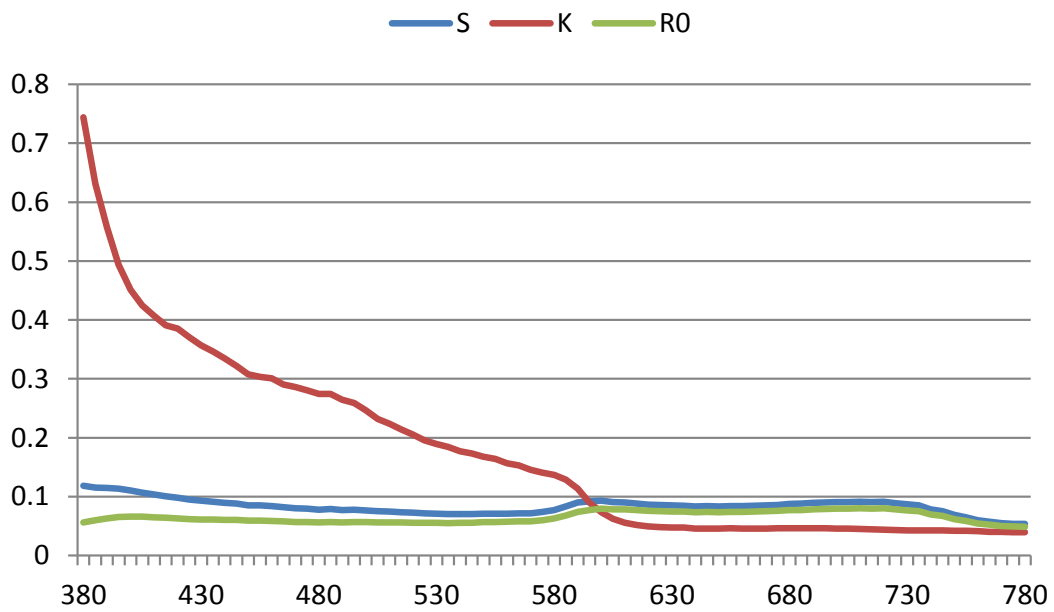


Figure 5.47: the fitting data of sample L5.

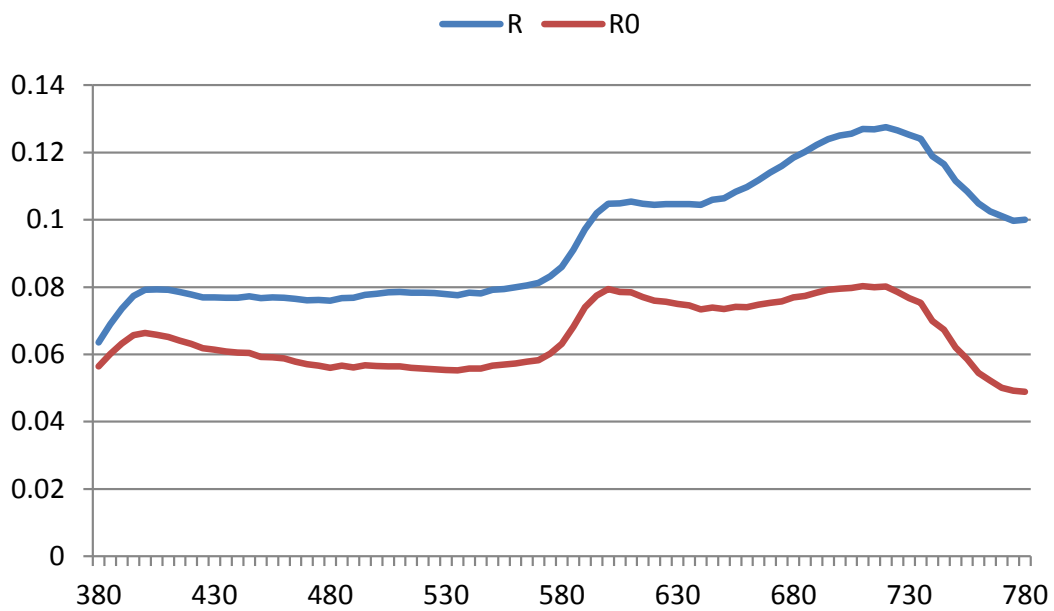


Figure 5.48: the comparison between R and R0 of sample L5.





Figure 5.49: the rendering result of sample L5. Left: the thickness is 0.2. Medium: the thickness is 1.0. Right: the thickness is 2.0.

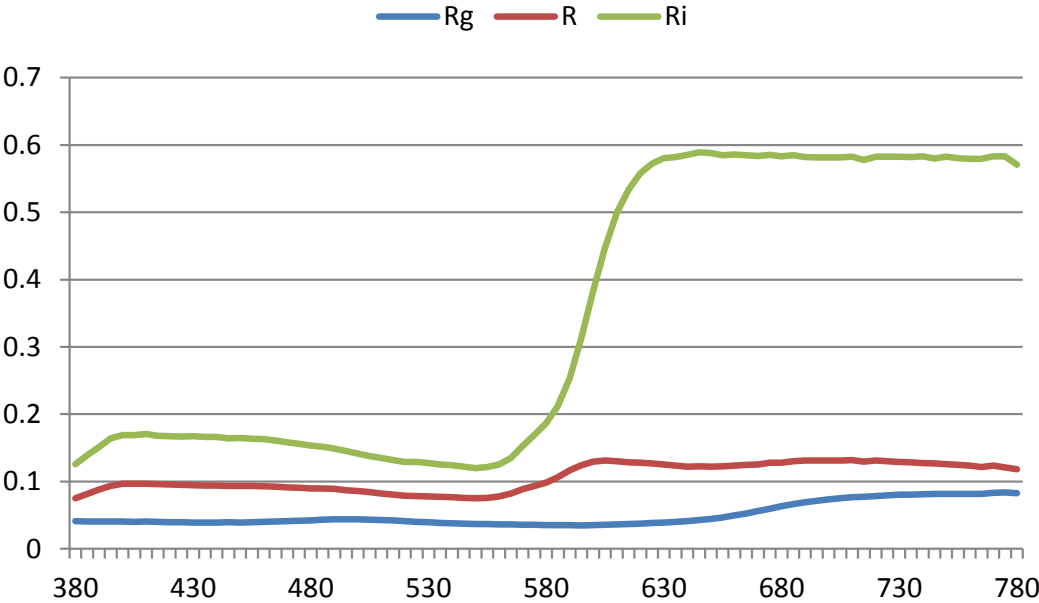


Figure 5.50: the measuring data of sample L6.

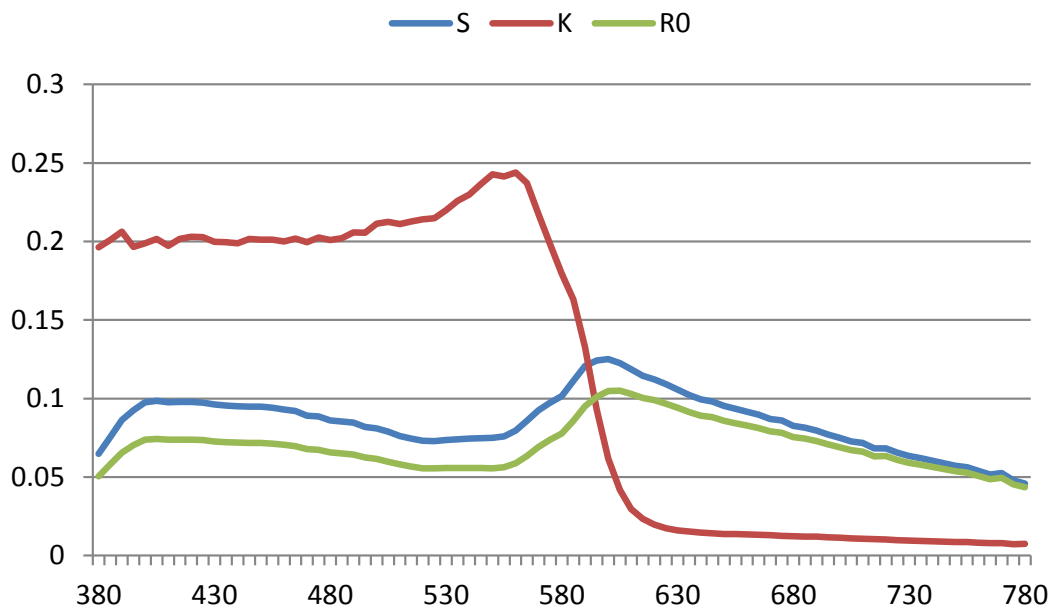


Figure 5.51: the fitting data of sample L6.

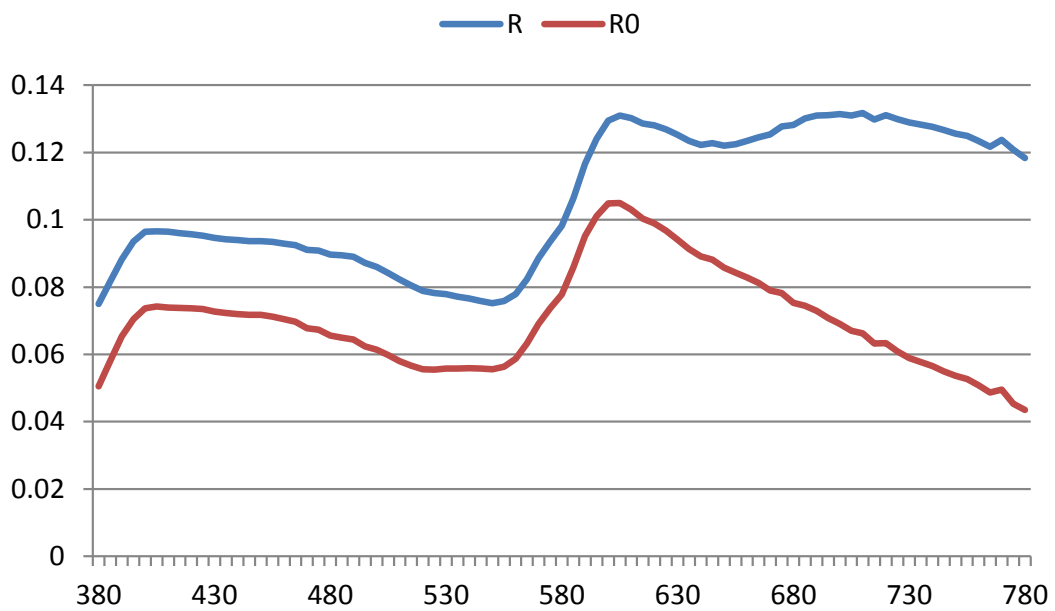


Figure 5.52: the comparison between R and R0 of sample L6.



Figure 5.53: the rendering result of sample L6. Left: the thickness is 0.2. Medium: the thickness is 1.0. Right: the thickness is 2.0.

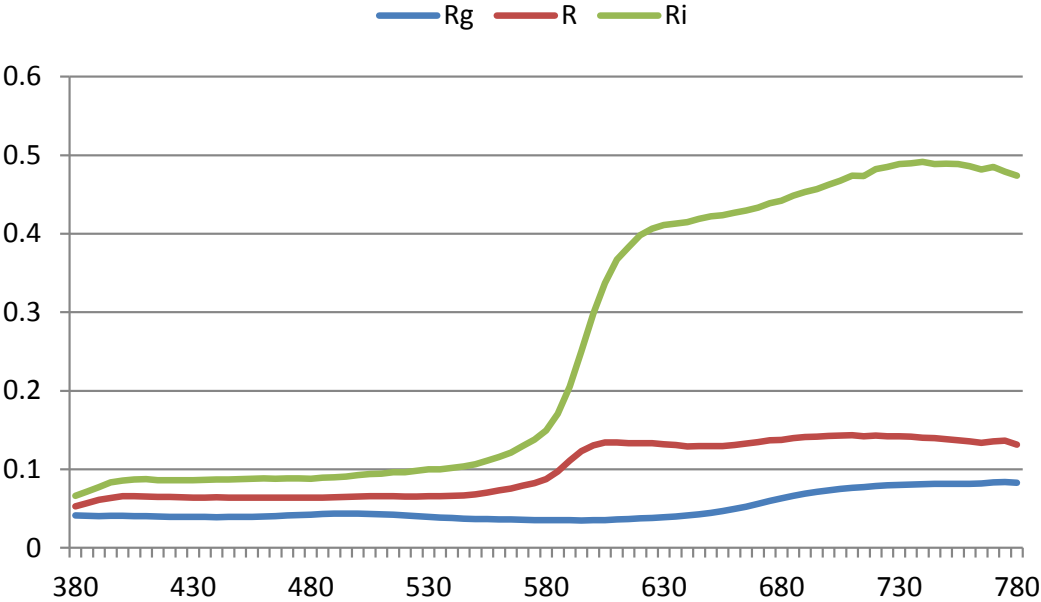


Figure 5.54: the measuring data of sample L7.

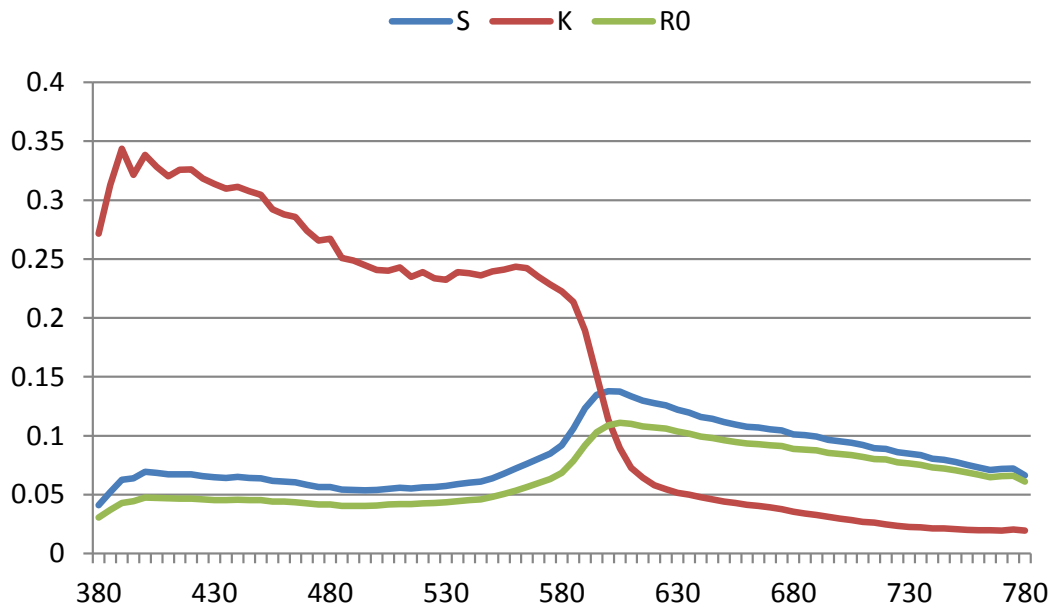


Figure 5.55: the fitting data of sample L7.

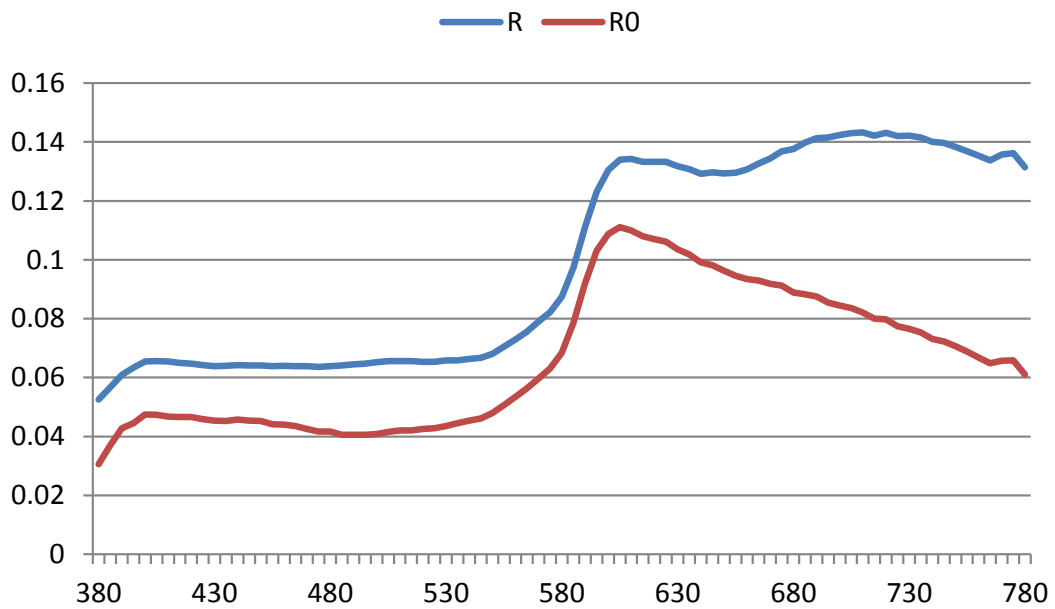


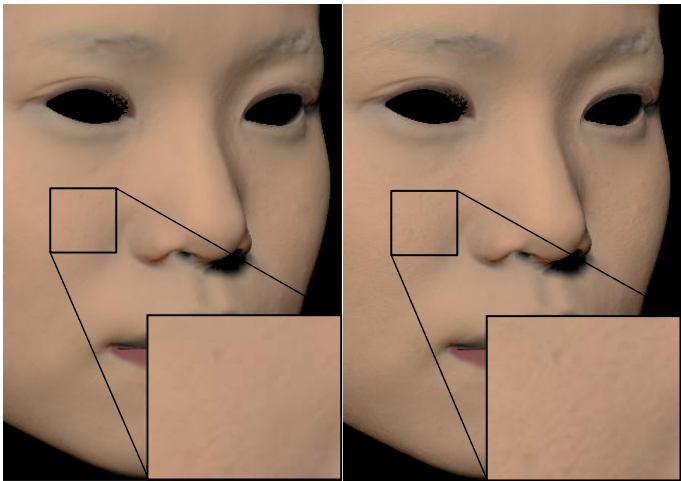
Figure 5.56: the comparison between R and R0 of sample L7.



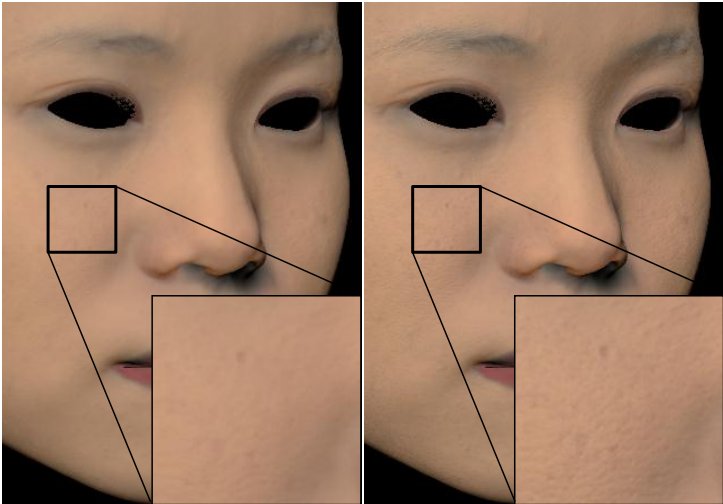
Figure 5.57: the rendering result of sample L7. Left: the thickness is 0.2. Medium: the thickness is 1.0. Right: the thickness is 2.0.

## 5.2 The makeup rendering

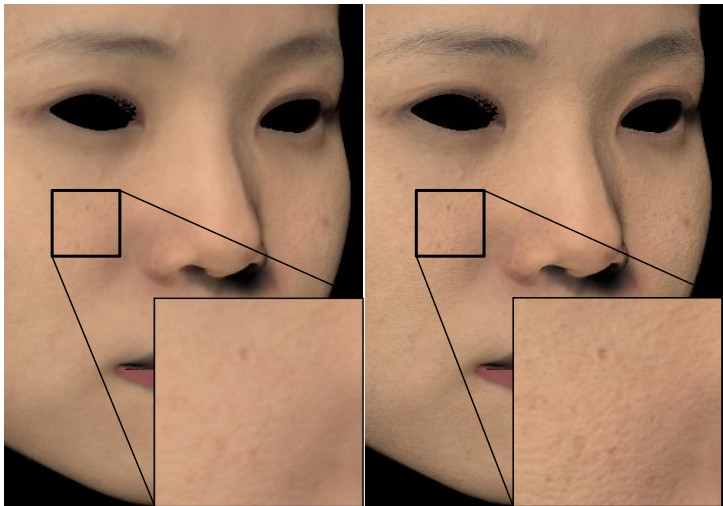
Makeup effect can combine different component. For example, some females just smear the foundation and let the appearance of skin is natural; some females select multiple cosmetics to decorate their face. Our method uses screen-space translucent rendering technique to render the skin and uses multilayered structure to combine the skin with cosmetics. User can give the cosmetic map to rendering its result, and select different cosmetics to render. Figure 5.58 gives two-columns rendering results with different thickness 1.0, 0.5 and 0.1. Left column is rendered with screen-space subsurface rendering technique and is combined with liquid foundation, and right column does not contain any subsurface effect. The rendered result of screen-space subsurface rendering technique generates more smooth and natural result. Figure 5.59, figure 5.60 and figure 5.61 show the cosmetic map and its rendering result. Figure 5.62 and Figure 5.63 compare our rendering result with ground truth, and we observe our rendering result gives a similar appearance with reference image (Ma et al. 2007 [20]).



(a) The thickness is 1.0.

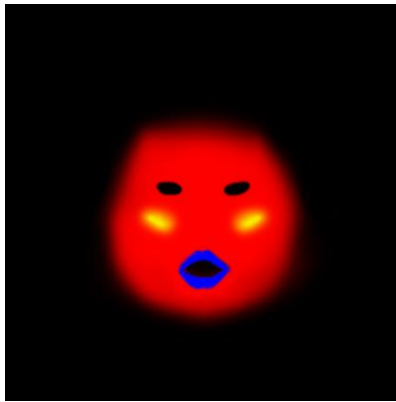


(b) The thickness is 0.5.



(c) The thickness is 0.1.

Figure 5.58: the comparing result of with SSS and without SSS. The left column shows the



(a) Cosmetic map. Red: foundation area. Blue: lipstick. Yellow: blush + foundation.



(b) The appearance of skin



(c) The rendering result. Foundation: Sample F1. Lipstick: Sample L1. Blush: Sample B1.



(d) The rendering result. Foundation: Sample F5. Lipstick: Sample L1. Blush: Sample B1.

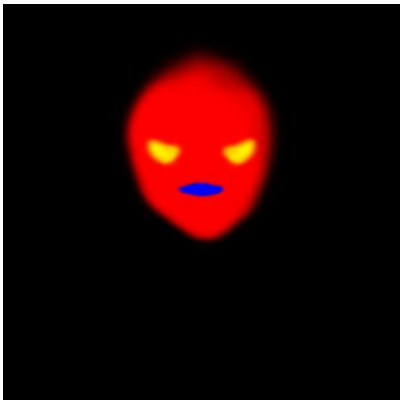


(e) The rendering result. Foundation: Sample F5. Lipstick: Sample L3. Blush: Sample B2.



(f) The rendering result. Foundation: Sample F3. Lipstick: Sample L3.

Figure 5.59: combination with different cosmetics and apply on Digital Coco.



(a) Cosmetic map. Red: foundation area. Blue: lipstick. Yellow: blush + foundation.

(b) The appearance of skin



(c) The rendering result. Foundation: Sample F1.

(d) The rendering result. Foundation: Foundation: Sample F5. Lipstick: Sample L1. Blush: Sample B1.

Figure 5.60: combination with different cosmetics and apply on a man head.





(a) Cosmetic map. Red: foundation area. Blue: lipstick. Yellow: blush + foundation. (b) The appearance of skin area.



(c) The rendering result. Foundation: Sample F1. Lipstick: Sample L6. Blush: Sample B1. (d) The rendering result. Foundation: Sample F2. Lipstick: Sample L7. Blush: Sample B1.

Figure 5.61: combination with different cosmetics and apply on Digital Orange.



Figure 5.62: comparison rendering result with reference image.



Figure 5.63: comparison rendering result with reference image. (do not contain eyelashes and eyebrows)

## CHAPTER 6

---

# Conclusions

---

In this chapter, we summarize our cosmetic simulation algorithm, and proposed several future works.



### 6.1 Summary

Our approach provides a simple way to simulate the makeup effect. We combine the screen-space algorithm with traditional Kubelka-Munk theory to simulate the final result. Instead of traditional method that warp the example image to the subject, the style of our makeup simulation system can be changed by user. This approach can be used in cosmetic industry to help them to simulate the makeup effect. Our system is rendering in real-time frame rate, and user can change the thickness in interactive time.

## 6.2 Limitation and Future work

In our assumption, we assume the cosmetics are no pearl effect and no sparkle effect. Because these effects are view-dependent, it is very difficult to simulate. But, these effects are other important parts of cosmetics. In the research of car painting, there are some articles give some hints, and we could try to use these methods to simulate the pearl effect or the sparkle effect, such as Takagi et al [4].

We also assume the materials are liquid or cream, but many cosmetics are loose powder. In our observing, if the makeup is smeared evenly, the different between liquid or cream and loose powder are hard to differentiate. In the future work, we could add view-dependent effects and loose powder effect to our system and let system to simulate more makeup effects.

The cosmetic map is most important part to mark makeup area and we use some auxiliary tool to help us to paint this map. Actually, we can add 3D mesh painting algorithm to our system, and then user can paint makeup area and observe the result directly.

We can also combine the cosmetic map with cosmetic transferring algorithm. In the cosmetic transferring, it extracts the makeup effect by some examples and this effect contains makeup style, color and view-dependent effect. In the future, we can give some examples and extract the makeup style, and then we can use our system to simulate different makeup result with this style.

## CHAPTER A

---

# Converting reflectance spectra to CIE RGB color space

---



Converting reflectance spectra to CIE RGB color space is another important process in our simulation system. We use traditional Kubelka-Munk theory to simulate each material's spectrum, so we need to convert it to color space and render to screen. In this section, we describe how to convert spectra data to CIE RGB color space. In traditional converting, it converts radiant energy to CIE color space. In our conversion, we convert the reflectance spectra rather than the radiant energy of material  $E_m$ .

Original measured data is radiant energy of material  $E_m$  which represents the amount of light reflected from surface to observer. Therefore,  $E_m$  needs to be divided by the "standard white" and we can obtain the reflectance. Figure A.1 shows a simple diagram about this process.

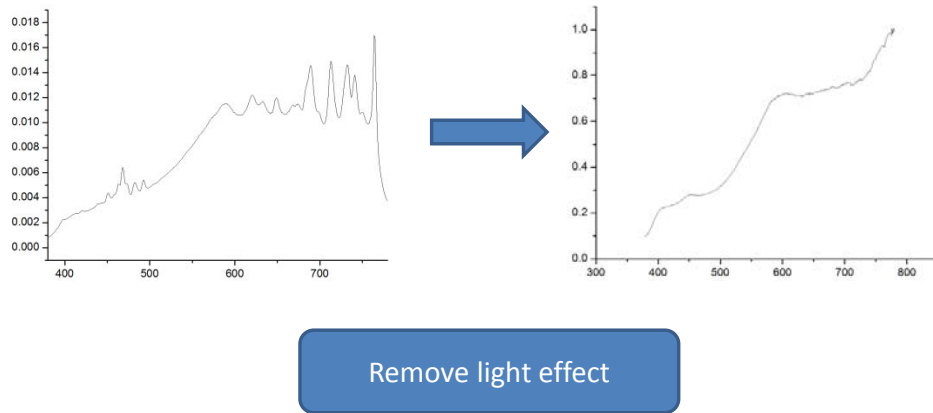


Figure A.1: Obtaining reflectance by remove light effect.

Converting spectra to CIE RGB includes two simple steps: First, converting spectra to CIE XYZ trisimulus values by CIE 2-degree color matching functions. Second, convert CIE XYZ color space to CIE RGB by transform matrix.

The first step uses color matching functions to convert spectra into trisimulus values. This process is a convolution operation and its integral formula is defined in equation 1. These color matching function curves are notated  $\bar{x}(\lambda)$ ,  $\bar{y}(\lambda)$  and  $\bar{z}(\lambda)$ . Figure A.2 shows these curves. It is noteworthy that the color matching function  $\bar{y}(\lambda)$  converts the spectra to luminance. The reflectance  $R(\lambda)$  convolutes these functions and we can obtain CIE XYZ color space value.

$$X = \int_{380}^{780} R(\lambda) \bar{x}(\lambda) d\lambda \quad (\text{A.1})$$

$$Y = \int_{380}^{780} R(\lambda) \bar{y}(\lambda) d\lambda \quad (\text{A.2})$$

$$Z = \int_{380}^{780} R(\lambda) \bar{z}(\lambda) d\lambda \quad (\text{A.3})$$

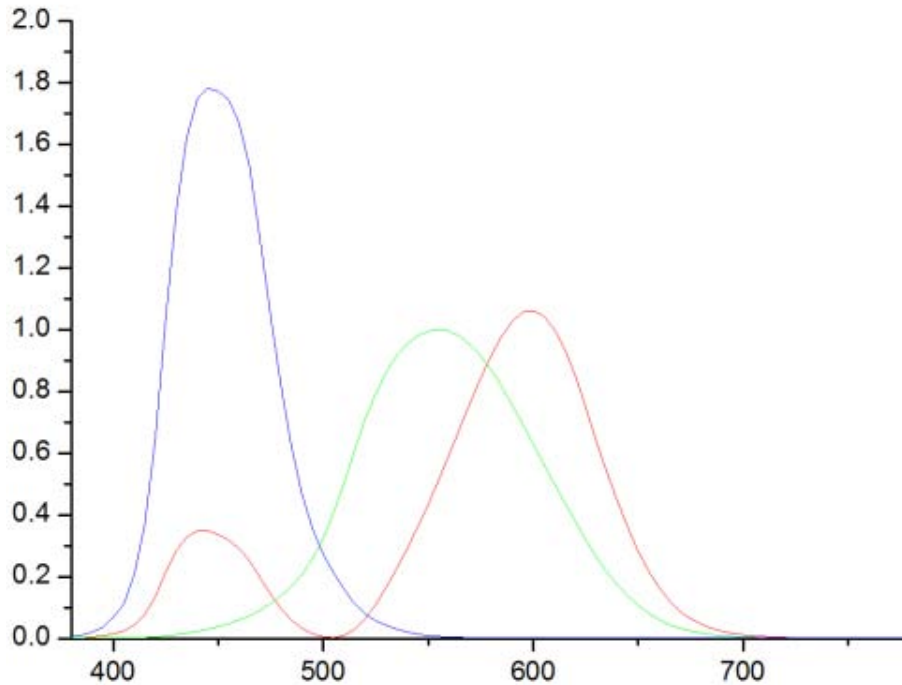


Figure A.2: CIE 2-degree color matching functions.

After convolution finished, we convert CIE XYZ color space to CIE RGB color space. This conversion is a linear transformation and we can be done by a matrix:

$$\begin{pmatrix} R \\ G \\ B \end{pmatrix} = \begin{pmatrix} 2.370674 & -0.90004 & -0.47063 \\ -0.51389 & 1.425304 & 0.088581 \\ 0.005298 & -0.04169 & 1.009397 \end{pmatrix} \begin{pmatrix} X \\ Y \\ Z \end{pmatrix} \quad (\text{A.4})$$

This matrix uses CIE standard illuminant E, and we can obtain the color of material directly.

Figure A.3 shows converting diagram.

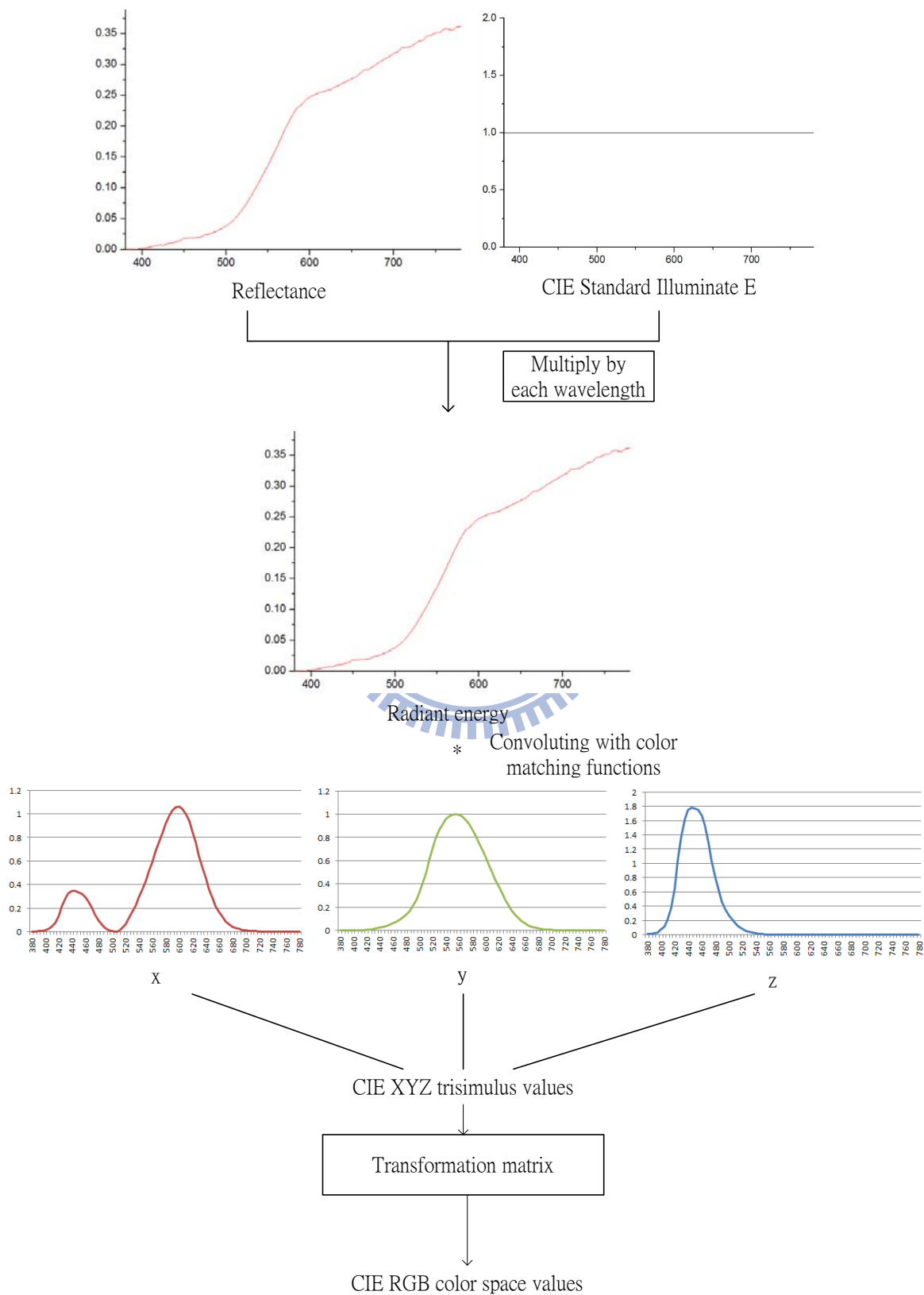


Figure A.3: converting diagram.



---

# Bibliography

---

- [1] W.-S. Tong, C.-K. Tang, M. S. Brown, and Y.-Q. Xu, “Example-based cosmetic transfer,” *Computer Graphics and Applications, Pacific Conference on*, vol. 0, pp. 211–218, 2007.
- [2] D. Guo and T. Sim, “Digital face makeup by example,” in *Proc. CVPR*, 2009.
- [3] K. S. and Tobias Ritschel and Matthias Hullin, T. T. and Volker Blanz, and H.-P. Seidel, “Computer-suggested facial makeup,” *Comp. Graph. Forum (Proc. Eurographics 2011)*, vol. 30, no. 2, 2011.
- [4] Y. Moriuchi, S. Tominaga, and T. Horiuchi, “Precise analysis of spectral reflectance properties of cosmetic foundation,” in *Image Analysis (A.-B. Salberg, J. Hardeberg, and R. Jenssen, eds.)*, vol. 5575 of *Lecture Notes in Computer Science*, pp. 138–148, Springer Berlin / Heidelberg, 2009.
- [5] H. W. Jensen, S. R. Marschner, M. Levoy, and P. Hanrahan, “A practical model for subsurface light transport,” in *Proceedings of the 28th annual conference on Computer graphics and interactive techniques, SIGGRAPH '01*, (New York, NY, USA), pp. 511–518, ACM, 2001.
- [6] C. Donner and H. W. Jensen, “Light diffusion in multi-layered translucent materials,” *ACM Trans. Graph.*, vol. 24, pp. 1032–1039, July 2005.

- [7] E. d'Eon and D. Luebke, *GPU Gems 3*, ch. Advanced techniques for realistic Real-Time skin rendering, pp. pp.293–347. Addison Wesley, July 2007.
- [8] D. L. Eugene d'Eon and E. Enderton, "Efficient rendering of human skin," in *The Eurographics Symposium on Rendering*, 2007.
- [9] M. Doi, R. Ohtsuki, and S. Tominaga, "Spectral estimation of skin color with foundation makeup," in *Image Analysis* (H. Kalviainen, J. Parkkinen, and A. Kaarna, eds.), vol. 3540 of *Lecture Notes in Computer Science*, pp. 70–82, Springer Berlin / Heidelberg, 2005.
- [10] H. W. Jensen and J. Buhler, "A rapid hierarchical rendering technique for translucent materials," *ACM Trans. Graph.*, vol. 21, pp. 576–581, July 2002.
- [11] J. Jimenez, V. Sundstedt, and D. Gutierrez, "Screen-space perceptual rendering of human skin," *ACM Transactions on Applied Perception*, vol. 6, no. 4, pp. 23:1–23:15, 2009.
- [12] E. D'Eon and G. Irving, "A quantized-diffusion model for rendering translucent materials," *ACM Trans. Graph.*, vol. 30, pp. 56:1–56:14, August 2011.
- [13] W. T. Reeves, D. H. Salesin, and R. L. Cook, "Rendering antialiased shadows with depth maps," in *Proceedings of the 14th annual conference on Computer graphics and interactive techniques*, SIGGRAPH '87, (New York, NY, USA), pp. 283–291, ACM, 1987.
- [14] J. Jimenez and D. Gutierrez, *GPU Pro: Advanced Rendering Techniques*, ch. Screen-Space Subsurface Scattering, pp. 335–351. AK Peters Ltd., 2010.
- [15] S. N. Thennadil, "Relationship between the kubelka-munk scattering and radiative transfer coefficients," *The Journal of the Optical Society of America A*, vol. 25, pp. 1480–1485, 2008.
- [16] J. E. Lohr, *Reflectance Spectroscopy*. Springer-Verlag, 1969.
- [17] J. Dorsey and P. Hanrahan, "Modeling and rendering of metallic patinas," pp. 387–396, 1996.

- [18] C. Kelemen and L. Szirmay-Kalos, "A microfacet based coupled specular-matte brdf model with importance sampling," *EUROGRAPHICS*, vol. Short Papers, p. 2534, 2001.
- [19] C. J. Curtis, S. E. Anderson, J. E. Seims, K. W. Fleischer, and D. H. Salesin, "Computer-generated watercolor," in *Proceedings of the 24th annual conference on Computer graphics and interactive techniques*, SIGGRAPH '97, (New York, NY, USA), pp. 421–430, ACM Press/Addison-Wesley Publishing Co., 1997.
- [20] P. P. C.-F. C. M. W. P. D. Wan-Chun Ma, Tim Hawkins, "Rapid acquisition of specular and diffuse normal maps from polarized spherical gradient illumination," *Eurographics Symposium on Rendering*, 2007.
- [21] A. Takagi, A. Watanabe, and G. Baba, "Prediction of spectral reflectance factor distribution of automotive paint finishes," *Color Research & Application*, vol. 30, no. 4, pp. 275–282, 2005.

